CANADIAN THESES

THÈSES CANADIENNES

NOTICE

The quality of this microfiche is heavily dependent upon the quality of the original thesis submitted for microfilming. Every effort has been made to ensure the highest quality of reproduction possible.

If pages are missing, contact the university which granted the degree.

Some pages may have indistinct print especially if the original pages were typed with a poor typewriter ribbon or if the university sent us an inferior photocopy.

Previously copyrighted materials (journal articles, published tests, etc.) are not filmed.

Reproduction in full or in part of this film is governed by the Canadian Copyright Act, R.S.C. 1970, c. C-30. Please read the authorization forms which accompany this thesis.

AVIS

La qualité de cette microfiche dépend grandement de la qualité de la thèse soumise au microfilmage. Nous avons tout fait pour assurer une qualité supérieure de reproduction.

S'il manque des pages, veuillez communiquer avec l'université qui a conféré le grade.

La qualité d'impression de certaines pages peut laisser à désirer, surtout si les pages originales ont été dactylographiées à l'aide d'un ruban usé ou si l'université nous a fait parvenir une photocopie de qualité inférieure.

Les documents qui font déjà l'objet d'un droit d'auteur (articles de revue, examens publiés, etc.) ne sont pas microfilmés.

La reproduction, même partielle, de ce microfilm est soumise à la Loi canadienne sur le droit d'auteur, SRC 1970, c. C-30. Veuillez prendre connaissance des formules d'autorisation qui accompagnent cette thèse.

THIS DISSERTATION
HAS BEEN MICROFILMED
EXACTLY AS RECEIVED

LA THÈSE A ÉTÉ
MICROFILMÉE TELLE QUE
NOUS L'AVONS REÇUE

Canada

WIND INDUCED RESPONSE OF LONG SPAN CABLE-STAYED BRIDGES WITH SHALLOW BOX GIRDER

by

Edward Shun Wah Tsui

A thesis
presented to the University of Ottawa
in partial fulfillment of the
requirements for the degree of
MASTER OF APPLIED SCIENCE
in
CIVIL ENGINEERING.

OTTAWA, Ontario, 1983

ABSTRACT

In the beginning of Chapter I, the characteristics and the types of cable-stayed bridges are introduced. The necessity of wind tunnel testing and the summary of aerodynamic behaviour of long span bridges are also included in the first Chapter. Comments on different model testing techniques are made at the end of Chapter I.

The work is concentrated on the aerodynamic problems of shallow box girder bridge using the Proposed Annacis Island Bridge as an example. A brief introduction of the bridge as well as the previous wind tunnel study at NAE/NRC are presented in Chapter II . In this previous study, the 1/60-scale sectional model was tested only in smooth flow. A part of the experimental results are summarized here.

For the present study, the 1/500-scale taut strip model and 1/500-scale sectional model were tested under six flow conditions as is described in Chapter III . Results of the flow measurements are discussed. From the non-turbulent flow results of the 1/500-scale models, the 1/60-scale sectional model test results are confirmed.

The buffeting response increases proportionally to turbulence intensity as was expected. The buffeting

response of the 1/500-scale taut strip model (3-D) and the sectional model(2-D) agreed satisfactorily. It is noteworthy, however, that this agreement was found to be less satisfactory in boundary layer flow conditions, in which, the three-dimensional characteristics of the flow are more pronounced.

Finally, a series of parametric studies on buffeting response has been done using a mathematical model. The summary of the results is given in the Appendix<B>.

ACKNOWLEDGEMENTS

The author wishes to express his gratitude to his supervisor, Dr. H. Tanaka . His continuous guidance and encouragement during the course of study is sincerely appreciated.

The author is also grateful to Mr. R.L. Wardlaw for allowing him to use the facilities at the National Aeronautical Establishment, National Research Council of Canada. The assistance provided from Mr. M. Savage in running the test at these facilities is greatly appreciated.

The Annacis Bridge Consultants and the Ministry of Transportation and Highways, Province of British Columbia are gratefully acknowledged for their allowance to use some valuable information about the Proposed Annacis Island Bridge - concrete version.

The author also extends his gratitude to Mr. Tommy Kan for his valuable help in both experimental work and preparation of the thesis.

Finally, the support from the author's family is gratefully acknowledged. Their ever-lasting encouragement can never be repaid.

CONTENTS

LIST OF FIGURES

LIST OF TABLES

NOMENCLATURES

b = A half of the chord length, or B/2

B = Width of the section

C_L = Lift force coefficient

C_m = Pitching moment coefficient

e = Eccentricity of section, the centre of gravity from the elastic axis

F = Frequency

FA = Torsional frequency

FZ = Vertical bending frequency

Hg = Bridge deck height

Iu = Turbulence intensity of u-component

Iw = Turbulence intensity of w-component

ℓ = Bridge span length

L = Lift force

m = Mass per unit length of the bridge

M = Pitching moment

R = Correlation function

S(f) = Spectral density function

t = Time

V = Mean wind speed

Vr = Reduced velocity

V/(B X FZ) or V/(B X FA)

$u(t)$ = Time dependent, instantaneous velocity component in u-direction

$v(t)$ = Time dependent, instantaneous velocity component in v-direction

$w(t)$ = Time dependent, instantaneoous velocity component in w-direction

ζ_z = Flexural damping in vertical bending

ζ_ϕ = Torsional damping

η = Reduced vertical displacement z/b

θ = Mass moment of inertia per unit length (about the elastic axis)

μ = Mass ratio defined by $(m/\pi\rho b^2)$

ν = Dimensionless mass parameter given by $\left(\frac{\theta}{\pi\rho b^4}\right)$

ξ = Ratio of frequency to flexural frequency (F/FZ)

ρ = Air density

ω_z = Circular frequency in flexural mode

ω_ϕ = Circular frequency in torsional mode

RMS = Root-mean-square

σ_η = RMS flexural response

σ_ϕ = RMS torsional response

$S_\eta(f)$ = Response spectrum of vertical bending

$S_\phi(f)$ = Response spectrum of torsion

Chapter I

INTRODUCTION

1.1 CABLE-STAYED BRIDGES

The selection of a specific type of bridge superstructure for a particular site is not an automatic engineering process. The principal parameters to be considered are : the span lengths of the bridge, the foundation conditions, environmental forces to be considered, the aesthetic considerations for the site, and finally the relative cost of one type of bridge with another comparable design.

The aesthetic and safety considerations are common for many types of bridges but their relative cost is highly dependent on the design selection. When the main span length of a bridge exceeds 250 metres, the suspension bridge (Fig. 1.1.1) and the cable-stayed bridge (Fig. 1.1.2) tends to dominate all other designs, not only because their erection is more economical, but also because of their elegance and graceful beauty.

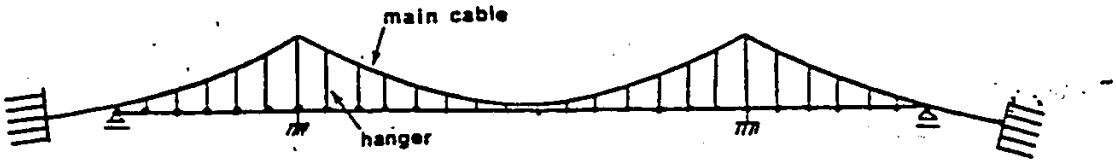

Figure 1.1.1: Suspension bridge

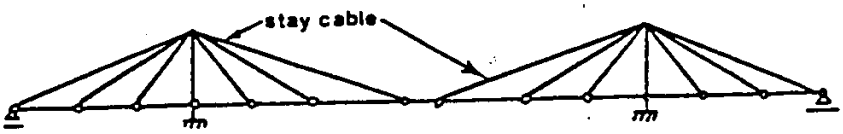

Figure 1.1.2: Cable-stayed bridge

The major structural difference between the cable-stayed bridge and the suspension bridge design is the orientation of the cables. For a suspension bridge, the main cable, which is connected to the bridge deck by the hangers, is anchored at both ends in the ground. On the other hand, the cable-stayed bridge is a self-supporting system. All the stay cables are anchored along the bridge deck and are attached to the tower.

As stated previously, the cost of building a bridge is one of the factors in selecting the type of bridge to be built. The economic survey of suspension bridge vs. cable-

stayed bridge, which was done by Podolny [16], indicated that if the main span length of a bridge is within the range of 200 to 700 metres, the cable-stayed bridge is more economical than the suspension, arch or cantilever designs. The main spans of most of the bridges built fall within the 200 to 700 metres range.

The modern cable-stayed bridge design was developed in West Germany during the post war years of reconstruction in Europe. West Germany found that approximately 15,000 bridges had been destroyed during the war. In this peroid of time, steel was in short supply and a great emphasis was placed on minimum weight design. As a result, an orthotropic type of bridge deck combined with cable-stayed design was adopted. This bridge structure in some cases reduced weight by as much as 40 percent of their original design.

A common type of the cable-stayed steel bridge is the Severin Bridge in Cologne, West Germany, 1959(Fig. 1.1.3). The bridge consists of six continuous spans with lengths of 161-292-157-990-494-172 ft (49-89-48-301.8-150.6-52.4 m). The two large spans are stiffened by a system of 12 cables intersecting at the top of an A-shape tower. This cable arrangement provides a very good torsional rigidity to the bridge. The cross section of the bridge consists of two box girders 10.5 ft (3.2 m) wide, with a depth varying from approximately 10 ft (3.05 m) at the end abutments to 15 ft (4.57 m) at the middle of the bridge.

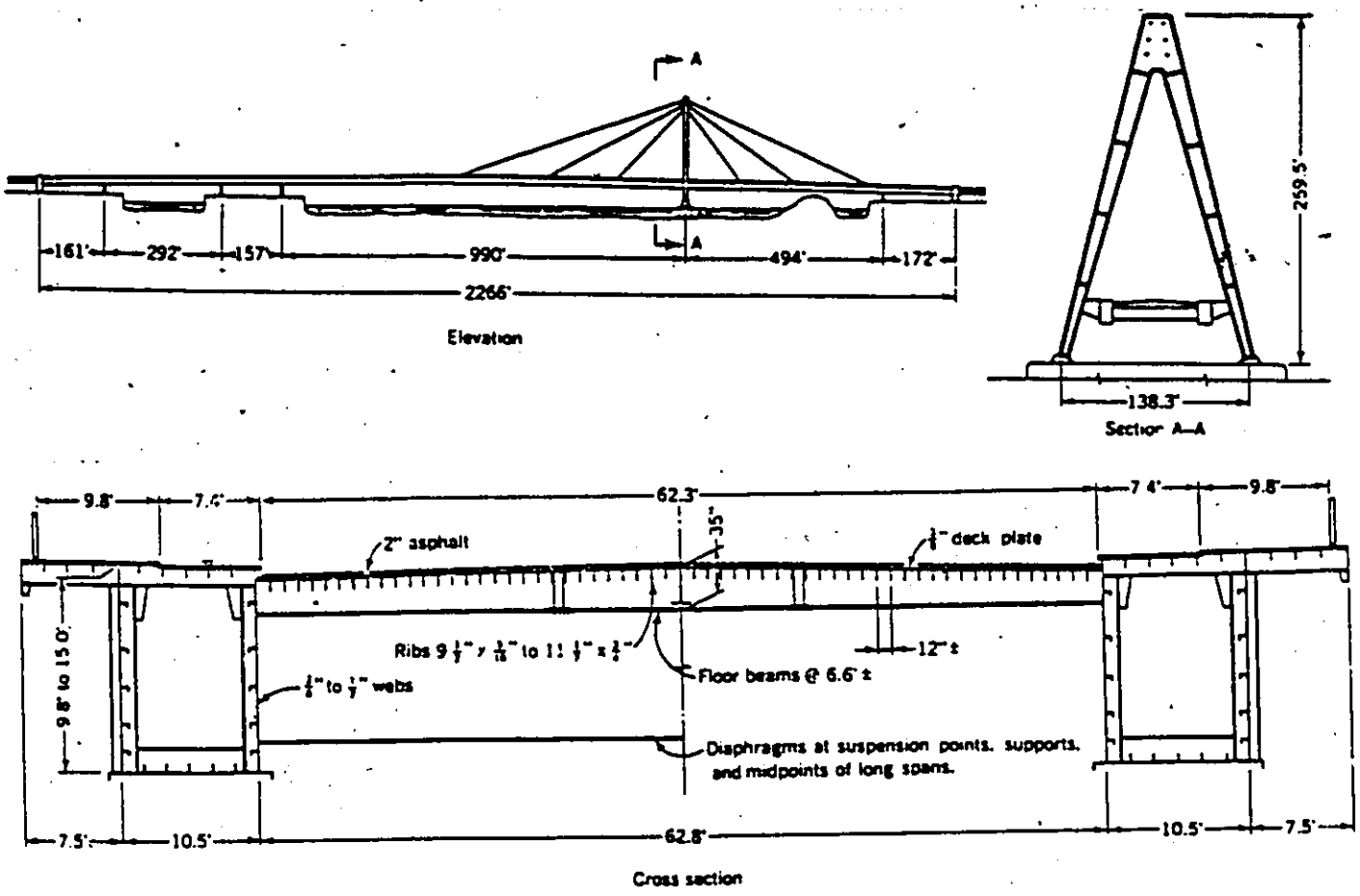

Figure 1.1.3: Severin Bridge , Cologne, West Germany,(After [1])

Spans of cable-stayed concrete girder bridges have been recently expanded to compete with their traditional steel counterparts for long span constructions. Given adequate foundation conditions, the centre span of cable-stayed bridges can be extended into the range of 500 metres where previously only an arch or a suspension bridge was feasible.

The first cable-stayed concrete structure was the Tempul aqueduct across the River Tempul, Spain, 1925 (Fig. 1.1.4). In 1957, 32 years later, a bridge over Lake Maracaibo with a 400 metres cable-stayed centre span was originally designed

in prestressed concrete, but the design was never used. Instead, a multiple span cable-stayed concrete bridge was completed with shorter spans in 1962 (Fig. 1.1.5) [15]. This particular bridge, with span lengths of 160 m, 5 at 235 m and 160 m, has six A-shape towers. Four stay cables are anchored at the tops of the towers.

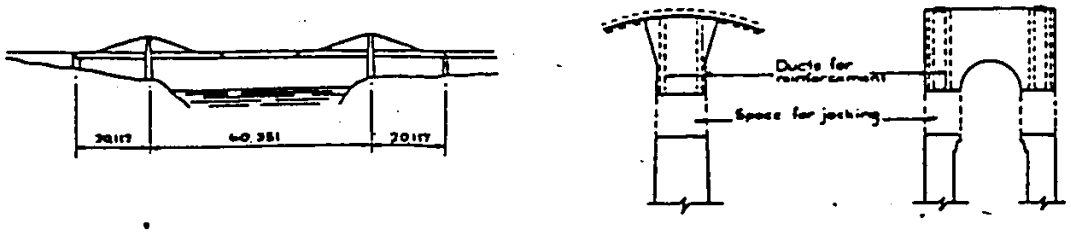

Figure 1.1.4: Tempul Aqueduct, Spain, 1925 (After [15])

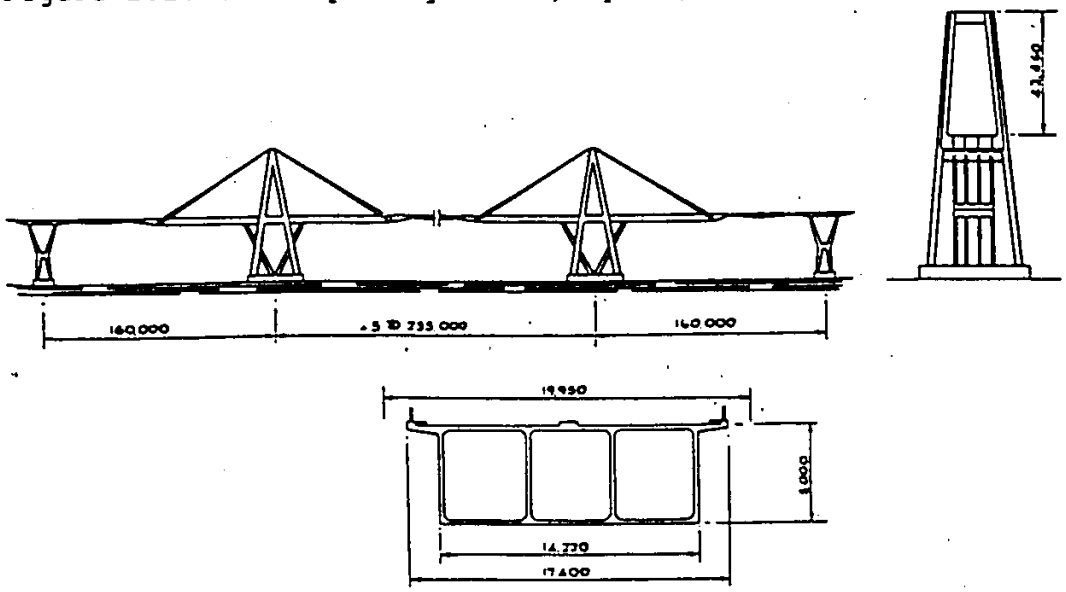

Figure 1.1.5: Lake Maracaibo Bridge, 1957 (After [15])

In modern cable-stayed bridge design, there are many types of configuration. The main characteristics of these configurations can be generally summarized as follows [15] :

A) Span arrangements

There are three basic types of span arrangement :

1. Two spans, symmetric or asymmetric (Fig. 1.1.6)
2. Three spans (Fig. 1.1.7).
3. Multiple spans (Fig. 1.1.8).

B) Cable arrangements

The cables are arranged either in two planes or in a single plane. Each of the two basic arrangements may have more than one variation as shown in Figure 1.1.9.

There are four basic configurations for the anchorage of cables (Fig. 1.1.10) :

1. The radiating or converging configuration where all the cables are spaced along the girder and are attached at a common point on the tower.
2. The harp configuration where the cables are parallel to each other and are spaced along the girder and the tower.
3. The fan configuration where the cables are spaced along the girder and the tower but are not parallel to each other.

4. The star configuration where the cables are spaced along the tower and converge at a common point on the girder.

C) Girder deck

For the design of girder bridges, I-shaped plate girders have been most frequently used. In the past 50 years, the bridge deck with single-celled or multi-celled box sections has come into fashion. For aesthetic or aerodynamic reasons, the box girders in some cases have been rounded at both edges. At the same time, the trend towards longer spans makes designers cautious about the choice of box girder configurations considering the dynamic behaviour of the bridges. Therefore, different kinds of theoretical and experimental methods have been developed to verify the reliability of the box design. Some of the box section examples are listed in Figure 1.1.11.

1.2 NECESSITY OF AERODYNAMIC CONSIDERATIONS

Response to wind is one of the most important factors in the design of long-span bridges particularly when the span of the bridge becomes so long that the possibility of structural failure becomes higher due to increasing flexibility. It is known that such bridges are susceptible to aerodynamic effects which include vortex-induced oscillation, buffeting and torsional instabilities.

The dynamic response of bridges to wind is strongly affected by the structure of wind. Natural wind is composed of mean flow and turbulence (i.e. fluctuations about the mean). Mean wind loading can be estimated using lift and drag forces and pitching moments measured in wind tunnels. However, the consideration of the insidious effects of an instantaneous localized gust is necessary; otherwise, peak loading will not be taken into account. The gusts of the wind can be described by its power spectrum (i.e. the energy distribution at different frequency of the wind). The correlations of the velocity fluctuations at different points on the bridge is also important for long span bridge design. The effect of spatial variations of wind velocity on bridge response is briefly discussed in the parametric analysis.

One of the first to consider the effect of gusts in the design of bridges was Sherlock in 1947 [9]. His conclusion was to use the mean wind velocity and the "gust factor", which would allow for the additional effect of gusts, to express the peak wind velocity. Later on, wind loads acting on a structure were found to depend upon various factors such as the features of the approaching wind flow and the geometry of the structure.

The instability criterion of galloping was first applied by Den Hartog in 1932 for iced power lines [8] . Later on,

Parkinson and Smith elaborated on the galloping characteristics in terms of dependency on the geometrical shape of structures and non-linearity of aerodynamic forces. In addition, vortex oscillation was studied by von Kàrmàn(1941), Roshko (1954), Brooks (1960), and Smith (1962) in connection with possible geometrical shapes of bridge structures [8] . The original Tacoma Narrows suspension bridge exhibited some vortex-excited bending oscillation months prior to its fatal torsional vibration. Substantial research on the collapse of the Tacoma Narrows Bridge in 1940 did not consider turbulence effects.

It has been well established that a suspension bridge is often vulnerable under strong wind. The idea of using spectral analysis of random vibration theory was pioneered by Davenport [2] . However, with limited knowledge of workable analytical methods, the wind effects can be studied in wind tunnels and compared with actual observations. Davenport and his team [6] made a full scale observations on the Bronx-Whitestone Bridge in New York City and compared the results with different wind tunnel tests. They concluded that the effect of turbulence on bridge buffeting and torsional instability was significant. Similar wind tunnel tests are now needed for cable-stayed bridges because they show the same aerodynamic problems as suspension bridges when the span lengths of the cable-stayed bridges are increased.

1.3 BRIEF DESCRIPTION OF WIND-INDUCED BEHAVIOUR OF BRIDGES IN GENERAL

As long span bridges are generally extremely flexible both in torsion and bending, they are prone to several forms of aerodynamic excitation which may result in vertical bending or torsional motion or in coupled vertical and torsional motion. Some different types of aerodynamic excitation mechanisms that affect structures are buffeting, vortex excitation, galloping, torsional instability and classical flutter. However, galloping is not a problem for bridge deck motion. The amplitude response of buffeting and vortex excitation are generally limited in magnitude, while galloping, torsional instability and flutter tend to be destructive or catastrophic. All these aerodynamic mechanisms can be found in previous research works and can be summarized as follows :

1. Buffeting

Buffeting is a turbulence induced oscillation caused by wind gusts in various modes of the bridge. The vibration has a random nature in both amplitude and frequency content. The random fluctuations of the gust, which can be depicted in statistical terms, are distributed over a wide range of frequencies. Therefore, either an experimental approach or a mathematical approach using statistical models has to be used to estimate the buffeting response of a given

system. One of the simplified statistical approaches is referred in Appendix<B>.

2. Vortex-induced oscillation

When the bluff cross section of the bridge deck is exposed to an air flow, a double row of air vortices is often formed in the wake of the body.This is referred to as a Kàrmàn vortex street. The vortex street behind a circular cylinder is shown in Figure 1.3.1. The vortices form as a result of separation of flow at the top and bottom of the bridge deck. These vortices produce oscillatory forces on the body transverse to the flow. The frequency of these vortices can be given as follows :

$$f = S \times V / D$$

in which f = frequency of vortex formation
S = Strouhal number
D = linear dimension of the body projected on a plane normal to the mean flow velocity
V = mean speed of oncoming flow.

Figure 1.3.1: von Kàrmàn vortex street

The Strouhal number depends on the structural shape and Reynolds number. For bluff bodies with sharp corners, S is usually constant for Re > 10^3 and yet with curved boundaries, S is a function of Re.

When a bridge structure is at rest, the strouhal number of the bridge deck can be assumed constant. A straight line, which shows the frequency of the vortices is proportional to the wind speed, can be drawn as shown in Figure 1.3.2 . When the frequency of the vortices is close to the natural frequency of the structure, the vortices are important source of excitation of motion of the structure. Once the motion starts, the vortices shed from the oscillating body may be "locked-in" to the motion of the bridge itself. In this circumstance, the rhythm of vortex discharge ceases to conform exactly to the strouhal rule and becomes instead the structure rhythm, i.e., the pattern of alternating vortices begins to be

governed by the motion of the body rather than the original vortex shedding. At this stage, the vortex-induced forces on a structure are coupled with the fluid flow pattern and the dynamic behaviour of the overall system will become "self-controlled". There is usually a narrow range of wind speed (the "locked-in" region as shown in Figure 1.3.2), above and below which loss of structural rhythmic control of vortex shedding occurs. This oscillation is termed vortex-induced oscillation.

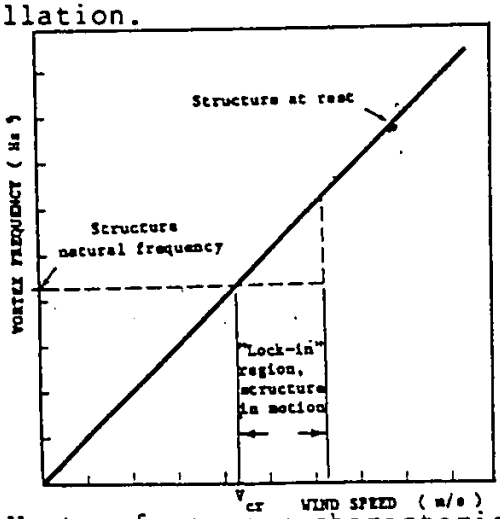

Figure 1.3.2: Vortex frequency characteristics with and without motion

The presence of turbulence in the air stream can break up the mechanism of vortex shedding.

The vortex excitation is generally not catastrophic to the structure but fatigue damage may be encountered.

3. Galloping

Galloping is a single-degree of freedom self-excited oscillation. When a slender bluff structure oscillates transverse to the flow, there is a corresponding variation in the apparent angle of incidence(Fig. 1.3.3). Considering that the rate of displacement is relatively slow compared with the wind speed, i.e. $\dot{Z}/V << 1$, the quasi-steady approach is applicable; i.e., the aerodynamic forces on the structure are determined solely by the instantaneous relative velocity and the angle of attack of the flow to the structure. This implies that the information about aerodynamic forces can be given by wind tunnel tests on stationary model held at various angles. Because flow separation occurs on bluff bodies, the aerodynamic forces may be non-linear functions of relative angle to the flow.

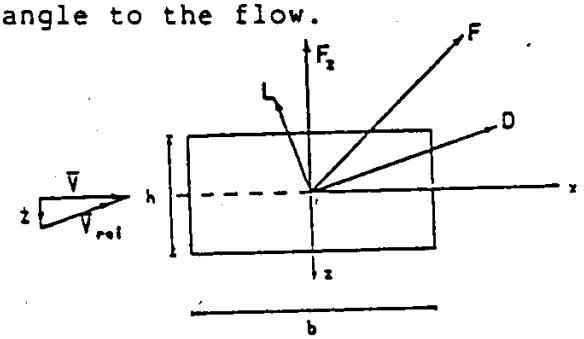

Figure 1.3.3: The mechanism of vertical motion of a bluff body

The variation of aerodynamic forces acting on the body has in general two terms: one is the "in-phase" force or the force proportional to the displacement; and another is the "out-of-phase" term or the force proportional to the displacement rate. The latter term is called aerodynamic damping, which may be positive or negative, depending on the conditions. The total damping of the bridge, which is the sum of structural damping and aerodynamic damping, is a function of velocity. If the total damping becomes negative, the amplitude response of the structure will grow. This is a self-excited oscillation.

Galloping, as was mentioned previously, is not a problem for bridge deck motion. This mechanism may occur if the bridge deck is deep compared to its chord(chord/depth > 4). Most existing long span bridges have a chord/depth ratio greater than 4.

4. Torsional Instability

The cause of the torsional instability phenomenon has not been clearly established in the literature.

It is a single-degree of freedom self-excited oscillation in the torsional mode. The existence of torsional instability is substantiated by the presence of negative total damping in the torsional mode.

5. Classical flutter

The name "flutter" is used in the field of aeronautical engineering to designate a special kind of aeroplane wing oscillation which may occur about a certain critical velocity. The wing must have at least two degrees of freedom, and the coupling between different modes due to the aerodynamic forces is essential. The vibration modes are in different phases and the motion is therefore called "flutter" and the amplitude response is divergent.

The classical treatment of an aerofoil flutter in a steady air flow can be applied to a bridge deck with a plate-like section because of their close similarity in aerodynamic characteristics to an aerofoil section. This is called the "classical flutter" theory which was developed in 1930's and then first applied to bridge structures by F. Bleich in connection with the collapse of the Tacoma Narrows.

The presence of classical flutter phenomenon with bridge decks is not easily established. The essential phase shift between torsional and flexural mode is seldom demonstrated. General characteristics are coupling of vertical and torsional modes and sudden increase of amplitude which immediately leads to the structure to destruction.

1.4 COMMENTS ON BRIDGE MODEL TESTING TECHNIQUES

A considerable amount of work has been done on the modelling techniques for prediction of the behaviour of long span bridges under wind action. Due to the limited availability of facilities, it is necessary to make a number of assumptions for the simulation. These assumptions should be made as realistically as possible without sacrificing essential information in reality. The models which have been often used in the wind tunnel tests are full models and sectional models.

The full model duplicates the entire prototype bridge to a smaller scale with proper physical scaling factors : length, mass, geometrical shape etc.. The elastic characteristics of the prototype are also simulated in dynamic studies. But the scale ratio of large structures may become very small because of the limited size of available wind tunnels. With such small ratios, it is rather difficult to construct the model with exact simulation in geometry and mechanical properties, and therefore, the reproduction of the behaviour of the prototype may not be satisfactory. Instead, rather than the testing of the entire model, the testing of two-dimensional section of a bridge has often been used. This is called a sectional model test which is popular because of relative ease in cost and handling compared to full model tests. The sectional model

represents a short, mid-span section of the deck and must be scaled in shape and mass; it is assumed to be rigid and must be supported by springs that simulate the dynamic characteristics of the structure.

Researches at the Boundary Layer Wind Tunnel Laboratory, University of Western Ontario, showed some difference in the response between sectional and full models. The paper[5] brought attention to the behaviour of sectional and full models of the Halifax Narrows Bridge, Nova Scotia, Canada. The dissimilarity of the results between two models in uniform flow caused suspicion of the technique of sectional model test. It was found that the sectional model indicated the instability characteristics at a distinctly smaller velocity value than the full model. The summary of the testing results of the Halifax Narrows Bridge is shown in Figure 1.4.1 below. The dramatic modification of onset wind speed of instability was the point focussed on. It is noteworthy because, in the past, Fraguharson & Vincent and Frazer & Scruton [5] had obtained satisfactory qualitative agreement between sectional and full models. Incidentaly, the sectional model tests have satisfactorily predicted the unstable behaviour of several full scale bridges including the Tacoma Narrows, Golden Gate and Deer Isle Bridge, at least qualitatively.

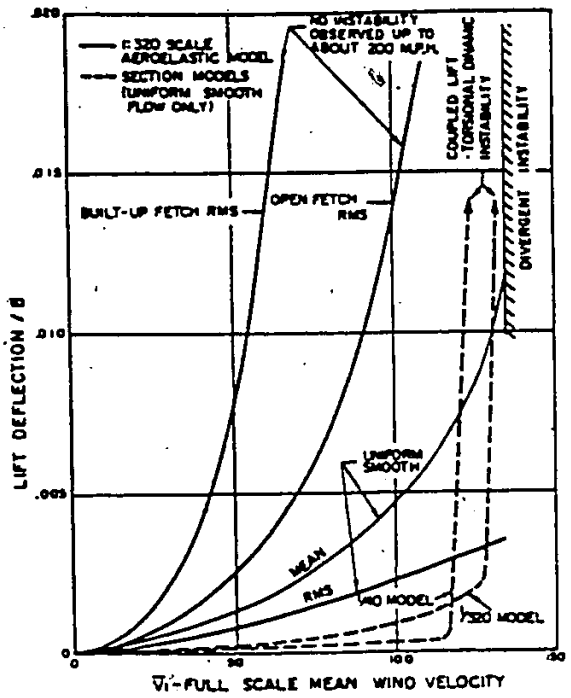

Figure 1.4.1: Summary of response of full model and sectional model (After [5])

Therefore, the fundamental question for the aerodynamic testing of long-span bridges again arises : can the section models predict the full bridge behaviour adequately? Also the conventional sectional models are seldom tested in turbulent wind because of their inherent two-dimensional characteristics. However, it is important to find out the role of turbulence in bridge aerodynamic stability studies. These difficulties in sectional model testing can be solved by performing the three-dimensional full model tests. But, as mentioned before, the sectional model test has been often used to replace the full model test. So, is there any

other testing method which could be employed to forecast the response of the long-span bridge under turbulent wind other than the full model?

Professor A.G. Davenport suggested a third alternative, the taut strip model, which has the convenience of sectional models and allows the direct measurement of the response in a three-dimensional turbulent wind. In the studies of the Bronx-Whitestone Bridge in New York City [6] and the Golden Gate Bridge in San Francisco [13] , it was found that the aeroelastic behaviour of the taut strip model in turbulent flow was found to agree well with full scale observations. An attempt to use taut strip models to observe the response of the proposed Annacis Island Bridge - Concrete version has been made in this study.

Chapter II

PREVIOUS WIND TUNNEL STUDY OF ANNACIS ISLAND BRIDGE AT NATIONAL RESEARCH COUNCIL

2.1 GENERAL DESCRIPTION OF THE ANNACIS ISLAND BRIDGE

The Annacis Island Bridge connects the Annacis Island on the Fraser River with a district of New Westminster, British Columbia, Canada (Fig. 2.1.1). A cable-stayed bridge is proposed. From Figure 2.1.2, it can be visualized that there is a long fetch of open water normal to the bridge direction. On the far side of the sketch, North-West of the bridge location, is a suburban area with vegetation. The wind flow over the bridge site presumably has low turbulence intensity; however, the wind flow may have higher turbulence intensity when the wind comes from the North-West quadrant. In general, the bridge site and its environment are topographically flat.

There are two different design versions for the bridge; one is a concrete design and the other is steel. The general sketch of the concrete design is shown in Figure 2.1.2. The total length of the bridge is 880 metres with a centre span of 440 metres. It is a three-span cable-stayed structure in which the cables are arranged in vertical double planes. A

large number of stay cables in harp configuration allow the distribution of the forces to the girder so that a shallow box girder can be used. The depth to width ratio of the concrete box is approximately 1 to 20. The shallow box girder design is favoured because the aerodynamic drag force acting on it is small. The advantage of adopting a large number of stay cables is to reduce the magnitude of maximum bending moment in the bridge girder. Consequently, the bending stiffness of the deck can be reduced, which is consistent with the previous point of using a shallow girder. It is worthwhile to pay special attention to the Annacis Island Bridge as an example to investigate the wind induced response of cable-stayed bridges because of these two characteristics.

2.2 STUDY AT NATIONAL RESEARCH COUNCIL OF CANADA ON 1/60-SCALE SECTIONAL MODEL

The consulting firm, Annacis Bridge Consultants, which proposed the concrete version of the Annacis Island Bridge, wanted to examine the wind-induced behaviour of the proposed bridge. The wind tunnel test was conducted at the National Aeronautical Establishment(NAE), National Research Council of Canada(NRC).

2.2.1 Description of the models

Three different shapes of sectional model were tested (Fig. 2.2.1.1). Each sectional model, approximately 2.1 metres long, had a length scale ratio of 1/60 to the prototype. The models were built effectively rigid and each of them contained different aerodynamically significant details of the box girder deck without cables. The aerodynamic forces acting on the cables and towers are assumed to be negligible. Thus, they were not modelled geometrically, however, their mass was taken into account by considering the generalized mass of the whole bridge for the given natural frequencies (Fig. 2.2.1.2). The summary of the scaling parameters for the study and the dynamic properties of the models are presented in Tables 2.2.1.1 and 2.2.1.2 respectively. The detail description of the models can be found in Ref 14.

2.2.2 Experimental procedures

The model was spring-mounted in the NAE vertical wind tunnel which has a modified square cross section of 2.1m x 2.1m(Fig. 2.2.2.1). By adjusting the movable weights and the spring spacing, the model moment of inertia and the frequency ratio FA/FZ (torsional frequency, FA, divided by bending frequency, FZ) could be altered into the desired values. Two of the supporting springs were attached to a

strain gauged elastic beam. The sum and difference readings of these two outputs can be calibrated to give vertical and torsional model responses respectively. Aerodynamic damping instead of amplitude response was measured in the experiment because the relationship between aerodynamic damping and reduced velocity shows the oscillatory trend of the bridge deck which may not be shown in amplitude response.

The signal received from the free vibration of the model in still air in either vertical or torsional mode was traced by the chart recorder. From the tracings, the corresponding natural frequency and structural damping of the vertical or torsional mode were calculated. When the model was excited manually at a certain wind speed, again in either vertical or torsional mode, the damping calculated from the tracing was the total damping, i.e. the summation of structural and aerodymanic damping. The negative value of the total damping indicates the aerodynamic instability. The trend of the aerodynamic damping over a range of wind speed can foretell the possibility of vortex-induced excitation, flutter and other forms of instability.

All tests were carried out in smooth flow only. The detailed of the experimental results are discussed in Ref 14.] Typical results of the option II sectional model are presented in Figures 2.2.2.2 , 2.2.2.3 and 2.2.2.4.

2.2.3 Results of 1/60-scale sectional model test

The typical results of the option II sectional model are presented in Figures 2.2.2.2 to 2.2.2.4. In this series, the turbulence induced buffeting response was not investigated. From the variation of response frequency and aerodynamic damping with respect to wind speed, the types of excitation mechanisms and aerodynamic instability of the structure were examined.

For the option II sectional model, a range of wind speed in which the aerodynamic damping decreases in both vertical and torsional mode was found (Fig. 2.2.2.2). In the vertical mode, the aerodynamic damping stayed positive and eventually increased at a wind speed of about 8.5 m/s (full scale). But in the torsional mode, when the mean angle of attack was ± 5 degrees, the negative aerodynamic damping was observed for the wind speed range of 45 to 70 m/s (full scale). The peak negative damping was found to be -0.4% of critical. The expected structural damping of the prototype was in the order of one percent. The bridge would be stable at this wind speed range and the bridge seems to be free from vortex-induced oscillations.

Beyond the speed range, in which vortex-excitation may occur, the aerodynamic damping increases with the wind speed (Fig 2.2.2.3). At extremely high wind speed, catastrophic aerodynamic instability was observed. In addition to zero

angle of attack, the model was also tested with four different angles relative to the flow; i.e., ± 5 and ± 7 degrees. However, according to the site investigation, flows with such large angles are unlikely to occur. Nevertheless, even considering such a large mean angle of attack, the torsional instability was the only instability mechanism observed with the option II model within the realistic range of wind speed. The critical wind speed or the onset of torsional instability was found to be greater than 140 m/s for the angle of + 7 degrees.

Chapter III

EXPERIMENTAL INVESTIGATION AND RESULTS

3.1 TAUT STRIP MODEL

The concept of the taut strip model can be interpreted as a semi-experimental, or half-theoretical aeroelastic model. For this particular experiment, the vibration of the centre span of the Annacis Island Bridge is assumed to be in its first symmetrical mode shape only. The model is constructed in a manner to achieve this assumption. However, in reality, the vibration of a long-span bridge is composed of more complicated mode shapes. Therefore, the response to turbulence of a taut strip model does not actually simulate the response of the prototype directly. However the model can be used as an input to the statistical theory of buffeting by turbulence [4] considering the test results together with the actual mode shapes of the structure. From this theory, the full-scale response is predicted.

The length scale ratio of 1:500 was used for the construction of the taut strip model of the Annacis Island Bridge. This ratio was chosen to match the scale of turbulence which the wind tunnel was able to produce. The model contained all the aerodynamically significant

geometrical details of the bridge deck, whose mass distribution and mass moment of inertia were also correctly scaled. The cross-section of the model is shown in Figure 3.1.1. Although the cables and towers are not modelled geometrically, their mass is taken into account by considering the generalized mass of the whole bridge. The model is suspended on a pair of parallel, taut-piano wires running at the level of the centre of rotation. The deck thus vibrates in the same way as the taut strings, primarily in a fundamental half-sine wave mode shape. The model consists of six small modules so that the deck section does not contribute to the stiffness or elastic characteristics. By adjusting the wire tension and wire spacing, the desired frequencies in vertical and torsional motion can be obtained. The length of the model corresponds to the main span of the bridge and runs the full width of the NAE wind tunnel. In addition to the three-dimensional(3-D) model test, a two-dimensional(2-D) model test was also carried out by taking a short length of the taut-strip model between internal partitions in the wind tunnel section. Only between these partitions was the model exposed to the wind. External wires outside the partitions were covered by aerofoil shaped sleeves. The layout of the two different set-ups are shown in Figure 3.1.2 and 3.1.3.

3.2 GENERAL DESCRIPTION OF TURBULENCE

It is difficult to give a perfect description of the structure of the wind mathematically but it can be said that wind is composed of turbulence as well as the mean flow.

The air flow inside the wind tunnel is generally irregular in space and time. Because of this irregularity, it is difficult to describe the motion exactly in all details as a simple function of space and time coordinates and it becomes necessary to describe it by its statistical properties. The values of various quantities, such as mean velocity, velocity fluctations and their spectra, can be detected by the hot-film anemometer, and these three quantities give the most important information relevant to structural design. However ,it should be kept in mind that the laboratory simulation of random air flow can only be judged adequate by comparing it to the actual site measurements.

Often, the turbulence is modelled in two categories. In the case where the mean velocity has a gradient, turbulence is non-isotropic since the mean velocity gradient is associated with the occurence of a shear stress. The expression " shear-flow turbulence" is often used to designate this class of flow condition. When the turbulence has quantitatively the same structure in any direction of the flow field, the turbulence is said to be homogeneous.

There is no average shear stress, and consequently, no velocity gradient is assumed for this case.

As the wind passes over the surface of the earth, because of the existance of the solid boundary and various roughnesses on it, the atmospheric flow becomes a shear flow; i.e., a boundary layer flow. In the present experiment, the bridge model was tested under both the homogeneous turbulence flow conditions and the boundary layer flow conditions. The purpose of testing in these two different types of turbulence is to investigate the sensitivity of bridge responses to the difference in turbulence structure.

The information about the flow condition at the site of the proposed Annacis Island Bridge is not known. The bridge site is in the open terrain over the Frazer River and the deck height is approximately 50 m above water surface. Considering these conditions the actual shear flow turbulence may be expected as a typical flow over open field with a power law exponent of 0.1 to 0.2 and turbulence intensity of up to 10% of the local mean speed.

3.2.1 Wind tunnel and flow conditions

The experiments were performed in a low speed wind tunnel with a test section 3 ft (91.4 cm) wide by 3 ft (91.4 cm) high and approximately 8 ft (243.8 cm) long. A

very uniform basic flow with a turbulence intensity less than 0.5 percent is produced to give a nearly smooth flow field, free of turbulence. Different square-mesh grids of rectanglar-section bars were used to produce isotropic homogeneous turbulence fields. The coarse grid has M = 7-7/8 inches (20.0 cm), b = 2 inches (5.1 cm); and the fine grid has M = 4 inches (10.2 cm), b = 1 inch (2.54 cm) (Fig. 3.2.1.1), where M = mesh size and b = bar size. Three types of spires and roughness set-ups were used to produce various boundary layer flows. The height of the spires was 20 inches (50.8 cm) and the base width was 3 inches (7.6 cm). The three types of set-up are as follows :

1. Bare tunnel and three spires only;
2. Three spires together with artificial roughness consisting of two different sizes of blocks; 0.79 in. x 0.79 in. x 0.79 in. (2 cm. x 2 cm. x 2cm.) and 0.79 in. x 0.79 in. x 1.18 in. (2 cm. x 2 cm. x 3 cm.);
3. Three spires with steel angles placed on the tunnel floor. The height of the angles was 1 inch (2.54 cm) and the thickness was 1/8 inch (0.32 cm).

The arrangements of spires and surface roughness elements are shown in Figure 3.2,1,2; and a sketch of surface roughness elements is shown in Figure 3.2.1.3.

3.2.2 Measurement of wind tunnel characteristics

The objective of this study was to observe the dynamic response of the proposed Annacis Island Bridge under different types of flow conditions. There were six kinds of wind flow conditions generated in the low speed wind tunnel. The flow measurements were carried out for two conditions: with partitions and without partitions (Fig. 3.1.2 and 3.1.3). The set-up of instruments is shown in Figure 3.2.2.1. The results are listed in Appendix<E>. For six various types of flow, vertical profiles of mean velocity and turbulence intensity in longitudinal & vertical directions were measured at the centre of the bridge deck location and the results are presented in Figures 3.2.2.2 and 3.2.2.3. The turbulence intensity is defined as the ratio of root-mean-square (RMS) value of the velocity fluctuation components to the longitudinal mean wind speed. In addition to the above measurement, the horizontal profiles across the wind tunnel with three spires arranged at the entrance of the tunnel were also measured. The flow at two different locations was examined : 45 inches (114.3 cm) and 90 inches (228.6 cm) from the spires. The results are presented in Figure 3.2.2.3.

For the boundary layer flow, the power law profile can be made to fit the data of mean wind speed by adjusting the values of two parameters Z_g & α in the equation :

$$V/V_g = (Z/Z_g)^{\alpha} \qquad (3.2.2.1)$$

Vg = mean velocity at top of boundary layer;

Zg = depth of boundary layer;

Z = height from ground surface;

α = power law index.

The power spectrum describes how the kinetic energy of turbulence is distributed with frequency and it can be obtained by analysing the signal received from the hot-film anemometer with the Fourier analyser. From each spectrum, the scale of turbulence can be calculated (Appendix <C>).

The results of flow measurement are summarized and presented in Table 3.2.2.1.

3.3 GENERAL COMMENT ON THE GENERATED WIND TUNNEL FLOWS - IN PARTICULAR BOUNDARY LAYER FLOWS

3.3.1 Mean speed profiles

1. Vertical profiles

The vertical profiles of mean wind speed have essential meaning only in simulated boundary layer flows generated as described in section 3.2.1 . By applying the power law concept (Eq.3.2.2.1), the power law index, α , and the depth of boundary layer, Zg, can be estimated to fit the flow measurements. The results are presented in Table 3.2.2.1.

Four different profiles were produced for the present study. The intention of having four different profiles is to examine the behaviour of the bridge deck in different types of boundary layer flows. Even in the smooth flow, a very shallow boundary layer flow was observed in the immediate vicinity of the floor but the flow field in which the bridge model is placed is almost free of turbulence.

2. Horizontal profiles

The horizontal profile of mean wind speed was measured for the boundary layer flow produced by three spires only. It is desirable to have the mean wind speed at the bridge deck location constant across the tunnel. The mean wind speed variation was found to be less than ±5% (Fig. 3.2.2.3). In addition to the measurement at bridge deck location, the measurement mid-way between the spires and the bridge model was also carried out. The results are shown in the same figure (Fig. 3.2.2.3). The horizontal distribution of mean wind speed was found to be more uniform at the downstream site.

3.3.2 Turbulence intensity

The turbulence intensity in the vertical and horizontal directions has been described in section 3.2.2 already. The

vertical component of turbulence is the major source of energy input to cause buffeting response of the bridge models. Generally speaking, the turbulence intensity in various types of 2-D flow conditions is close to the results for the 3-D case. The vertical profiles of turbulence intensity of u and w components are presented (Figs. 3.2.2.2, 3.2.2.3). The shape of the profile depends upon the type of flows.

3.3.3 Velocity spectrum

The high susceptibility of suspension bridges to gusts is due to their great flexibility and to the fact that their resonant frequencies fall in the range of broad energy input apparent in the horizontal and vertical gust spectra.

The nature of terrain exerts a strong controlling influence both on magnitude of the extreme winds attainable and also on the intensity of turbulence. This is the explanation why different roughnesses set-ups on the tunnel floor are employed in this experiment.

The agreement of the velocity spectrum with the von Kàrmàn type spectrum seems to be most satisfactory with regard to the general shape of the spectrum (Appendix <C>).

3.4 RESPONSE MEASUREMENT

Generally speaking, a bridge deck exhibits three types of response : torsional rotation about the bridge axis, vertical bending displacement and horizontal displacement along the wind direction. However, for a streamlined bridge deck section, the horizontal displacement is less important than the other two responses. Therefore, the horizontal displacement is not considered here.

In order to observe the aerodynamic instability as well as the vortex-induced excitation, the tension of the wires was adjusted to produce two different sets of frequency values. It was done for both 3-D and 2-D models. The natural frequency and structural damping are calculated from the traces of free vibration (Appendix<A>). The scaling factors of the 2-D and 3-D models are listed in Table 3.4.1 while the mechanical properties are presented in Table 3.4.2.

The set-up of instruments to measure the vertical and angular displacements is shown in Figures 3.4.1 and 3.4.2 . The procedures to find the calibration values , which are required to convert the two measured voltages into the corresponding vertical and angular displacements, are illustrated in Appendix<A>. The buffeting response data of 2-D and 3-D models are listed in Appendix<D>. They can be summarized as shown in Figure 3.4.3 to 3.4.6.

Chapter IV

DISCUSSION OF THE RESULTS

4.1 OBSERVED BEHAVIOUR OF THE SHALLOW BOX BRIDGE DECK

In section 1.3, five different types of aerodynamic excitation mechanisms were introduced. Because the Annacis Island Bridge has an almost streamlined bridge deck, the aerodynamic instability of classical flutter may be expected. However, the bridge should be examined against all potential instability mechanisms. With limited development of analytical approaches, at the present time, the most reliable way to predict the aerodynamic behaviour of the bridge seems to be the wind tunnel test. Sectional model and taut strip model wind tunnel tests have been carried out at the NRC to investigate the aerodynamic stability of the Annacis Island Bridge. The bridge was found to be very stable in the low wind speed range, but becomes aerodynamically unstable at extremely high wind speed as the sum of structural and aerodynamic damping becomes negative.

4.1.1 1/500-scale models

In addition to the previously described 1/60-scale sectional model test (section 2.2), three dimensional and two dimensional models at 1/500-scale were tested. The present thesis is based on this series of test. The three dimensional model used in this experiment is based on the concept of the so-called taut strip model. Tests were carried out in uniform flow as well as in various types of turbulent flow.

Because of the small velocity scale ratio, which can be referred to Table 3.4.1, it was rather impractical to cover the low wind speed range in which the vortex-induced excitation may be expected to occur. For example, considering a case where the flexural and torsional frequencies were tuned to 6.25 Hz and 17.5 Hz respectively, the corresponding velocity scale ratios were 0.05 and 0.10 (Table 3.4.1). From the 1/60-scale sectional model tests, it is indicated that the vortex-induced excitation may be observed at the wind speed range of 8.5 m/s to 10 m/s (full scale) for vertical and torsional modes, which corresponds to 0.4 m/s to 1.0 m/s in the 1:500 model test. This was approximately 20 to 50 percent of the lowest available wind speed of the tunnel. In order to observe whether the vortex-induced excitation existed or not, a higher frequency setting was adjusted as was described in Section 3.4. When

the frequency is higher, the velocity scale ratio is higher. Nevertheless, vortex-induced excitation was not observed.

The aerodynamic instability was observed in smooth flow for both the 3-D and 2-D tests. The vertical and torsional response spectra are plotted in Figure 4.1.1.1 through Fourier Analysis. These spectra are almost identical and show a peak response at the same frequency which is between the two natural frequencies of the model; i.e., there is a distinct coupling between the vertical and torsional excitations which is one of the characteristics of the classical flutter. However, the essential phase shift between vibration modes of classical flutter was not investigated.

Buffeting response was also observed and it is discussed in the following section together with the effects of various types of turbulence.

4.2 EFFECTS OF VARIOUS TYPES OF TURBULENCE (1/500-SCALE MODELS)

One of the objectives of this research work was to test the taut strip model in various types of turbulent flows to observe their effects on the bridge response. The principal reason for considering the effects of turbulence is because the natural wind is turbulent and its characteristics are more or less known. Although the two dimensional section

model is not suitable for testing in inherently three dimensional turbulent flow, by having a relatively long section of the model compared with the typical linear scale of turbulence, the testing is considered to make some sense, particularly in comparison with the 3-D taut strip model test.

The response amplitude of the model is expected to be affected by the intensity of turbulence contained in the flow and the length scale of turbulence (Appendix <C>). The effects of various types of turbulence were examined in 3-D and 2-D cases individually.

4.2.1 3-D model test

The experimental results discussed in this section are shown in Figure 3.4.3 and 3.4.4. As is mentioned in section 4.1.1, the vortex-induced oscillation was not expected in this test and therefore it is impossible to discuss the role of turbulence in this type of behaviour. In order to observe the effect of turbulence on buffeting response, the experimental results are rearranged and presented in Figures 4.2.1.1 and 4.2.1.2. It is observed that the bridge deck behaviour in 3-D testing is not very sensitive to the scale of turbulence. For example, the response amplitudes of the model at "coarse grid" and "spires and angles" flow conditions are close each other. These two different kinds

of flow conditions have different integral length scale of turbulence but similar turbulence intensity magnitude. The integral scale of turbulence in "spires & angles" flow is 1.5 times of "coarse grid" flow. The responses are, as they are shown in Figs. 4.2.1.1 and 4.2.1.2, very close each other. This seems to imply that the model response is related to the total energy input contained in the flow; i.e., the turbulence intensity but not much affected by the scale of turbulence, at least for this particular bridge section. The results of the testing with the spires and the surface roughness blocks were somewhat different. The response of this particular set-up is found to be smaller in spite of relatively higher turbulence intensity than the other flow configurations. The reason of this phenomenon is not immediately clear.

Within the maximum wind speed range that the NAE wind tunnel can reach, the onset of aerodynamic instability was not observed with high turbulence intensity. At reduced velocity, $V/(B \times FA) = 9.2$, there is a tendency towards instability with the turbulence given by the fine grid. However, the instability was not fully established within the tested wind speed range. There seems to be a non-linearity of aerodynamic forces in this case, which limits the response amplitude at various speed levels.

There is a possibility that the aerodynamic instability may not occur or, at least, the onset speed is pushed up to unrealistically high levels, because of the turbulence. Buffeting response at lower speeds, however, would probably become excessively high and eventually would reach the harmful amplitude levels for the structure.

4.2.2 2-D model test

The experimental results discussed here are shown in Figures 3.4.5, 3.4.6, 4.2.2.1 and 4.2.2.2. In general, the trend of the 2-D model responses to turbulence is similar to that of the 3-D model; i.e., increasing turbulence intensity increases the response amplitude. The complete comparison with the 3-D model test is in the next section.

4.3 COMPARISON OF 2-D AND 3-D TESTING RESULTS (1/500-SCALE MODEL)

The figures relevant to the discussion of this section are presented in Figure 4.3.1. It is difficult to achieve identical frequency and damping in the 2-D model as in the 3-D model because of the difference in the mechanical scheme. Nevertheless, comparison of the results between the 3-D and the 2-D model tests gives an insight to the validity of the testing of the 2-D model in three-dimensional turbulent flow.

For this comparison, it is necessary to consider the difference in frequencies and dampings between the two cases and proper adjustment needs to be done.

The dynamic charateristics of two model schemes are given as follows :

	FA/FZ	ζ_η	ζ_ϕ
3-D	2.8	2.84%	1.31%
2-D	1.8	0.92%	0.38%

The results of the 2-D model tests are adjusted and the adjustment is based on the results of parametric analysis. This particular analytical approach employs the combination of linear equations in vertical bending and torsion (Eq. B.2.1). The aerodynamic forces (Eq. B.3.1) acting on a vibrating model consist of unsteady self-excited forces and the random buffeting forces. The spectral analysis of random vibration theory is applied and the illustration of it is shown in Appendix<B>.

From a parametric analysis (see Appendix<B>, Fig. B.5.5), the effect of damping on buffeting response can be estimated. The buffeting response, both in bending and torsion, decreases when structural damping is increased. The parametric analysis suggests as follows :

1. Bending response :

In the reduced wind speed range of V/(B X FZ) = 5 to 10, the reduction of response amplitude is approximately 10% when structural damping is increased from 1% to 3%.

2. Torsional response :

In the reduced wind speed range of V/(B X FA) = 1 to 6, the reduction of response amplitude is approximately 14% when structural damping is increased from 0.5% to 1.5%.

The effect of frequency ratio is expected to be very small as the correlation between vertical and torsional response is negligibly small in buffeting response. This effect will be of course more pronounced as soon as instability, coupled flutter for this case, starts.

According to the parametric analysis, the adjustment of the 2-D response is shown in the shaded region of the comparison figures. The agreement of response amplitudes between the 3-D and the 2-D model tests is quite satisfactory in homogenous turbulence and smooth flow conditions. For the other three types of boundary layer flows, the situation becomes more complicated. The 2-D response is found to be smaller than the 3-D response in "spires and angles" flow condition. However, the above observation is reversed for the other two boundary layer flows.

The structure of turbulence seems to have effect on the agreement between the 2-D and 3-D response. The difference of the 3-D response and 2-D response may be caused by the different sensitivity of these two models to the structure of turbulence. For example, the turbulence intensities generated by the "coarse grid" and the "spires and angles" are close to each other. However, the response in the "coarse grid" flow shows good agreement between 2-D and 3-D model tests but the agreement is less satisfactory in "spires and angles" flow.

From above discussion, it seems that three-dimensional bridge model testing is required if the 3-D buffeting response of the bridge in boundary layer flow is required.

4.4 COMPARISON OF 1/500-SCALE TEST RESULTS TO 1/60-SCALE TEST RESULTS

Since the 1/60-scale was only tested in the smooth flow condition, a comparison of buffeting response is not possible. However, it is interesting to know the effect of model scale ratio on the onset wind speed for instability.

The 1/60-scale sectional model was tested with a frequency ratio of 1.25, which is different from the frequency ratios used in the 1/500-scale model test. Reference 11 suggests that the critical wind speed for the onset of coupled flutter is related to the frequency ratio as follows :

$$(V/(B \times FA))_{cr} \propto \sqrt{1 - (FZ/FA)^2} \qquad (4.4.1)$$

From Figure 2.2.2.3, the instability wind speed, $(V/(B \times FA))_{cr}$, of the option II sectional model is > 5.7 assuming extremely small structural damping. From this number, by making use of the above relationship(4.4.1) the critical wind speed can be suggested for the frequency ratio as follows :

1. FA/FZ = 2.8 : $(V/(B \times FA))_{Cr} = 8.9$

2. FA/FZ = 1.8 : $(V/(B \times FA))_{cr} = 7.9$

The experimental results of 1/500-scale models (Figure 4.3.1) :

1. 1/500-scale 3-D model, FA/FZ = 2.8, $\zeta_\phi = 1.3\%$

   $(V/(B \times FA))_{cr} = 9$

2. 1/500-scale 2-D model, FA/FZ = 1.8, $\zeta_\phi = 0.4\%$

   $(V/(B \times FA))_{cr} = 8.6$

In spite of the existence of structural damping in 1/500-scale models, the instability wind speed of the 1/500-scale 3-D model agrees with the instability wind speed of the 1/60-scale 2-D model. But for the 1/500-scale 2-D model, the instability wind speed is higher than the instability wind speed of the 1/60-scale 2-D model.

Chapter V

CONCLUDING REMARKS

Turbulence appears to have effects on the behaviour of the bridge deck system of the Proposed Annacis Island Bridge. The following results can be extracted from the present series of experiments :

1. Turbulence raises the critical wind speed for the aerodynamic instability of the bridge deck. The delay of onset speed of the instability with the turbulence given by the fine grid is an example.
2. Turbulence produces significant random movements of the bridge deck both in vertical and torsional mode. The amplitude of the vibration increases proportionally to turbulence intensity.
3. The response of the proposed Annacis Island Bridge section seems to be insensitive to the variation of the integral length scale of turbulence. The comparison of response between "coarse grid" and "spires and angles" flow conditions is an example.

The comparison between taut strip model test results with sectional model test results showed the following features :

1. The critical reduced velocity, $(V/(B \times FA))_{cr}$, of 1/60-scale model test was confirmed.
2. The buffeting response of the 1/500-scale model both in 2-D and in 3-D showed satisfactory agreement.

As far as the buffeting response is concerned, the taut strip model test may be a good alternative testing method in terms of ease in handling, cost and model making compared with a full model test having the advantage of three-dimensionality that is missing with the traditional section model test.

The above results were from the testing of a particular bridge section, Annacis Island Bridge. The results are just as would be expected for a flat plate structure. This is not very surprising considering how shallow the box girder of the bridge is. Consequently, the results can be easily extended to any bridge with an "extremely" shallow box girder, which is expected to become a trend for the long span cable-stayed bridges.

One more final remark should be added about model testing. The model test results can only be justified by full scale measurements. The comparison of full scale measurements to taut strip model results has been done for

some limited cases [6,13] before. As it is mentioned in section 2.3, the aeroelastic behaviour of the taut strip model agreed reasonably well with the full scale observation for these cases. In addition to the investigation of the wind induced response of shallow box bridge decks, there may be an opportunity to compare the taut strip model results with the full scale measurements of the Annacis Island bridge if it is completed in its concrete version. This comparison may provide valuable information for future research.

REFERENCES

1) American Institute of steel Construction, Inc., "Design manual for orthotropic steel plate deck bridges", AISC, 1963.

2) Davenport A.G., "Buffeting of a suspension bridge by storm winds", Proceeding of ASCE, ST3, 1962, page 233-268.

3) Davenport A.G., "The application of statistical concepts to wind loading of structures", Proc. I.C.E. Vol.19 (1961)

4) Davenport A.G., "The use of taut strip models in the prediction of the response of long span bridges to turbulent wind", Symposium on Flow-Induced Structural Vibrations, Karlsruhe, Germany,1972.

5) Davenport A.G., N. Isyumov and T. Miyata, "The experimental determination of response of suspension bridges to turbulent wind", Proceedings, Third International Conference on Wind effects on buildings and structures, Tokyo, Sept. 1971, Saikon Co. Ltd.

6) Davenport, A.G., N. Isyumov, H. Rothman and H. Tanaka, "Wind induced response of suspension bridges - Wind tunnel and full scale observation", Proc., Fourth International Conference on Wind Engineering, Fort Collins, Colorado, 1979.

7) Fung, Y.C., "Introduction to Aeroelasticity", Dover Publication, 1969.

8) Parkinson G.V., "Wind Induced Instability of Structures", Philosophical Transaction of Royal Society of London, Series A, Volume 269, 1971.

9) Sherlock R.h., "Gust factors for the design of buildings", Int. Assn. for Bridge and Structural Engineering, Volume 8, 1947, page 204-236.

10) Tanaka, H., "Study on response of Suspension Bridge to Fluctuating Wind", Proceedings,Third International Conference on Wind Effects on Buildings and Structures, Tokyo, Sept. 1971,Saikon Ltd. .

11) Tanaka, H., "Vibration of bluff sectional structures under wind action", Proceedings,Third International Conference on Wind Effects on Buildings and Structures, Tokyo, Sept. 1971,Saikon Ltd. .

12) Tanaka, H. and Davenport, A.G., "Response of taut strip model in turbulent wind", Proc. ASCE (108) EMI, 1982.

13) Tanaka, H. and Davenport, A.G., "Wind-induced response of Golden-Gate Bridge" Proc. ASCE (109) EMI, pp. 296-312, 1983.

14) Tanaka, H., Wardlaw R.L., "A wind tunnel investigation of the Proposed Annacis Island Bridge Concrete alternative, New Westminster, B.C.", Laboratory Technical Report LTR-LA-263, NAE/NRC, 1982.

15) The task Comittee on Cable-Suspension Structures "Commentory on the Tentative Recommendations for Cable-Stayed Bridge Structures", Jounal of Structural division, Proce. ASCE, May 1977, pg. 941-959.

16) Walter Podolny, Jr., "Cable-Stayed Vs. Classical Suspension Bridge", ASCE National Structural Engineering Convention, April 14-18, 1975.

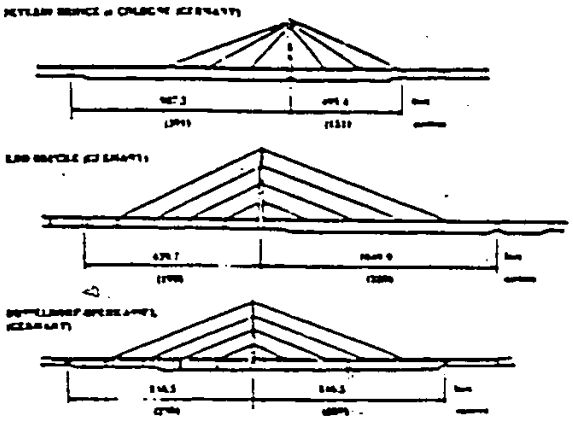

Figure 1.1.6: Example of Two-Span Cable-Stayed Structures (After [15])

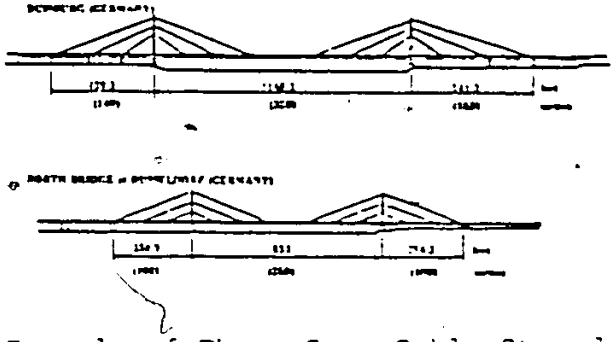

Figure 1.1.7: Example of Three-Span Cable-Stayed Structures (After [15])

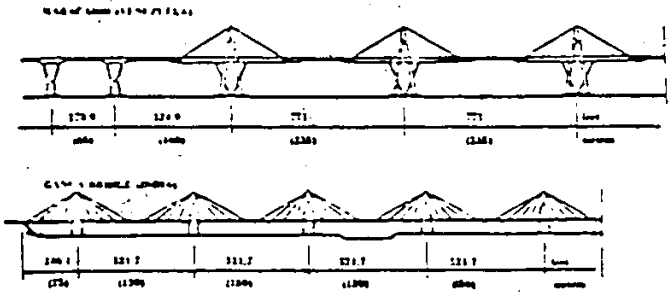

Figure 1.1.8: Example of Multi-Span Cable-Stayed Structures (After [15])

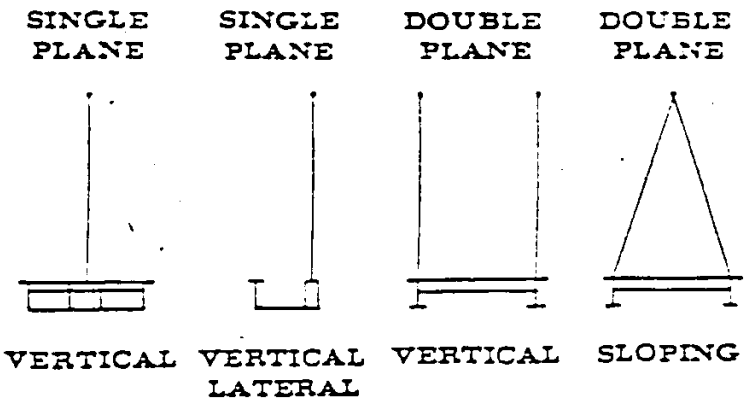

Figure 1.1.9: Transverse Cable Arrangement (After [15])

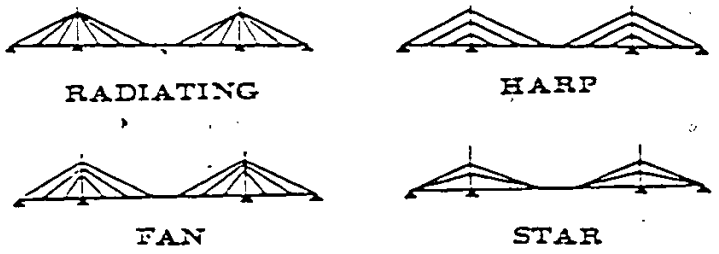

Figure 1.1.10: Longitudinal Cable configuration (After [15[)

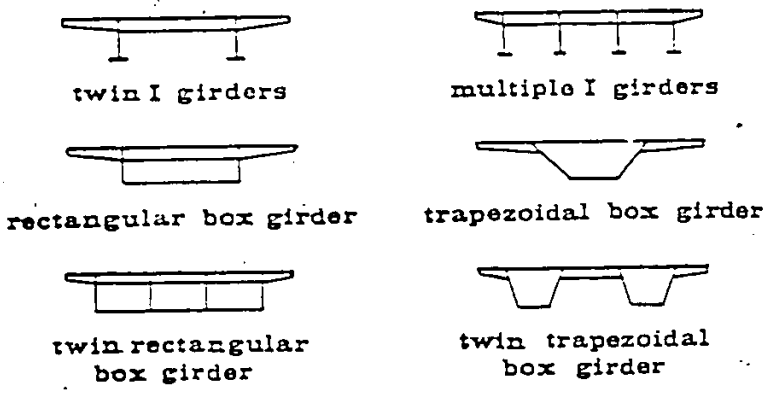

Figure 1.1.11: Bridge Deck Cross sections (After [15])

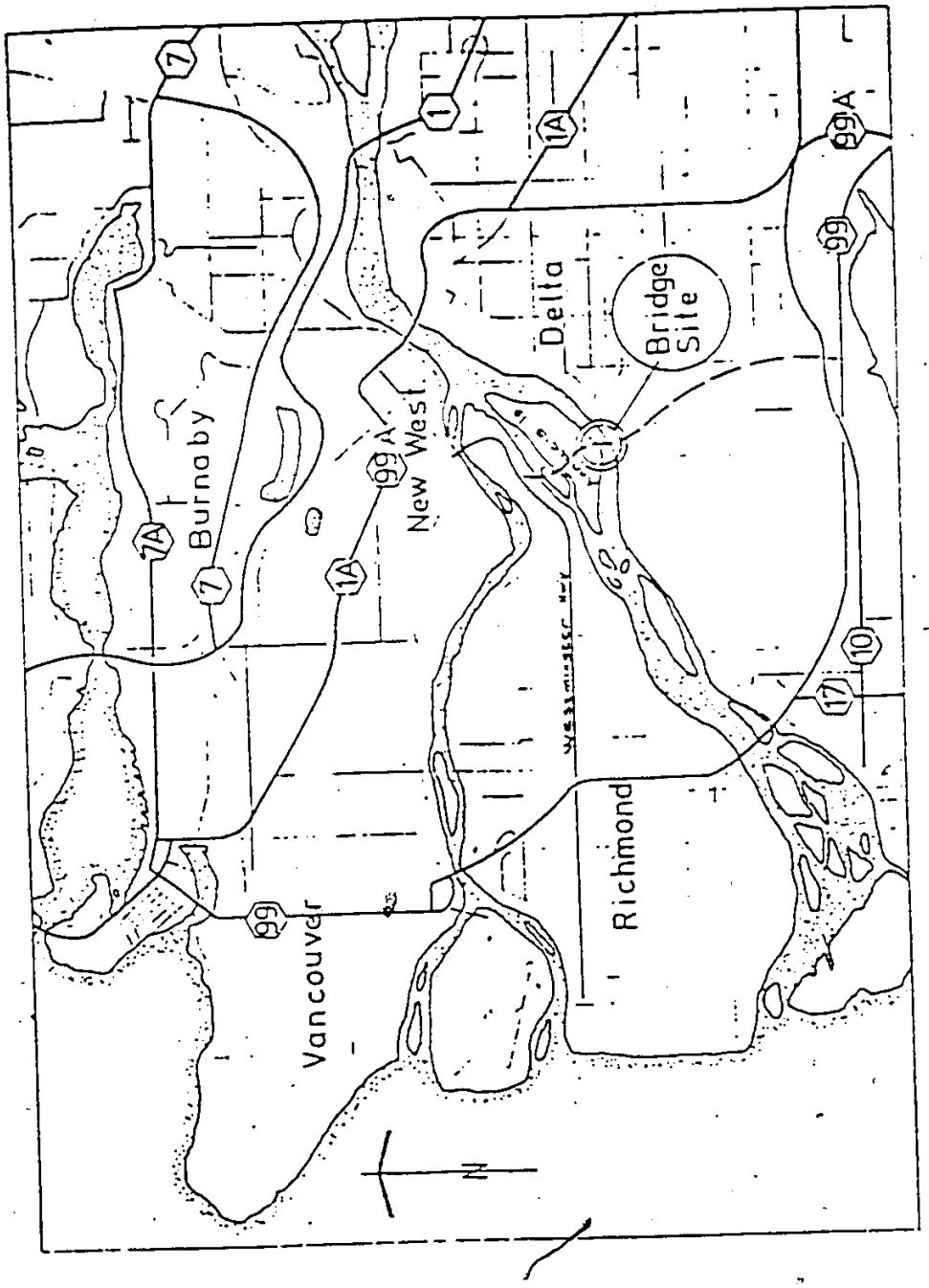

Figure 2.1.1: Annacis Island Bridge - Site Map (After [14])

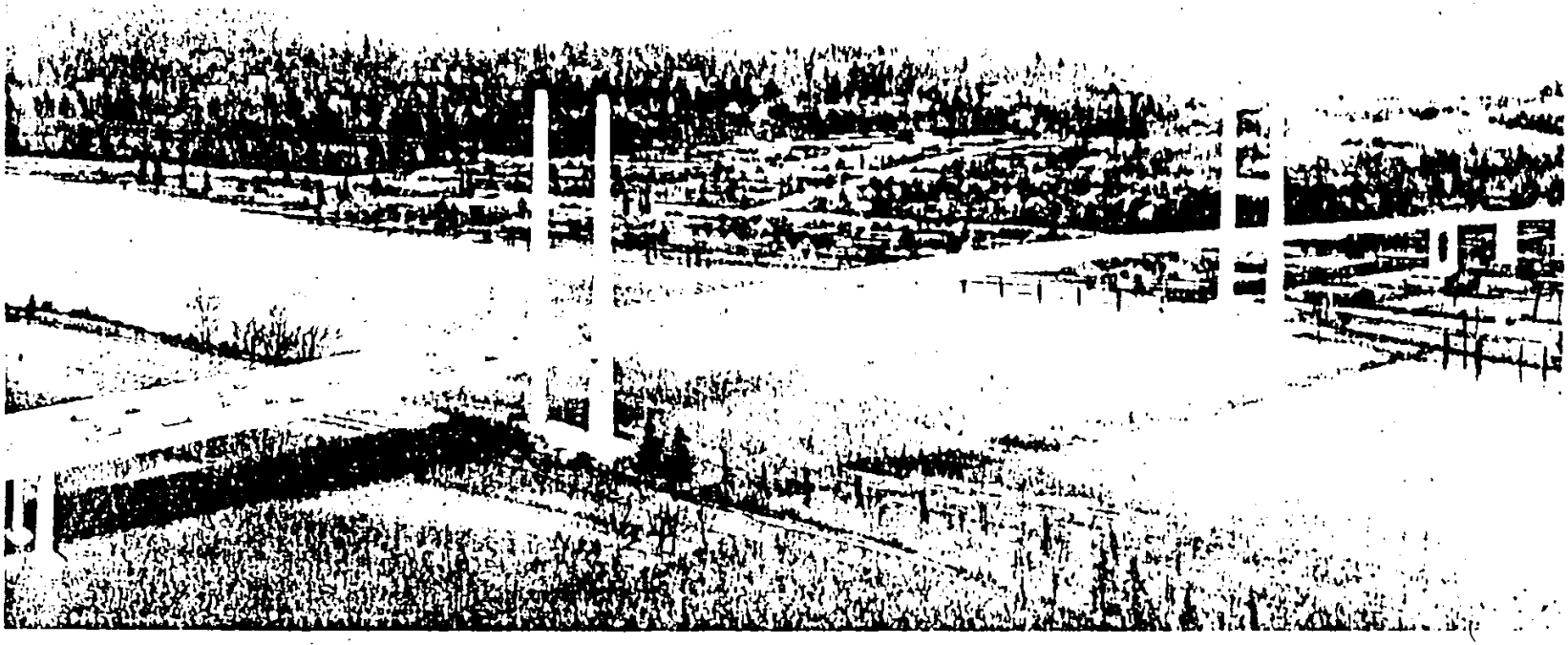

Figure 2.1.2: PROPOSED ANNACIS ISLAND BRIDGE – CONCRETE VERSION (After [14])

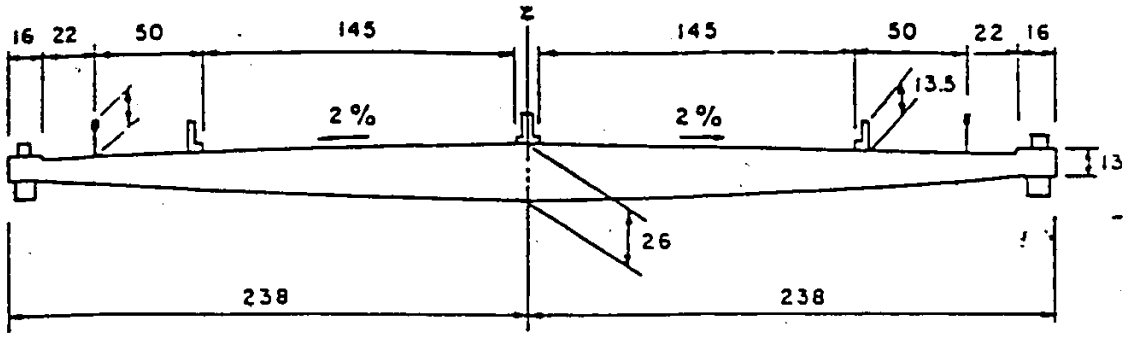

INITIAL SECTION

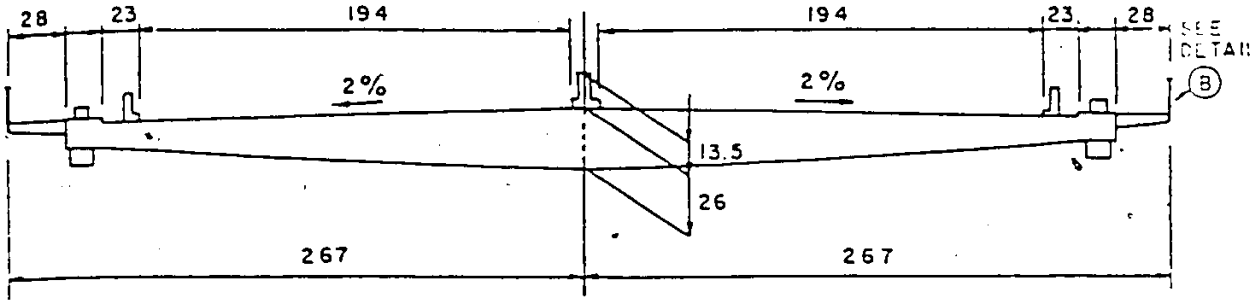

OPTION I

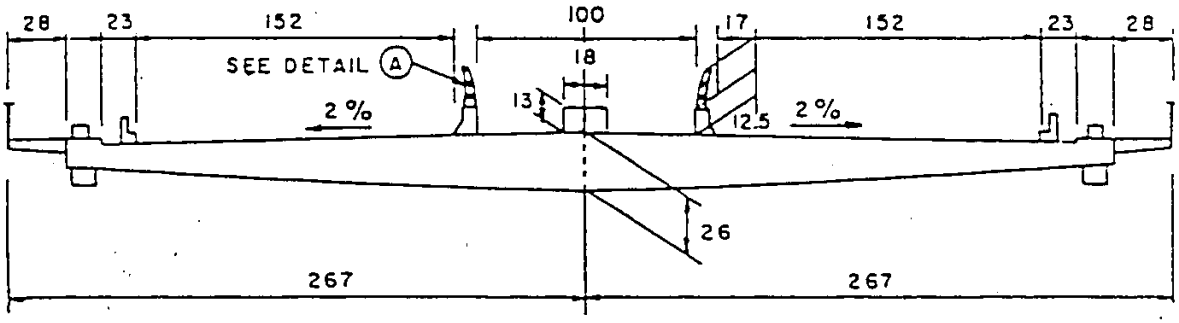

OPTION II

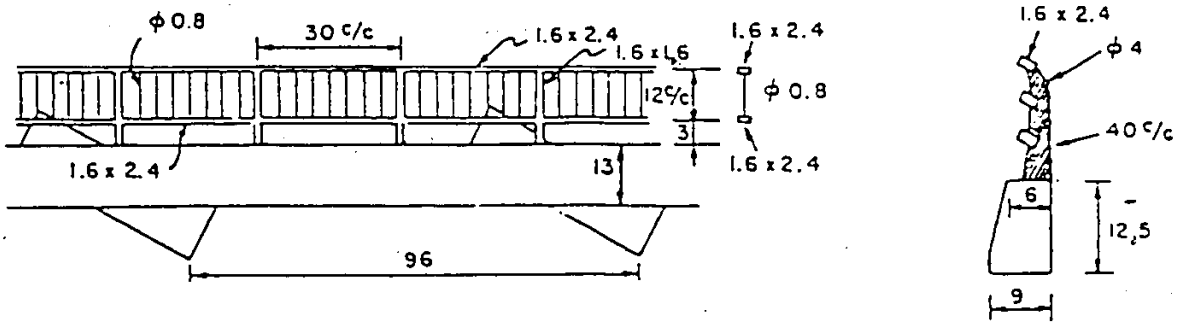

UNIT: millimeter

SIDE VIEW OF HANDRAILS

ALRT GUARDRAIL

Figure 2.2.1.1: 1/60-scale section models (After [14])

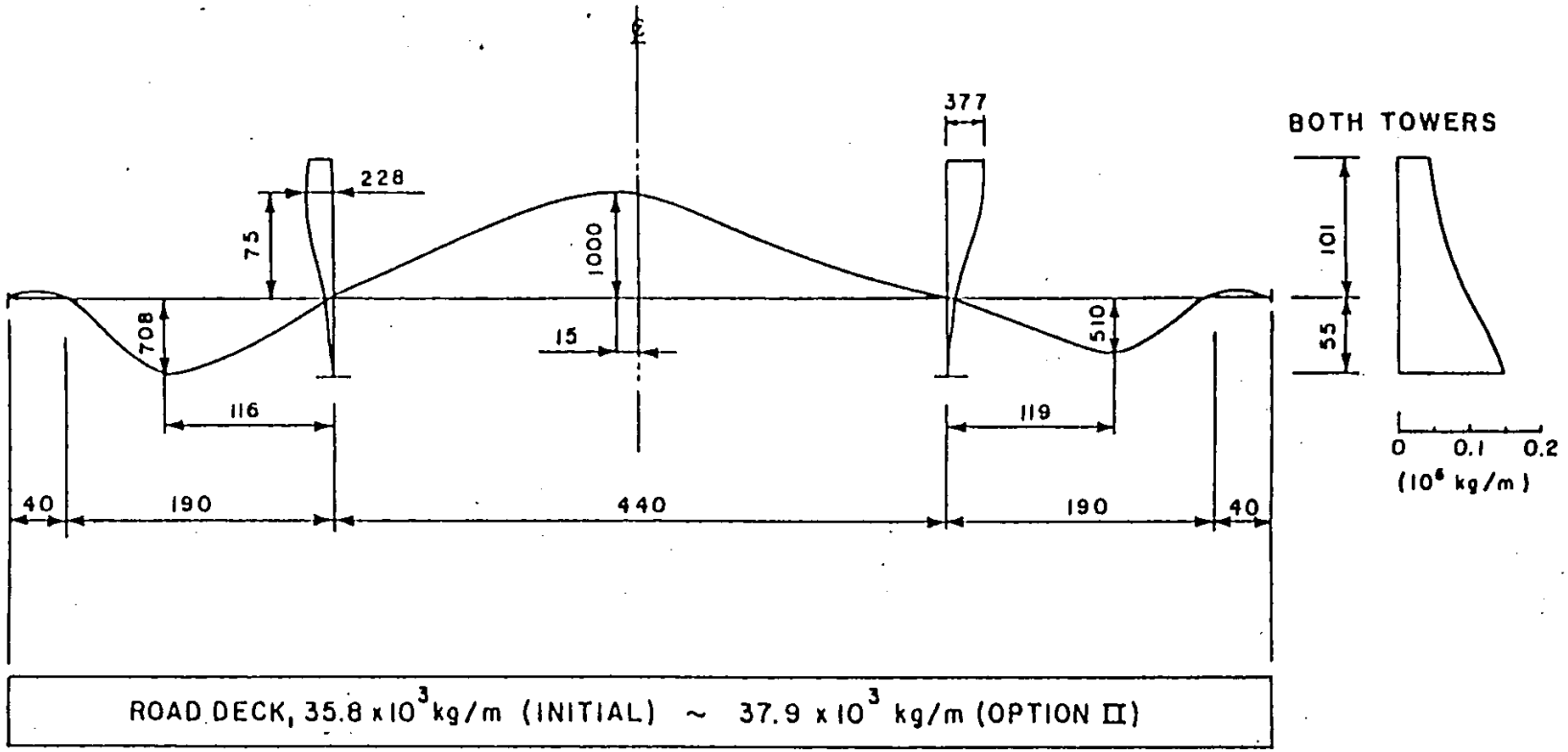

Figure 2.2.1.2: First Mode of Vibration and Generalized Mass (After [14])

TABLE 2.2.1.1

Summary of the Scaling Factors of 1/60-scale model (After [14])

Parameters	Scaling Factors used in Modelling
Length	$\lambda_L = 1/60$
Mass per unit length	$\lambda_M = \lambda_L^2 = 2.78 \times 10^{-3}$
Mass moment of inertia per unit length	$\lambda_J = \lambda_M \lambda_L^2 = 7.72 \times 10^{-6}$
Damping	$\lambda_\zeta = 1$
Time	$\lambda_T = 1/17.5$ (vertical mode) $= 1/2.9$ (torsional mode)
Frequency	$\lambda_f = 17.5$ (vertical mode) $= 2.9$ (torsional mode)
Velocity	$\lambda_{\bar{V}} = \lambda_L/\lambda_T = 1/3.43$ (vertical) $= 1/21$ (torsional)

TABLE 2.2.1.2

Mechanical Properties of the 1/60-scale Model (After [14]).

Generalized Properties	Prototype	1/60 Model	
Mass	Initial 35.8x10³ kg/m Option I 36.2x10³ kg/m Option II 37.9x10³ kg/m	Model 8.8 kg/m Attached weight 1.5 kg/m	
	Towers 3.0x10³ kg/m Cables at mid-span 5.5x10³ kg/m	Spring system 1.0 kg/m	Equivalent prototype values
		Total 11.3 kg/m	40.6x10³ kg/m
Polar mass moment of inertia	2.23x10⁶ kg.m²/m	0.156 kg.m²/m	2.02x10⁵ kg m²/m
Radius of gyration	7.88 m	0.133 m	7.98 m
Width	Initial 28.6 m Option 1 Option II 32.0 m	0.477 m 0.533 m	28.6 32.0
Frequencies		(i) (ii)	(i) (ii)
Vertical, f_V	0.243 Hz	4.3 Hz 2.7 Hz	0.24 Hz 0.15 Hz
Torsional, f_T	1.18 Hz	>13 Hz 3.4 Hz	>4.5 Hz 1.2 Hz
Frequency Ratio, f_T/f_V	4.83	>3 1.25	>3 1.25
Structural Damping	Vertical ς_V = 0.8% torsional ς_T = 0.8% (projected)	0.3 - 0.5% 0.3 - 0.5%	0.3 - 0.5% 0.3 - 0.5%

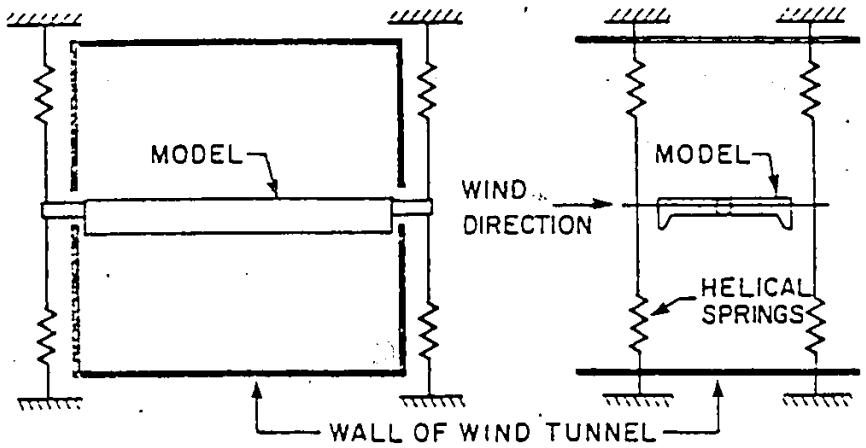

Figure 2.2.2.1: Section Model Suspension System (After [14])

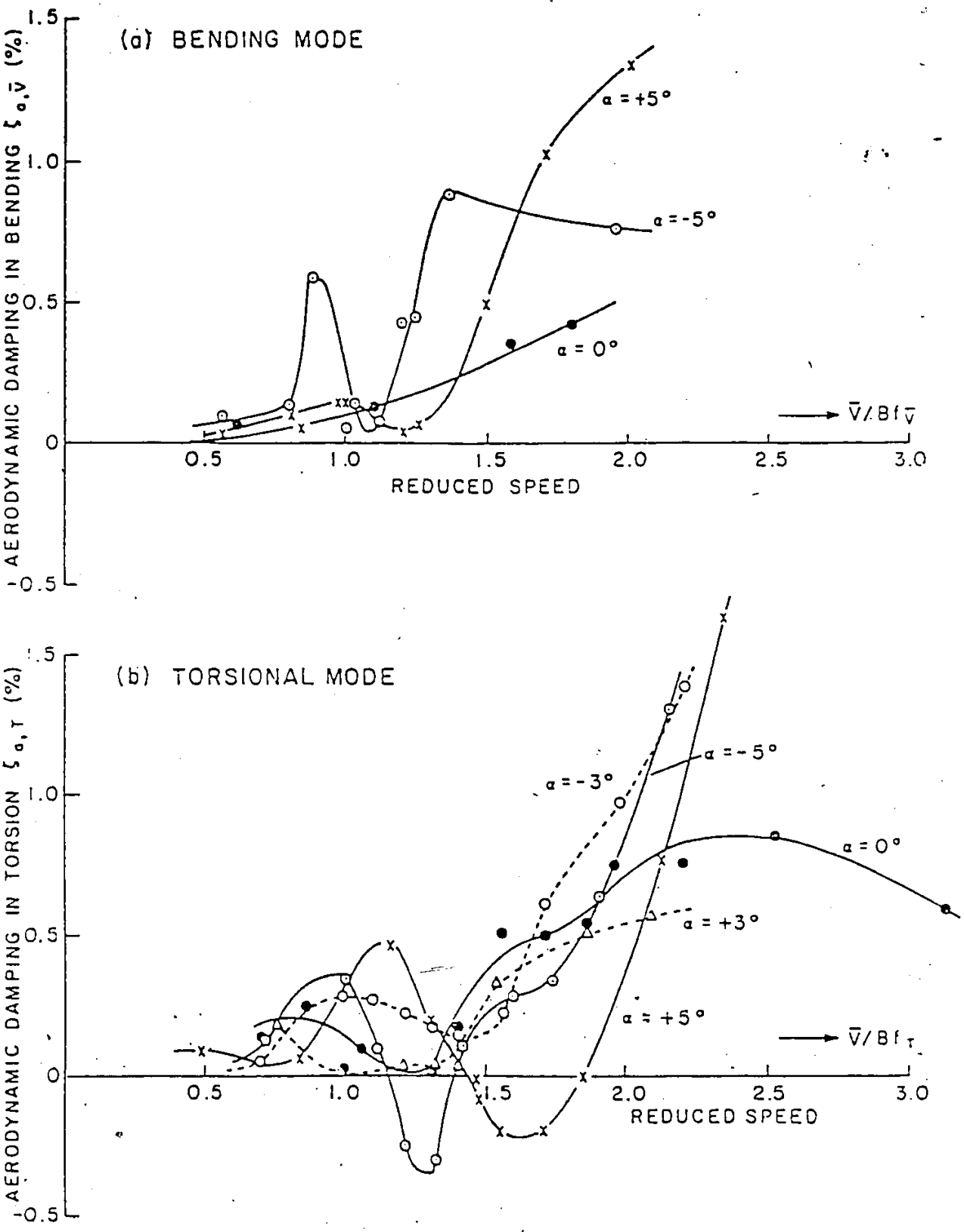

Figure 2.2.2.2: Aerodynamic Damping (After[[14])

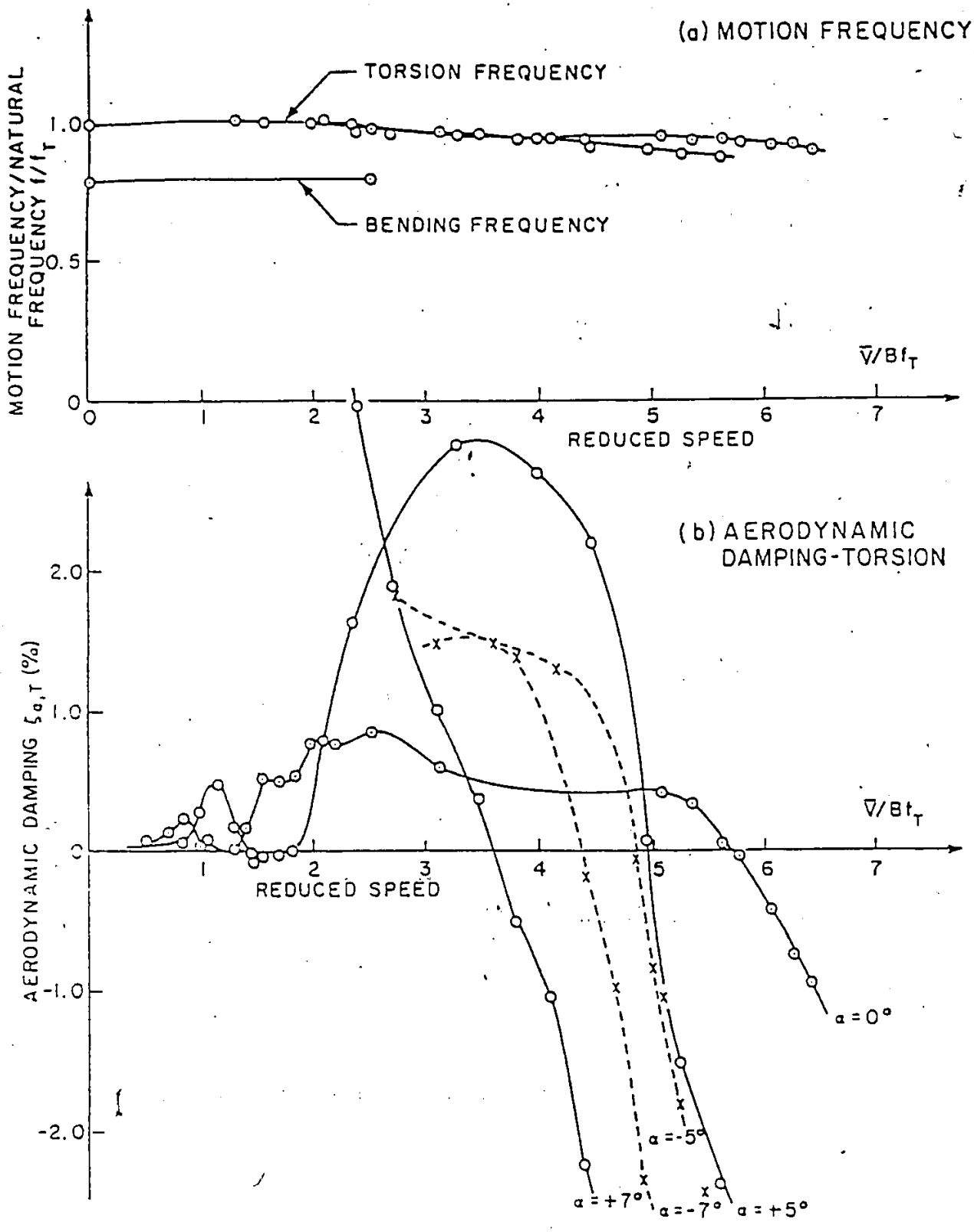

Figure 2.2.2.3: Aerodynamic Instability (After [14])

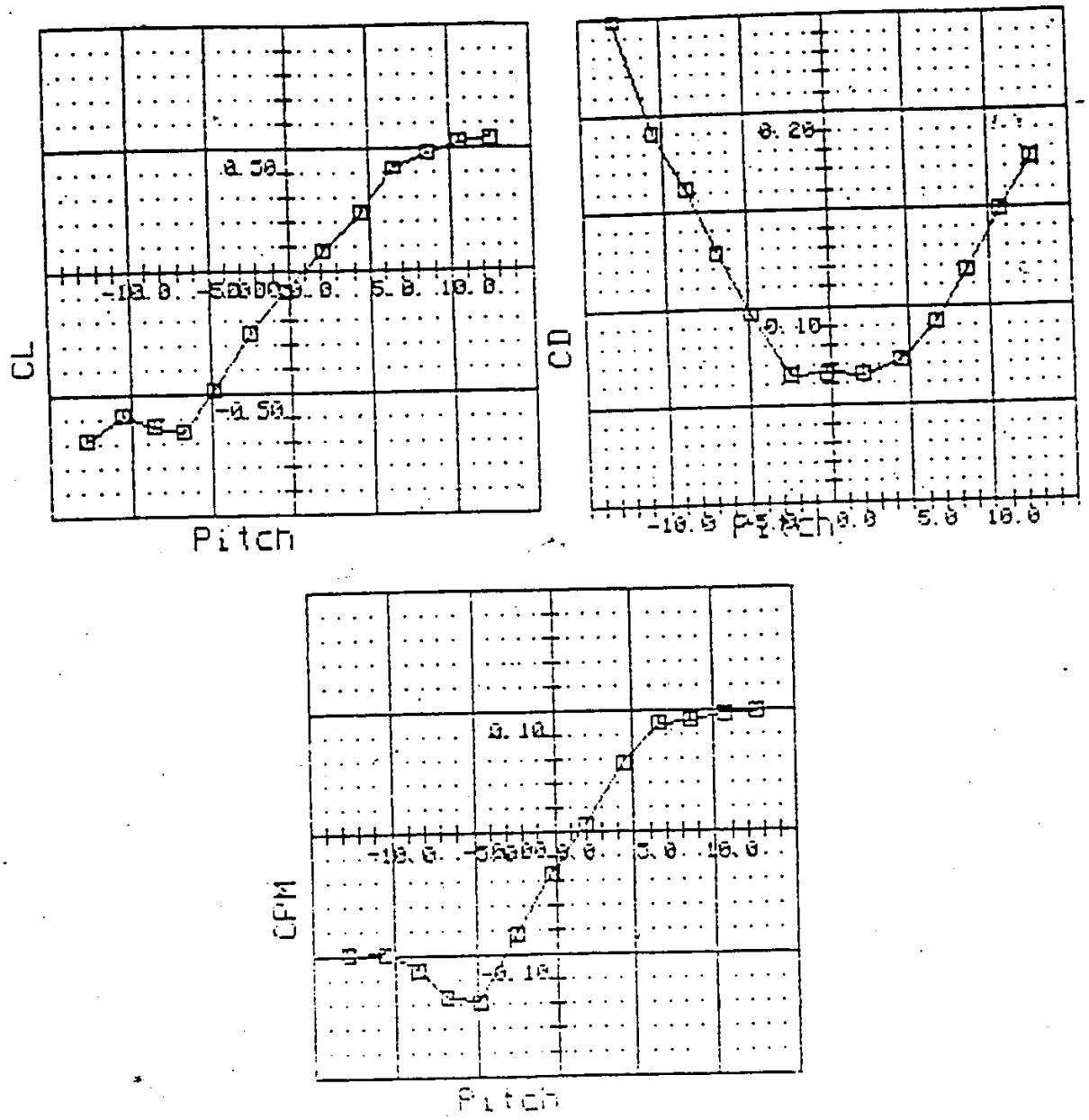

Figure 2.2.2.4: Mean Aerodynamic Forces (After [14])

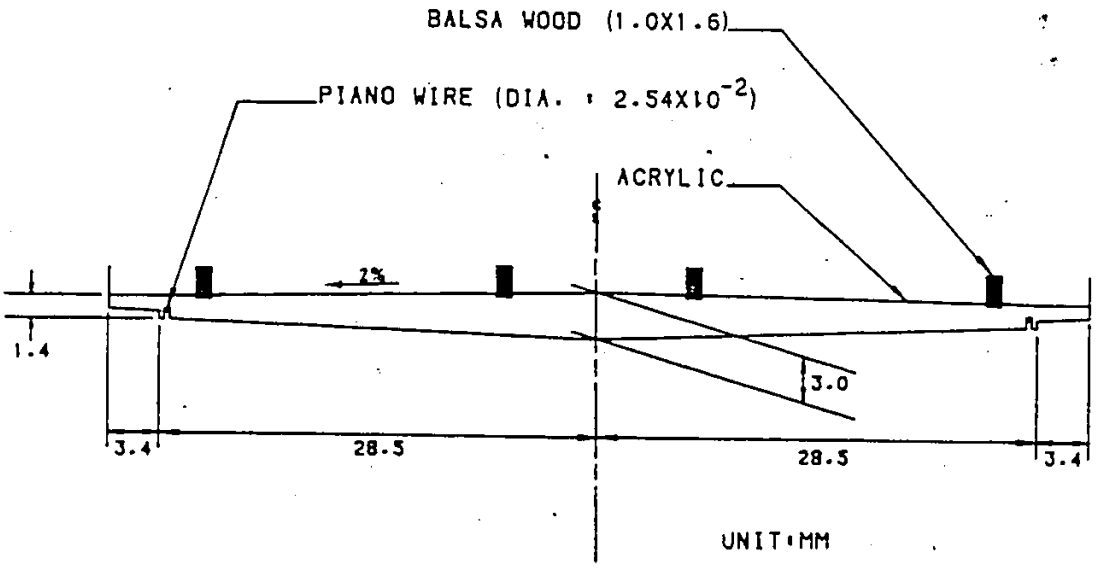

Figure 3.1.1: cross-section of 1/500-scale model

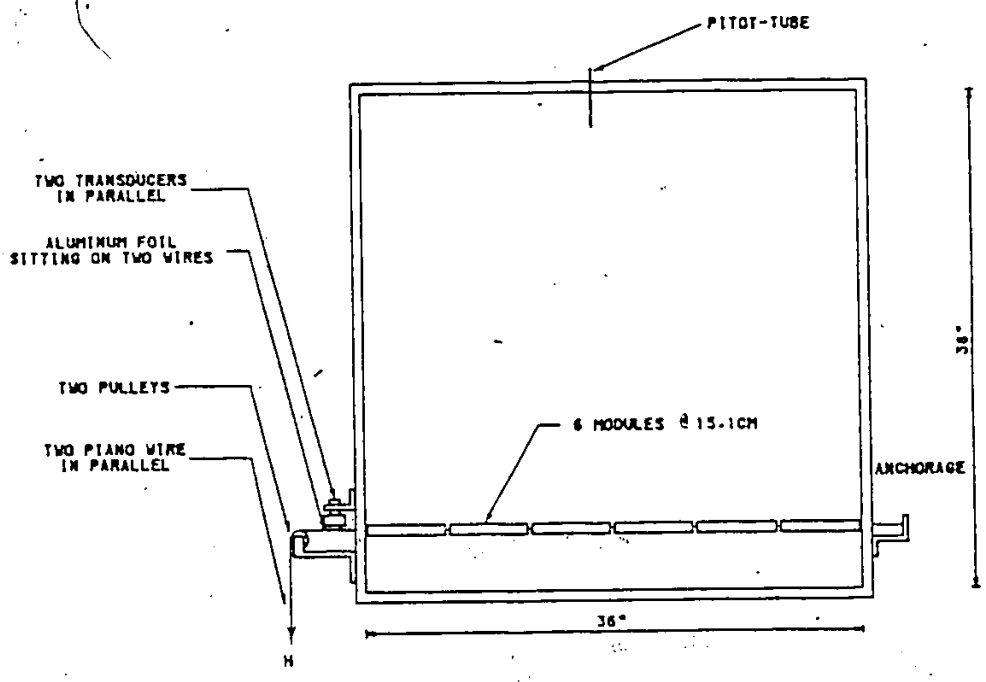

Figure 3.1.2: Layout 1

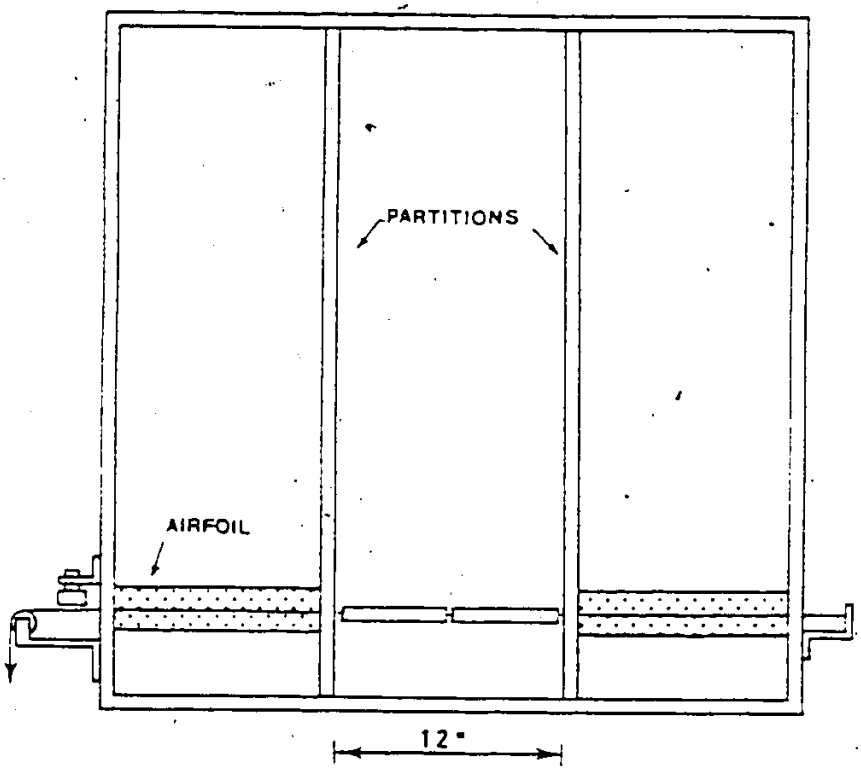

Figure 3.1.3: Layout 2

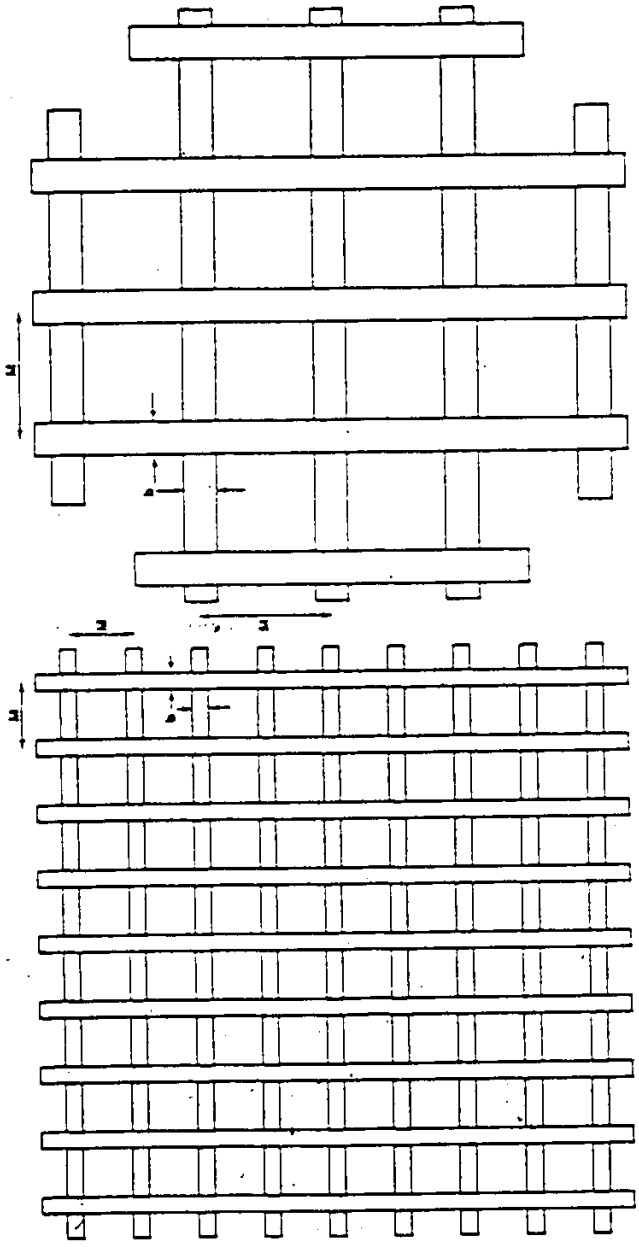

M 20 , b = 6.08

M 10.16 , b = 2.54

UNIT : CM

Figure 3.2.1.1: Grids

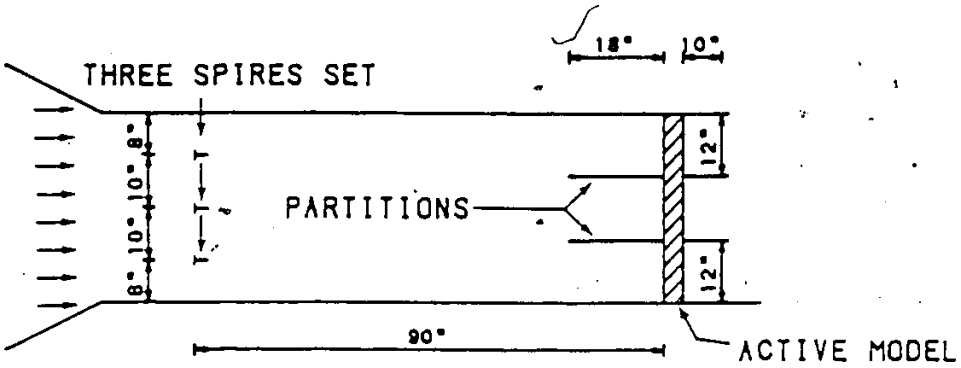

(a) Bare Tunnel and Spires

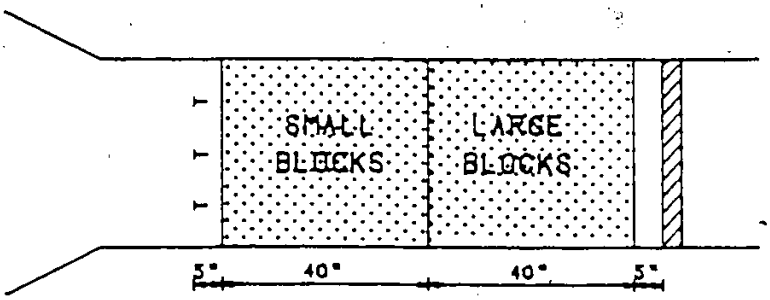

(b) Spires and Roughness

Figure 3.2.1.2: Top view of the tunnel with different arrangement of surface roughnesses

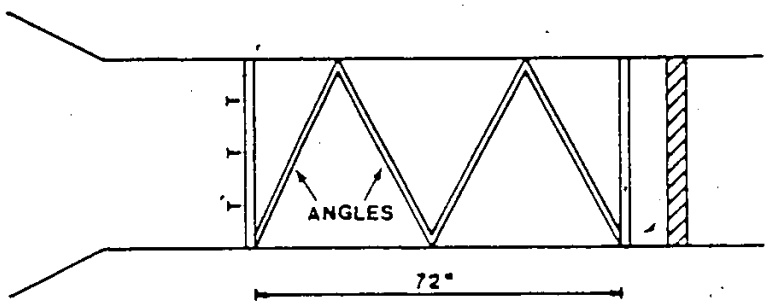

(c) Spires and Angles

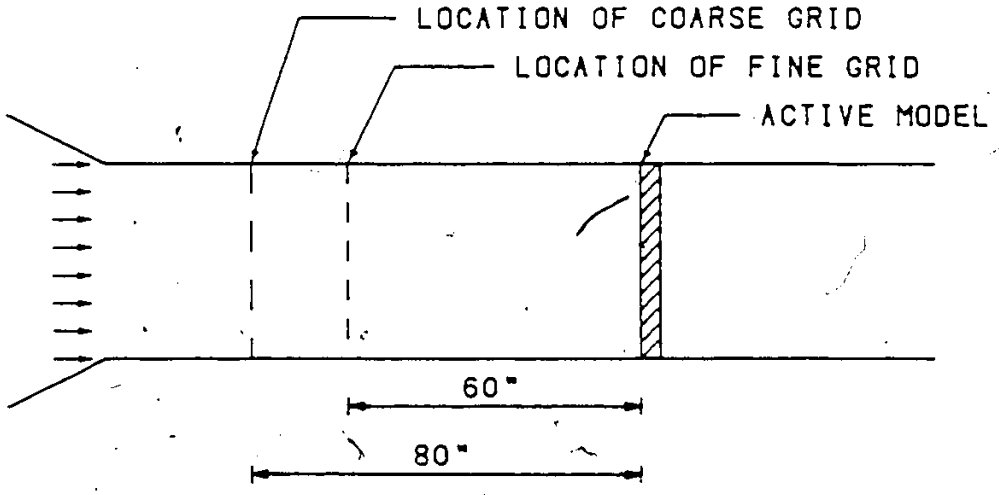

(d) Location of Fine Grid and Coarse Grid

Figure 3.2.1.2: Top view of the tunnel with different arrangement of surface roughnesses

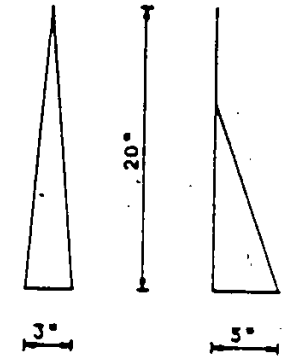

(a) Spire

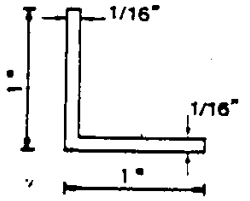

(b) Angle

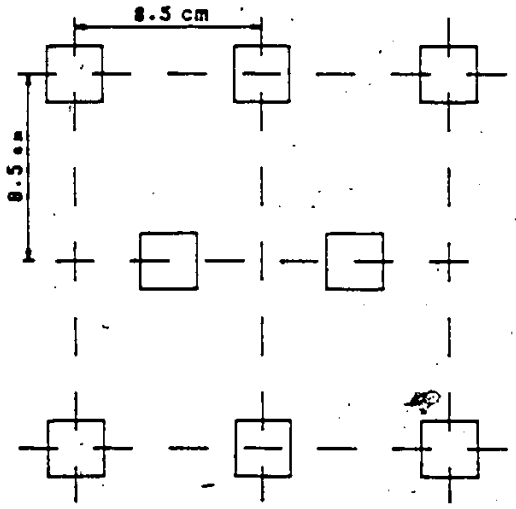

Small block :
0.79 in x 0.79 in x 0.79 in
(2 cm x 2 cm x 2 cm)

Large block :
0.79 in x 0.79 in x 1.18 in
(2 cm x 2 cm x 3 cm)

(c) Blocks Arrangement

Figure 3.2.1.3: Sketch of surface Roughness Elements

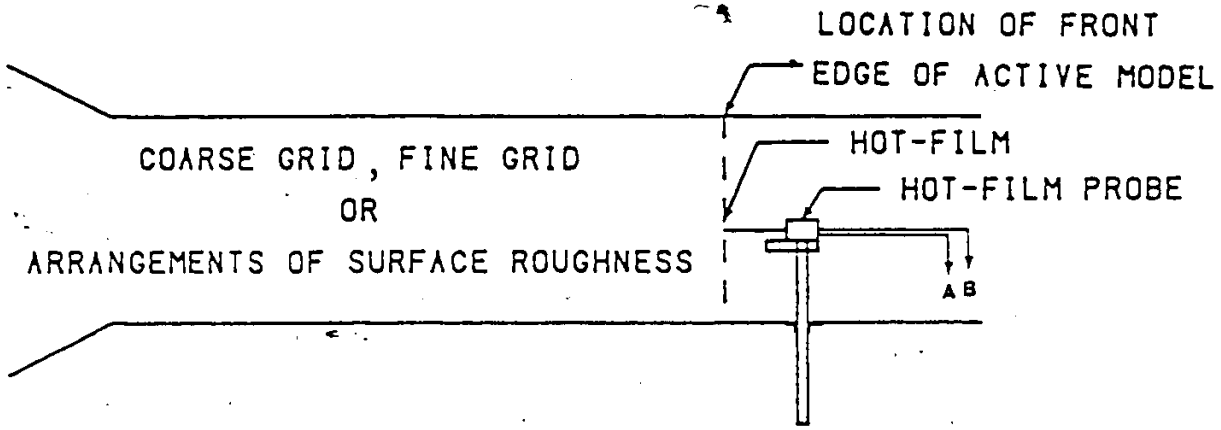

(a) Side View of Wind Tunnel

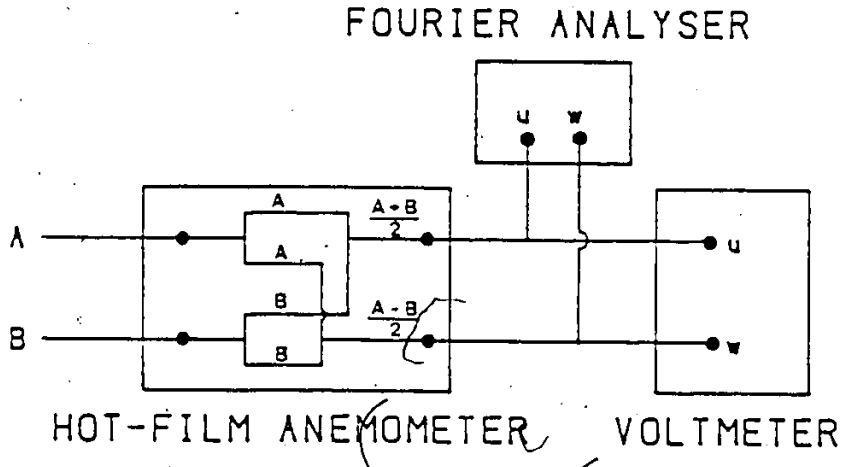

(b) Instrument Set Up

Figure 3.2.2.1: Set-up of instruments to measure wind characteristics

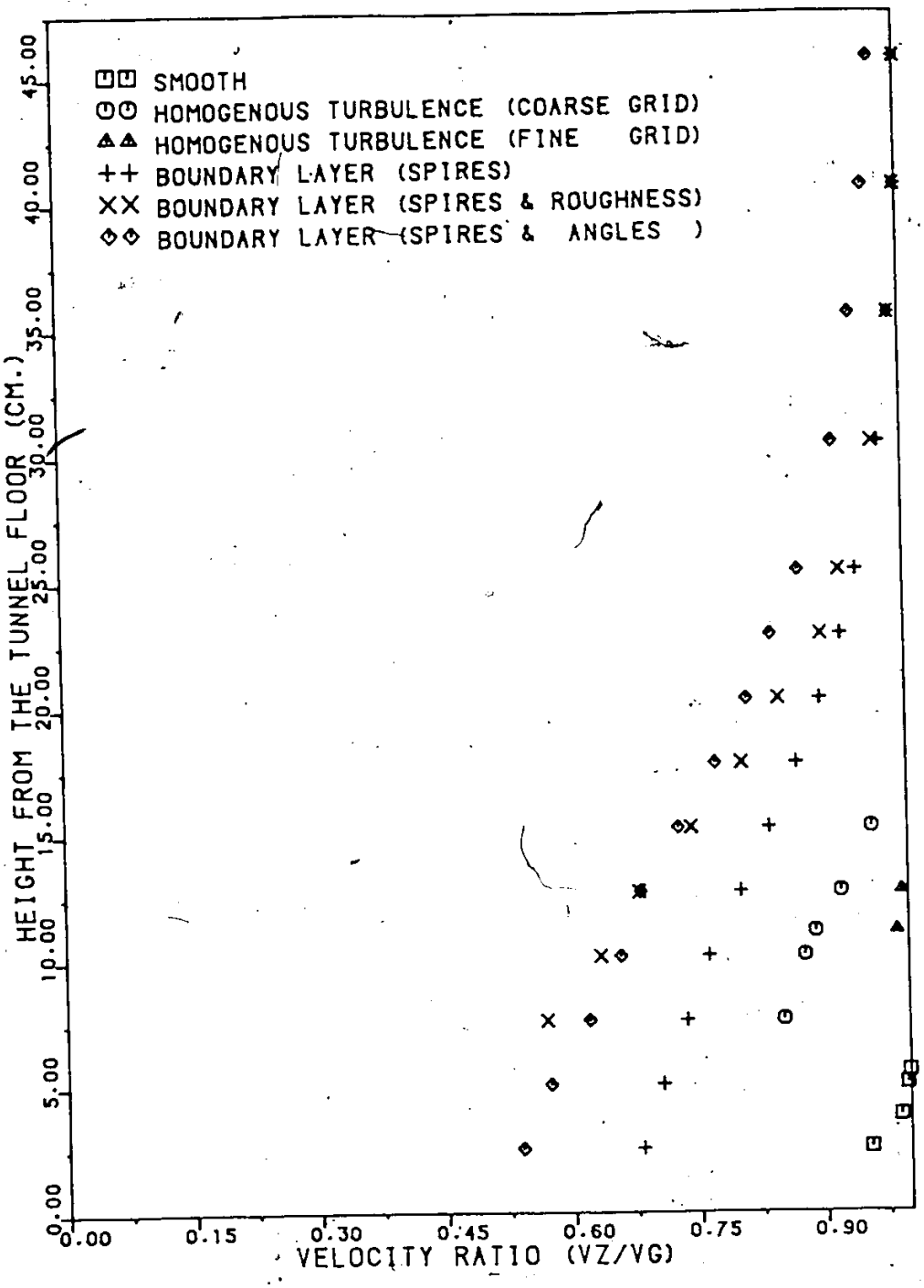

(a)

Figure 3.2.2.2: Vertical Profile of Mean Wind Speed (3-D)

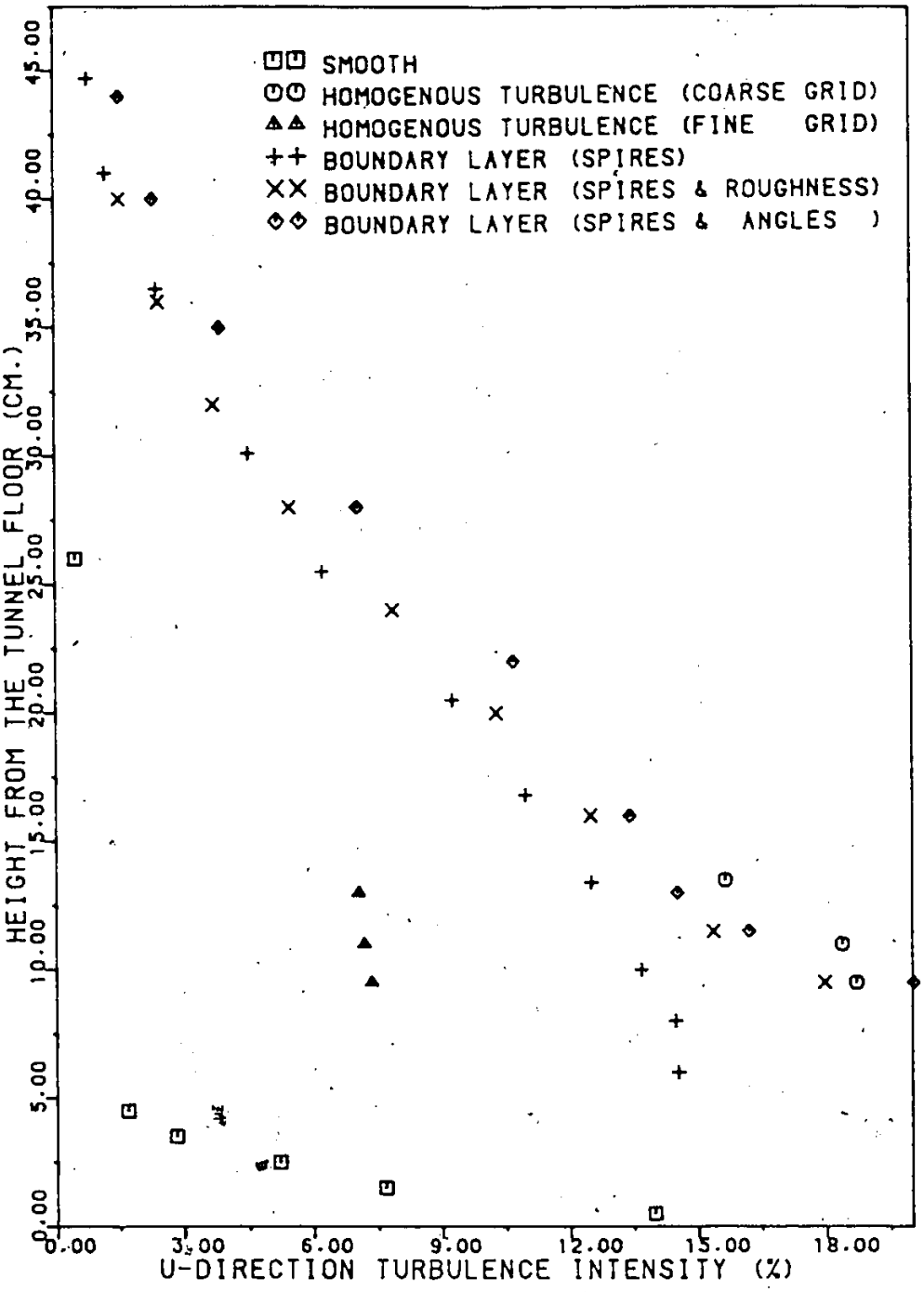

(b)

Figure 3.2.2.2: Vertical Profile of Turbulence Intensity (u) (3-D)

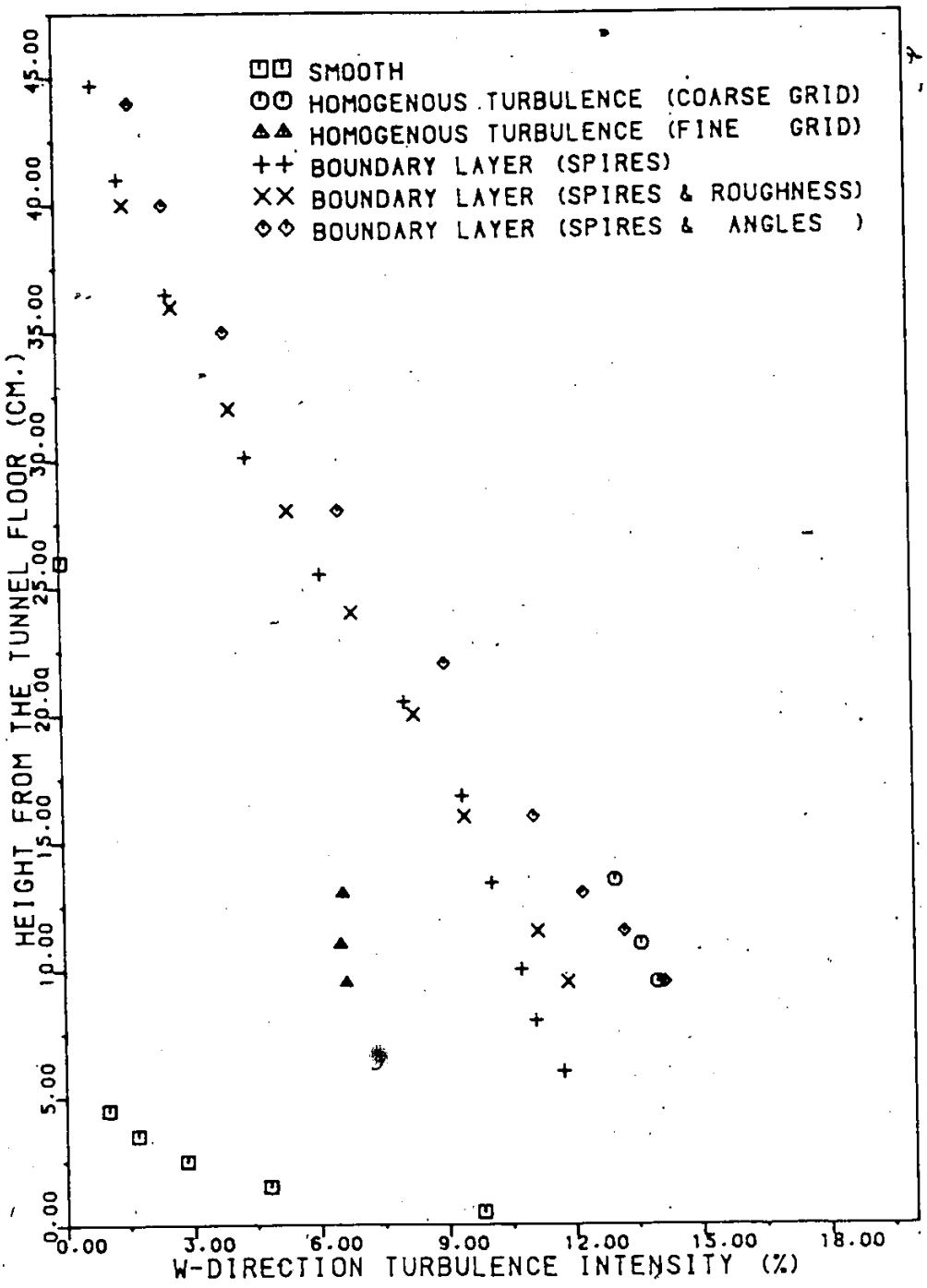

(c)

Figure 3.2.2.2: Vertical Profile of Turbulence Intensity (w) (3-D)

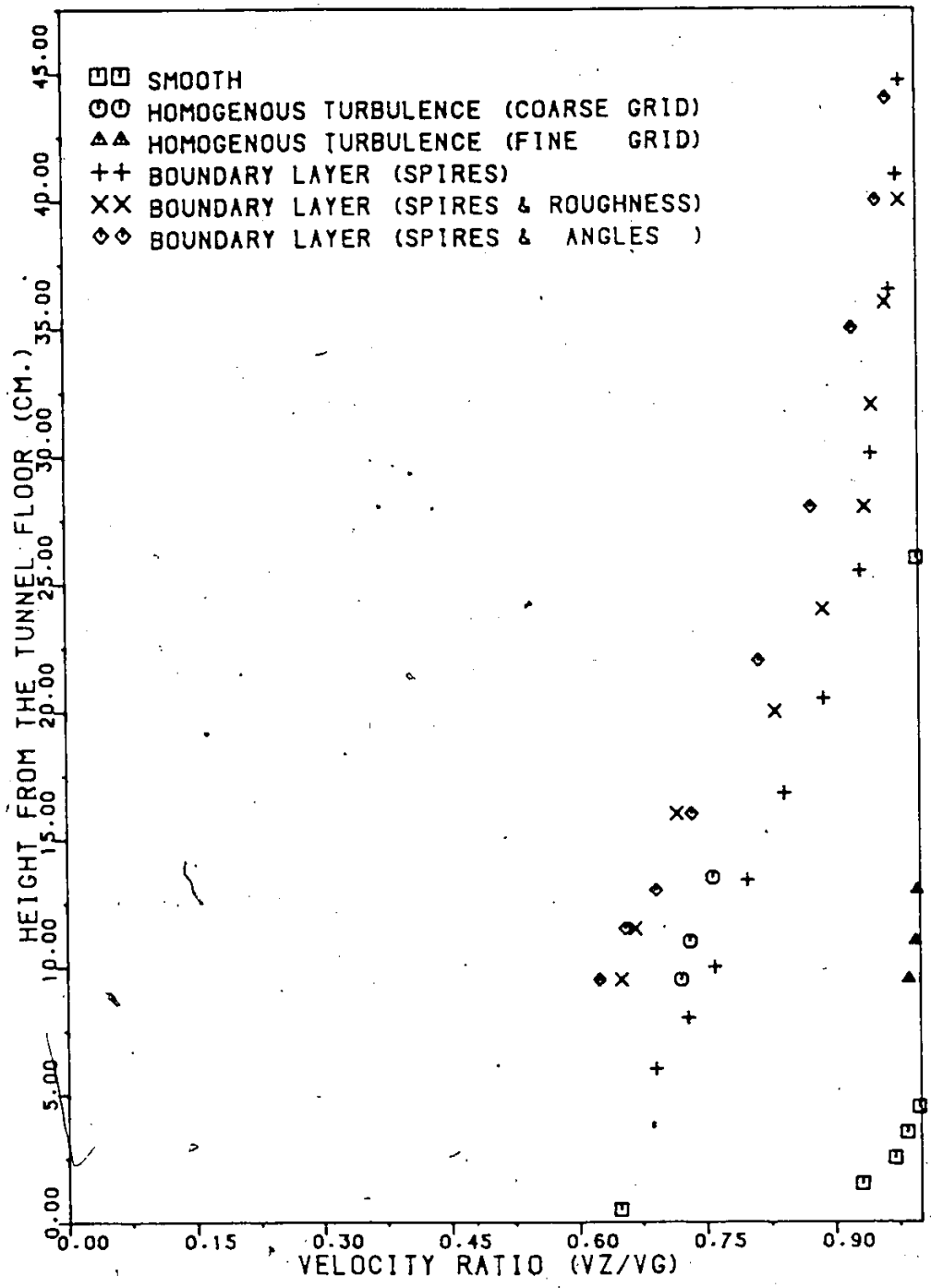

(a)

Figure 3.2.2.3: Vertical Profiles of Mean Wind Speed (2-D)

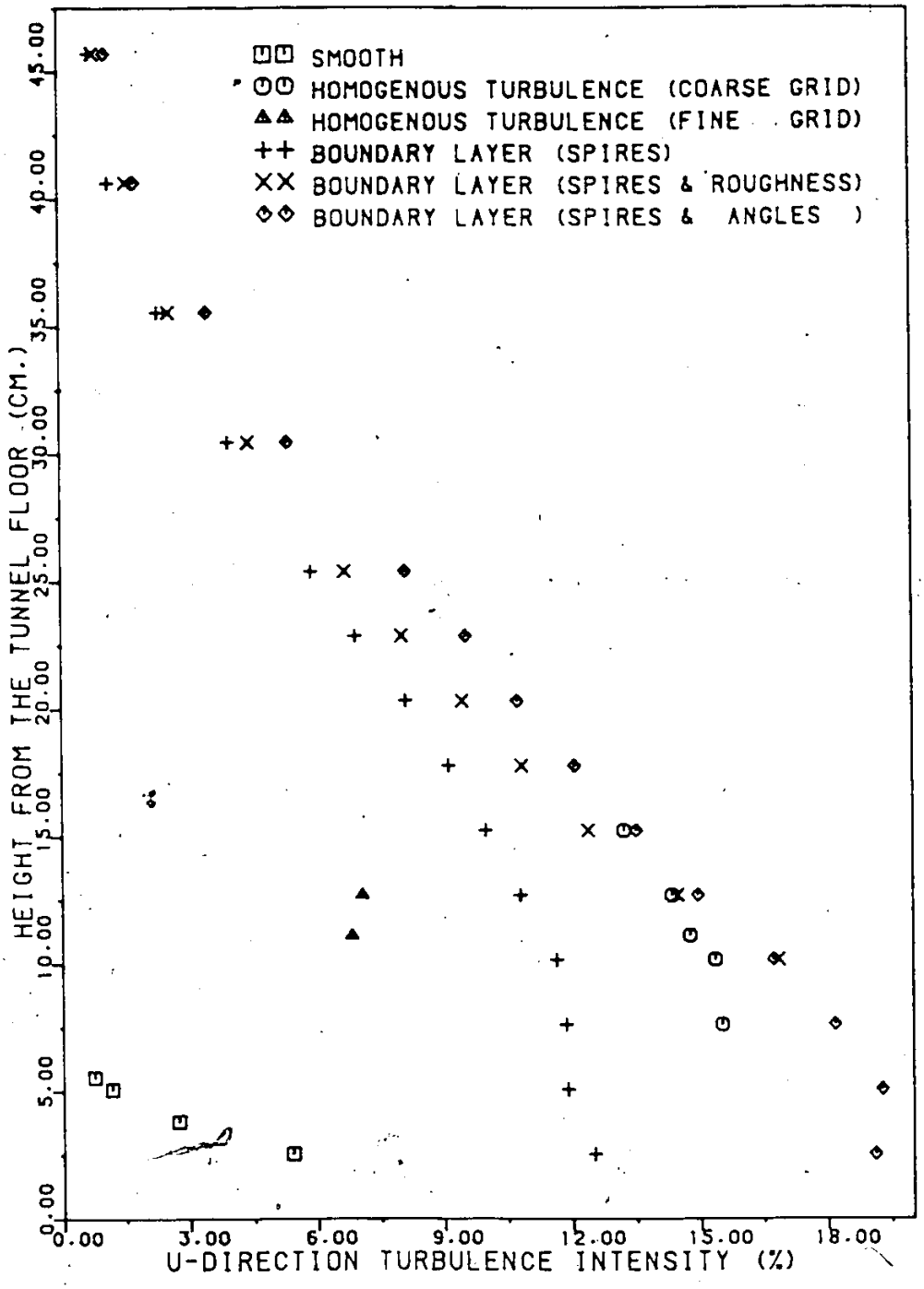

(b)

Figure 3.2.2.3: Vertical Profiles of Turbulence Intensity (u) (2-D)

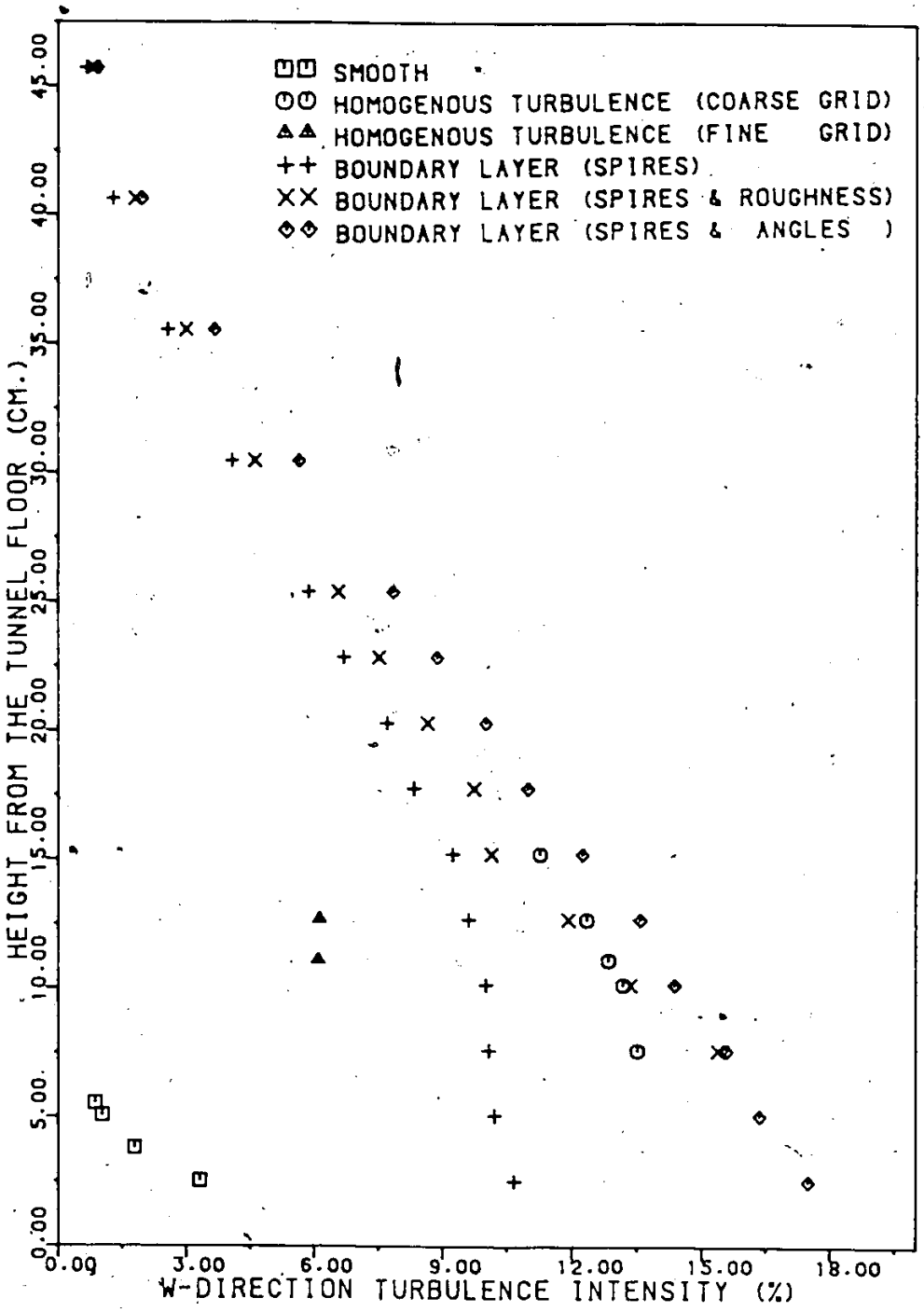

(c)

Figure 3.2.2.3: Vertical Profiles of Turbulence Intensity (w) (2-D)

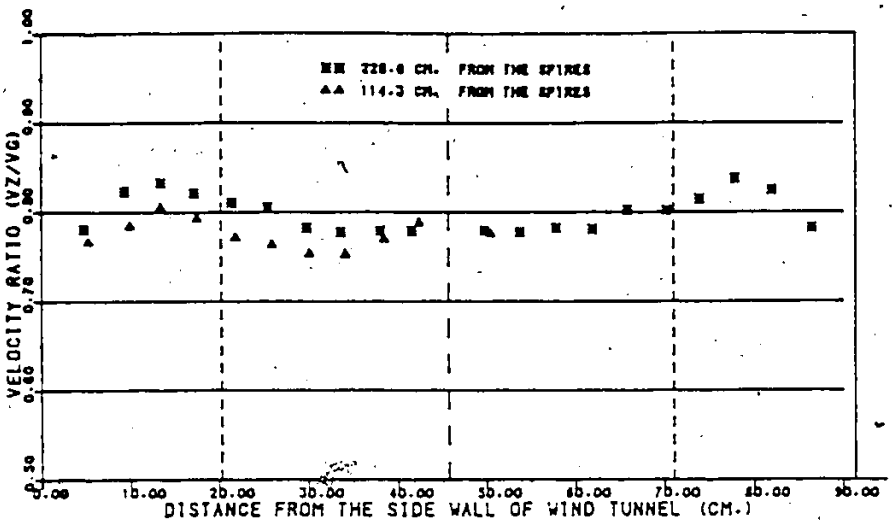

(a) Mean Velocity

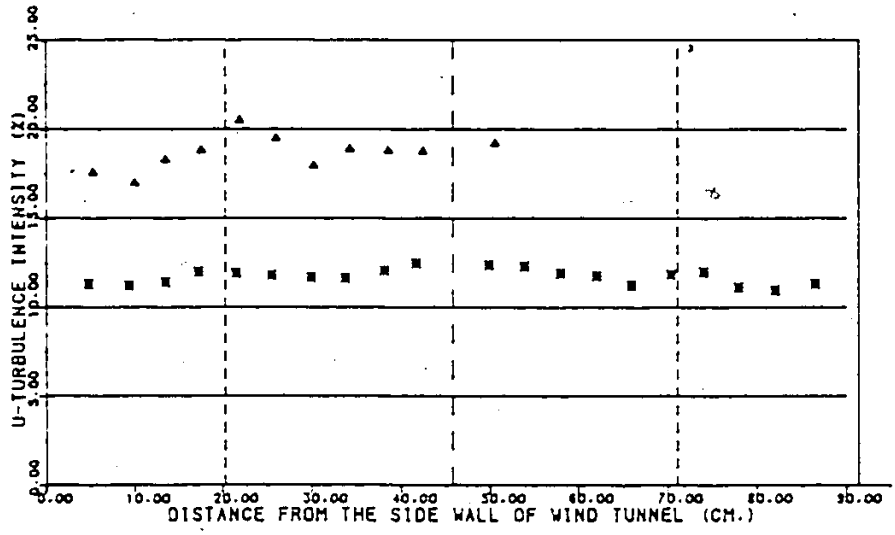

(b) Turbulence Intensity (u)

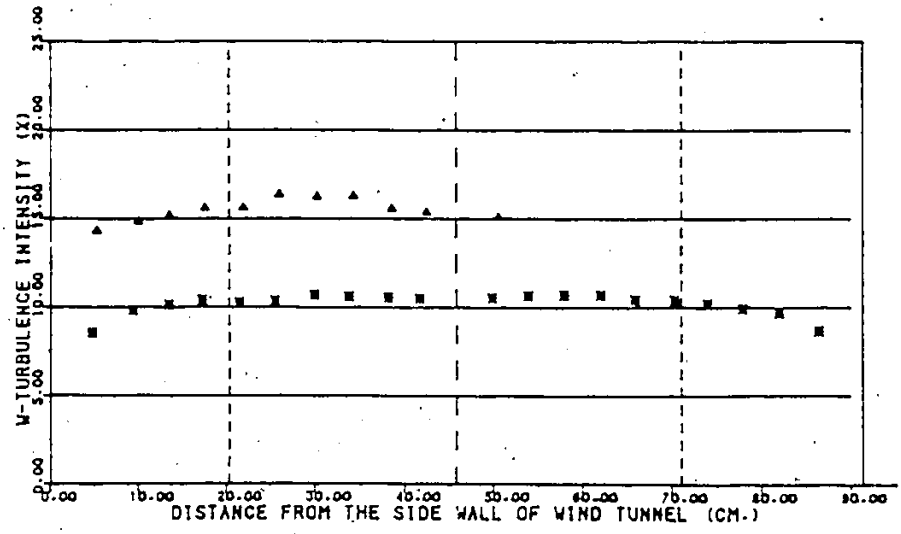

(c) Turbulence Intenstiy (w)

Figure 3.2.2.4: Horizontal Profiles

TABLE 3.2.2.1

Summary of the flow measurement

	FLOW CONDITION	Velocity profile : $V/Vg=(Z/Zg)^{\alpha}$		At deck height Z = 11.5 cm				
				Vz/Vg	Turbulence intensity(%)		Scale of turbulence mm	
		α	Zg(cm)		Iu	Iw	Lu	Lw
3-D	Smooth	0.06	4.5	1.0	0.5	0.25	/	/
	Coarse Grid	/	/	0.73	18.0	13.25	40	40
	Fine Grid	/	/	1.0	7.2	6.4	25	25
	Spires	0.18	40	0.8	13.0	10.5	50	45
	Spires and roughness	0.32	50	0.63	15.4	12.0	60	55
	Spires and angles	0.29	47	0.66	15.8	13.2	60	55
2-D	Smooth	0.06	5	1.0	0.0	0.0	/	/
	Coarse Grid	/	/	0.89	15	13.2	40	40
	Fine Grid	/	/	1.0	7	6.2	25	25
	Spires	0.19	40	0.79	11.3	9.8	50	45
	Spires and roughness	0.33	50	0.62	15.0	12.5	60	55
	Spires and angles	0.27	46	0.69	16.0	13.0	60	55

TABLE 3.4.1

Summary of scaling factors of 1/500-scale models

Parameters	Scaling factors used in modelling			
	3-D		2-D	
	1	2	1	2
Length scale, λ_L	1/500	1/500	1/500	1/500
Mass per unit length, λ_m	4×10^{-6}	4×10^{-6}	4×10^{-6}	4×10^{-6}
Mass moment of inertia per unit length, λ_J	1.6×10^{-11}	1.6×10^{-11}	1.6×10^{-11}	1.6×10^{-11}
Structural damping	1	1	1	1
Time, λ_T				
vertical mode	0.04	0.028	0.025	0.02
torsional mode	0.02	0.018	0.022	0.018
Frequency, λ_f				
vertical mode	25.7	36.2	40.3	49.4
torsional mode	43.4	54.1	44.4	54.6
Velocity, λ_v				
vertical mode	0.05	0.07	0.08	0.1
torsional mode	0.1	0.11	0.09	0.11

$\lambda_m = \lambda_L^2$; $\lambda_J = \lambda_m \lambda_L^2$

$\lambda_f = \frac{\text{model frequency}}{\text{prototype frequency}}$; prototype frequency: FZ=0.243, FA=0.403

$\lambda_T = 1/\lambda_f$; $\lambda_v = \lambda_L/\lambda_T$

TABLE 3.4.2

Mechanical Properties of 1/500-scale Models

Properties	1/500-scale taut strip model		1/500-scale sectional model	
	1	2	1	2
Mass	0.15 kg/m	0.15 kg/m	0.15 kg/m	0.15 kg/m
Mass moment of inertia	35.6×10^{-6} kgm^2/m	35.6×10^{-6} kgm^2/m	35.6×10^{-6} kgm^2/m	35.6×10^{-6} kgm^2/m
Width of bridge deck	0.064 m	0.064 m	0.064 m	0.064 m
Depth of girder	$3^{-1}.4 \times 10^{-3}$ m	$3^{-1}.4 \times 10^{-3}$ m	$3^{-1}.4 \times 10^{-3}$ m	$3^{-1}.4 \times 10^{-3}$ m
Frequencies				
vertical, FZ	6.25 Hz	8.8 Hz	9.8 Hz	12 Hz
torsional, FA	17.5 Hz	21.8 Hz	17.9 Hz	22 Hz
Damping				
vertical, ζ_η	2.84 %	0.78 %	0.92 %	0.54 %
torsional, ζ_ϕ	1.31 %	0.50 %	0.38 %	0.26 %
Frequency ratio, FA/FZ	2.8	2.5	1.8	1.79

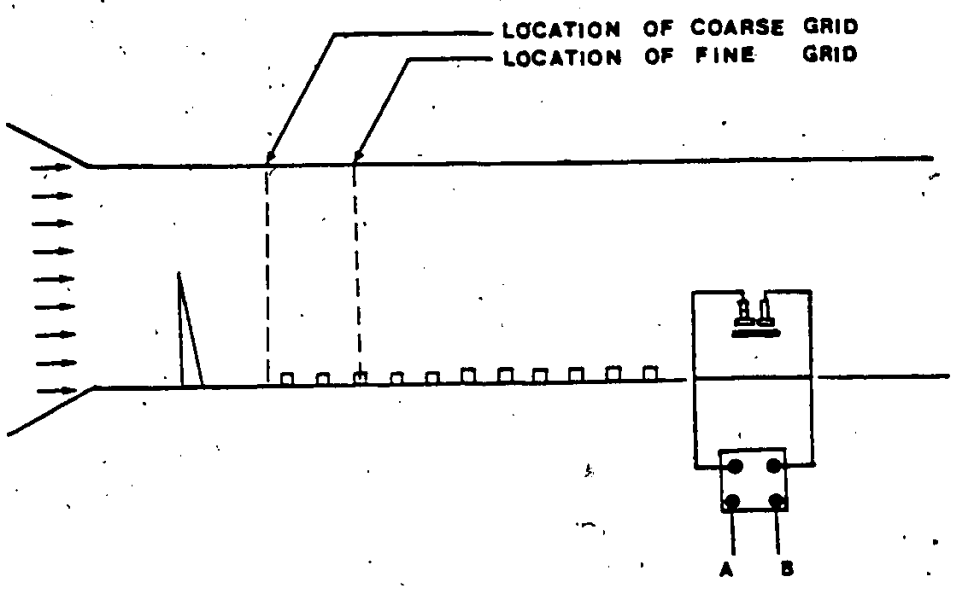

Figure 3.4.3: Side View of Wind Tunnel for Response Measurement

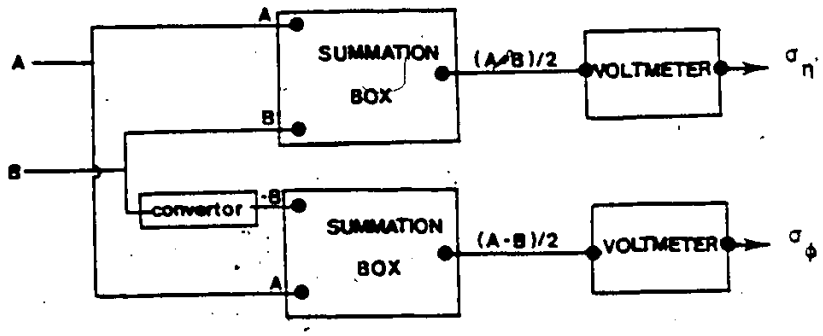

Figure 3.4.4: Set Up of Instruments to Measure Response

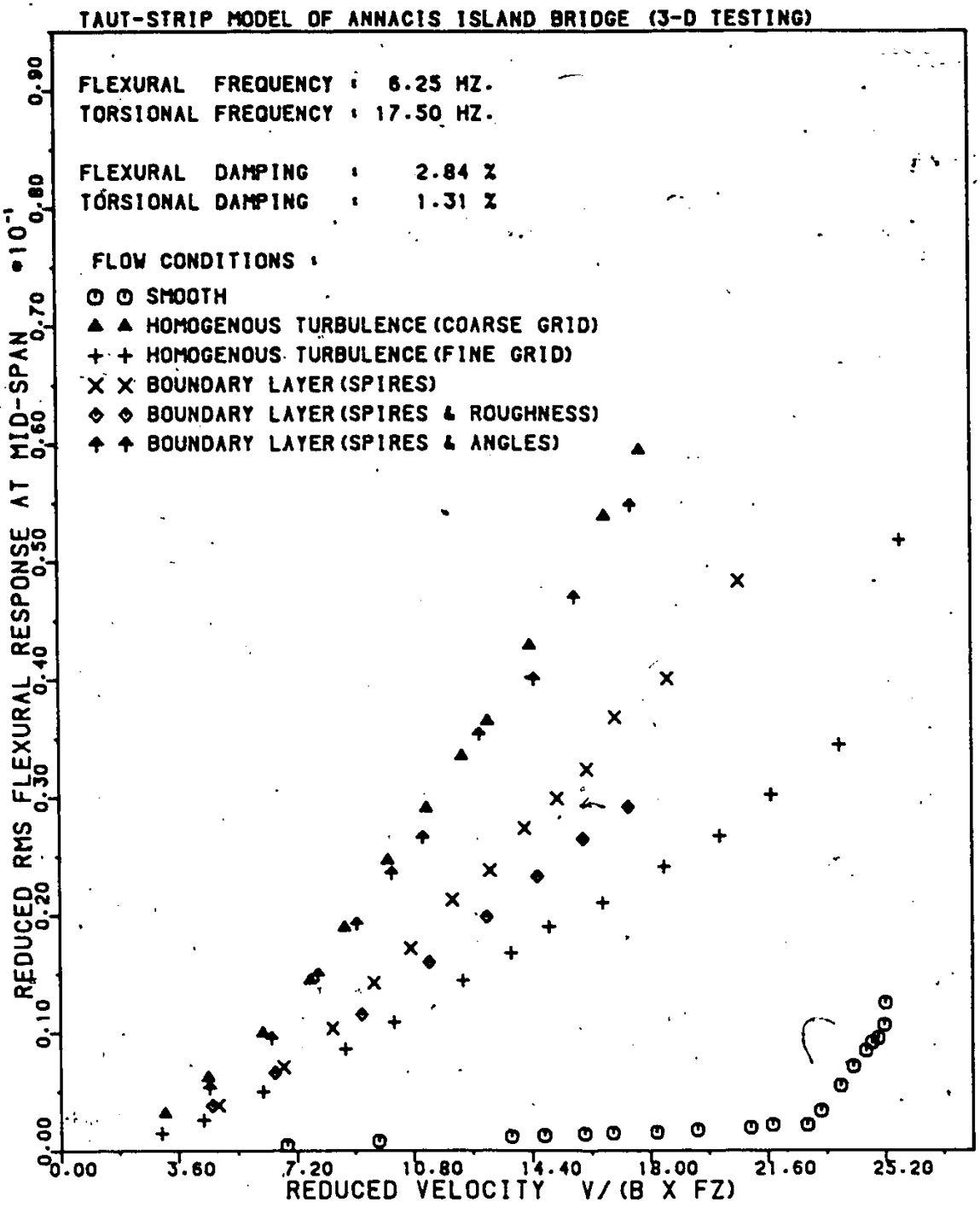

Figure 3.4.5: Buffeting Response against Reduced Velocity (3-D) : FA = 17.5 Hz , FZ = 6.25 Hz

(a) Flexural response

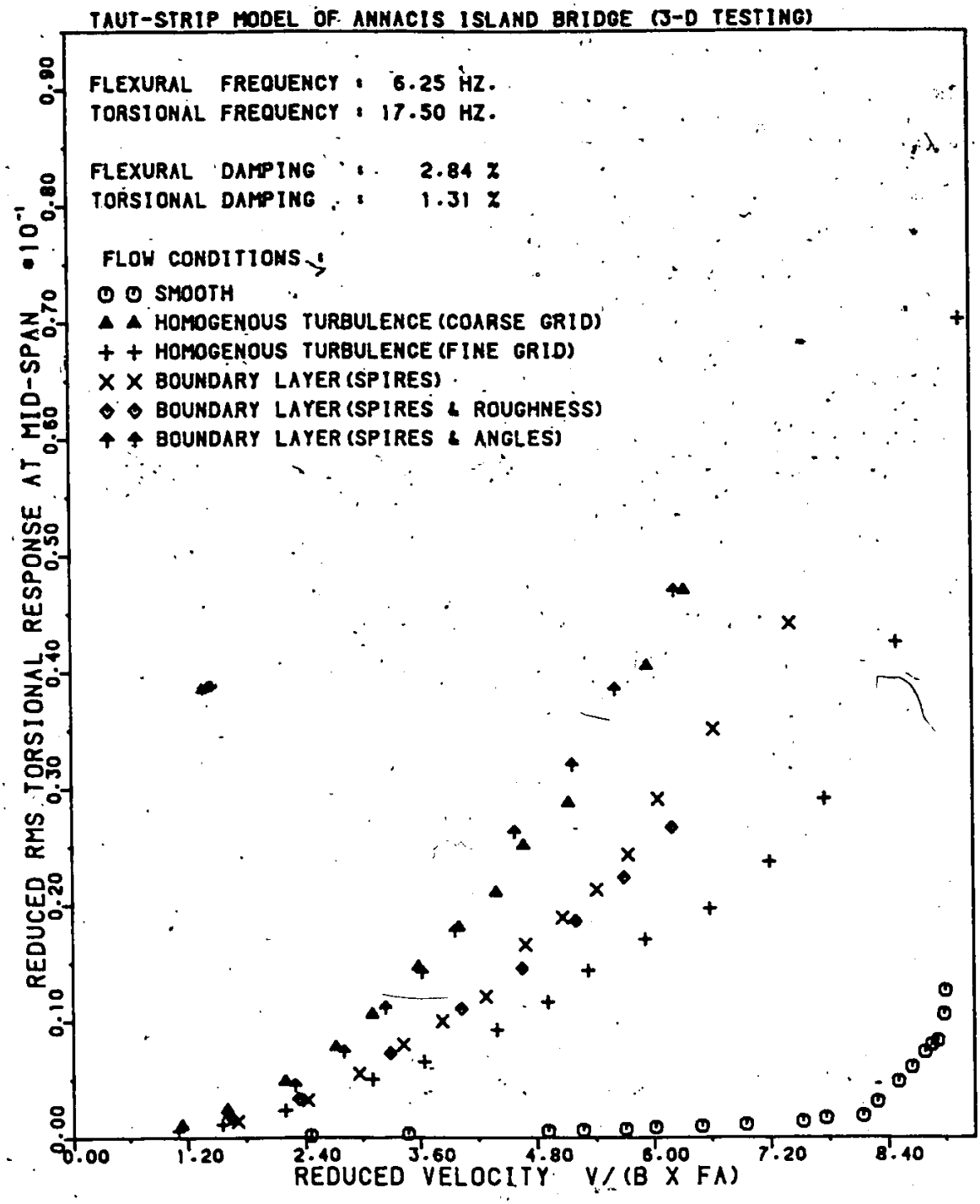

Figure 3.4.5: Buffeting Response against Reduced Velocity (3-D) : FA = 17.5 Hz , FZ = 6.25 Hz
(b) Torsional response

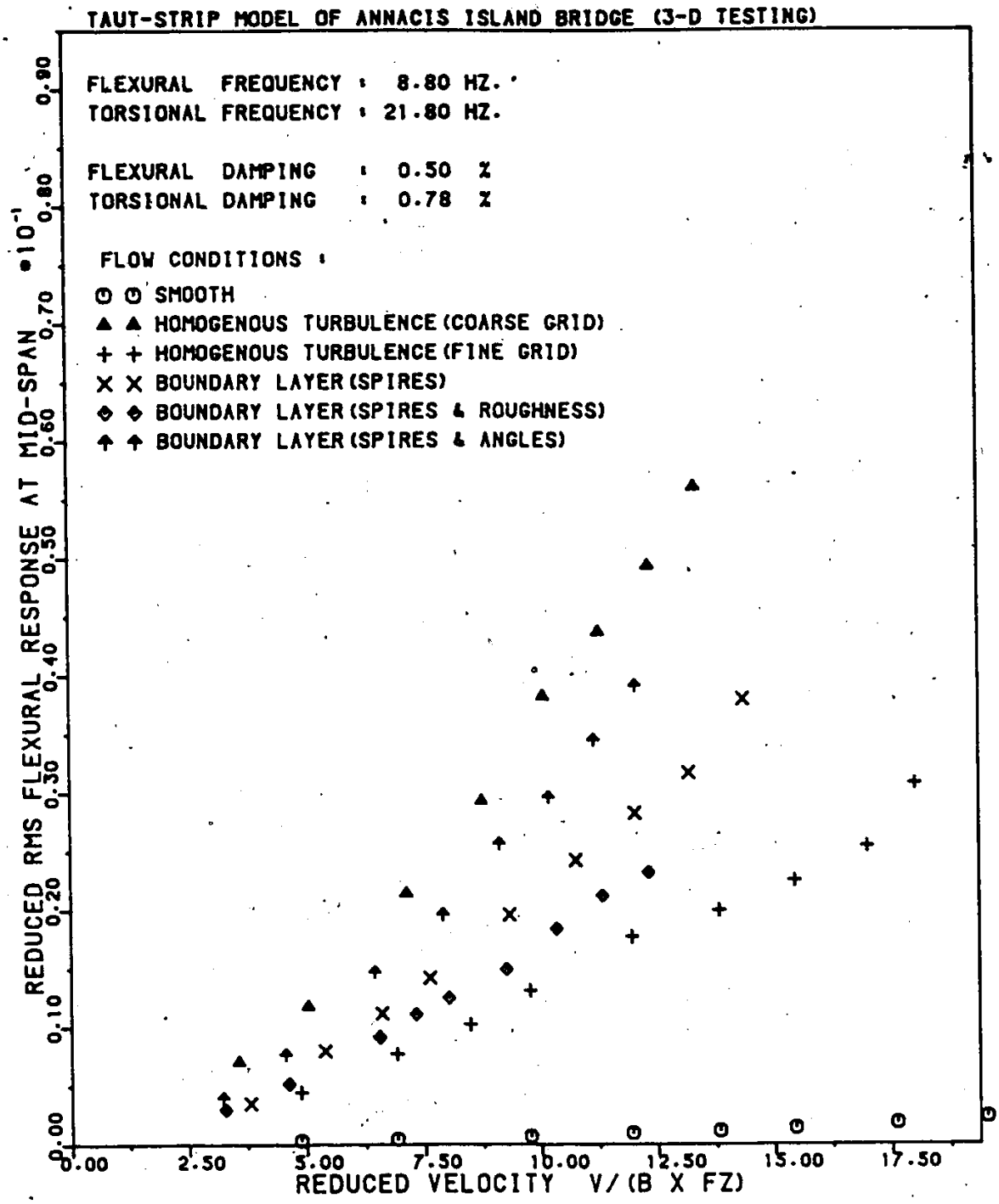

Figure 3.4.6: Buffeting Response against Reduced Velocity (3-D) : FA = 21.8 Hz , FZ = 8.8 Hz

(a) Flexural response

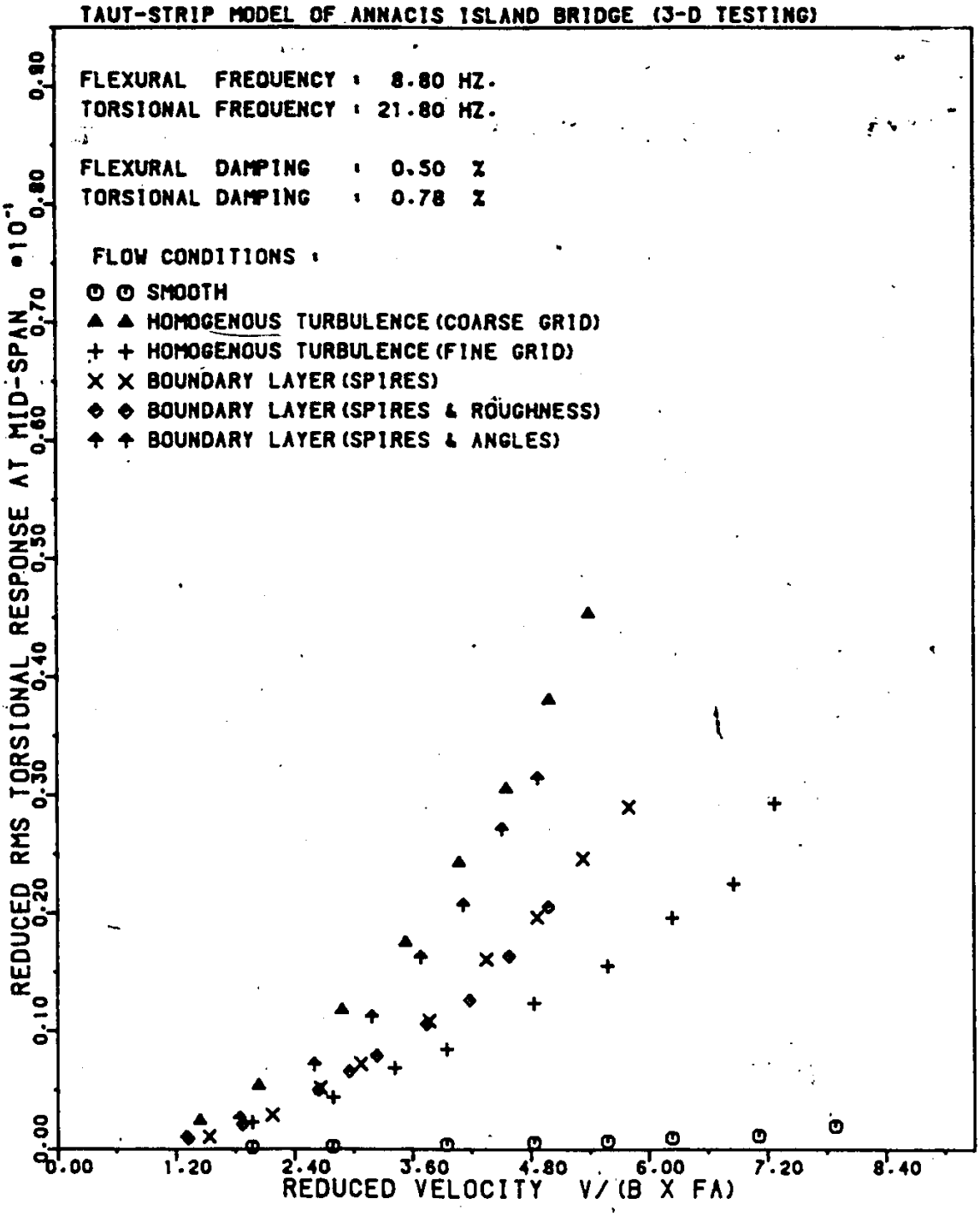

Figure 3.4.6: Buffeting Response against Reduced Velocity (3-D) : FA = 21.8 Hz , FZ = 8.8 Hz

(b) Torsional response

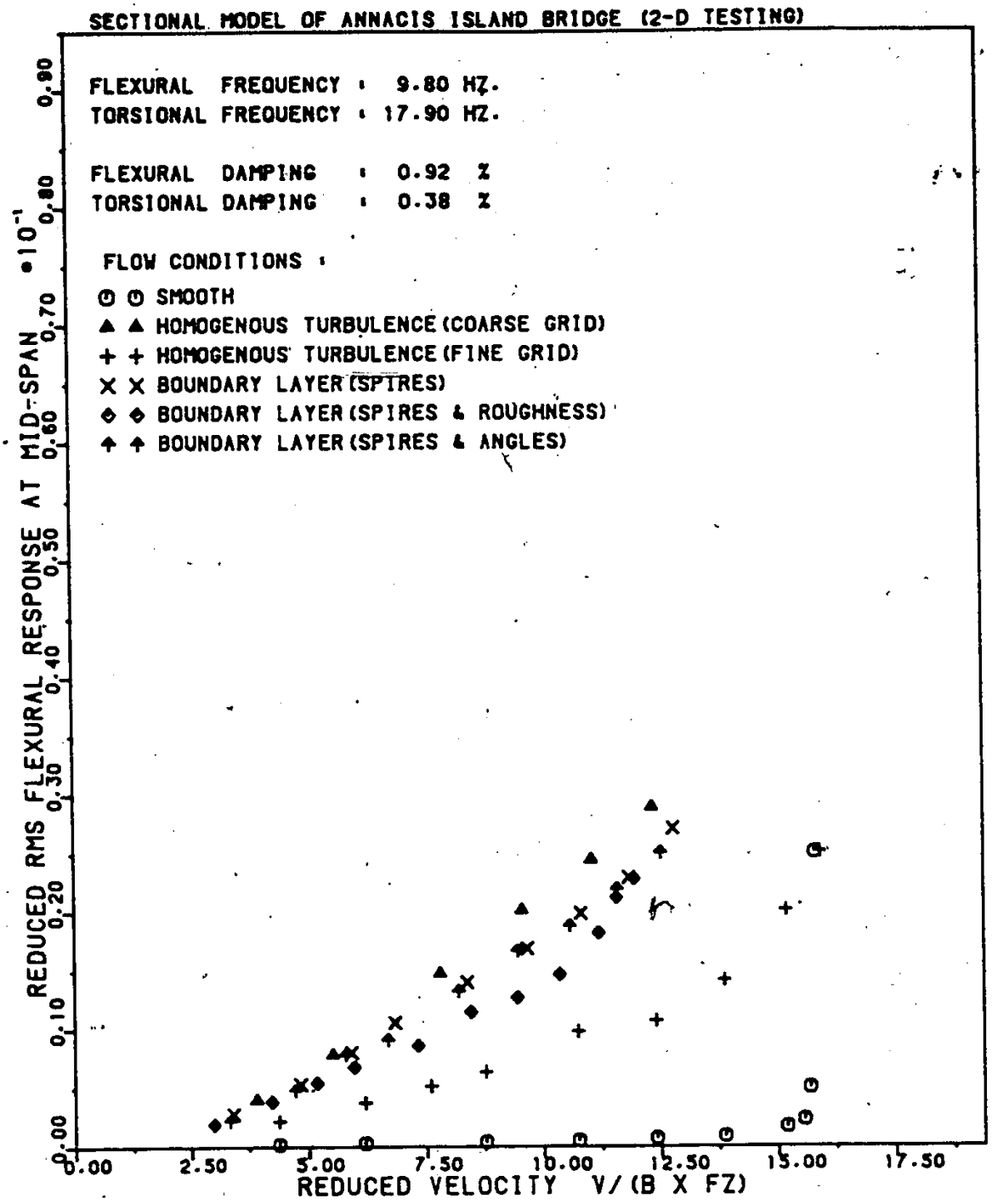

Figure 3.4.7: Buffeting Response against Reduced Velocity (2-D) : FA = 17.9 Hz , FZ = 9.8 Hz

(a) Flexural response

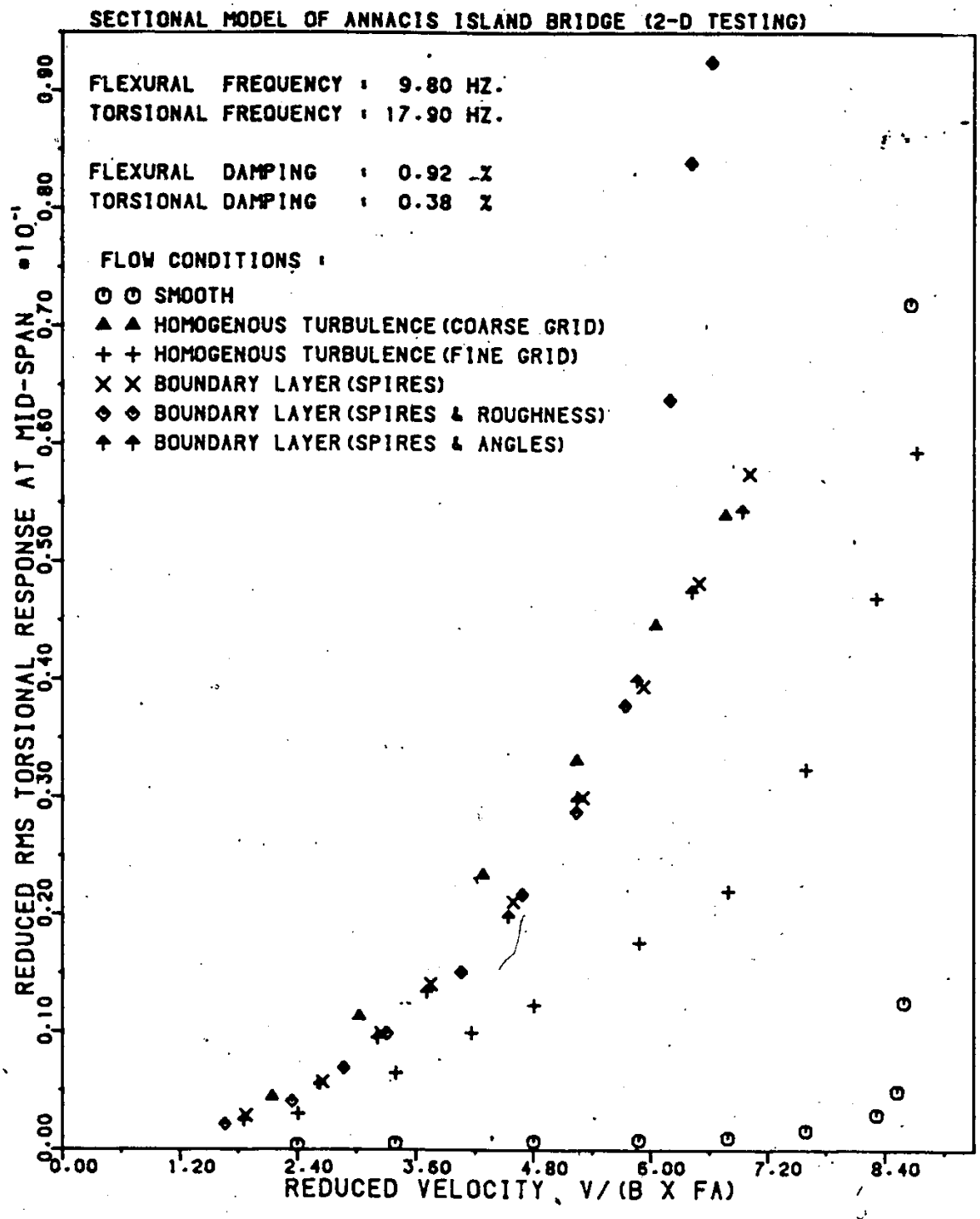

Figure 3.4.7: Buffeting Response against Reduced Velocity (2-D) : FA = 17.9 Hz , FZ = 9.8 Hz

(b) Torsional response

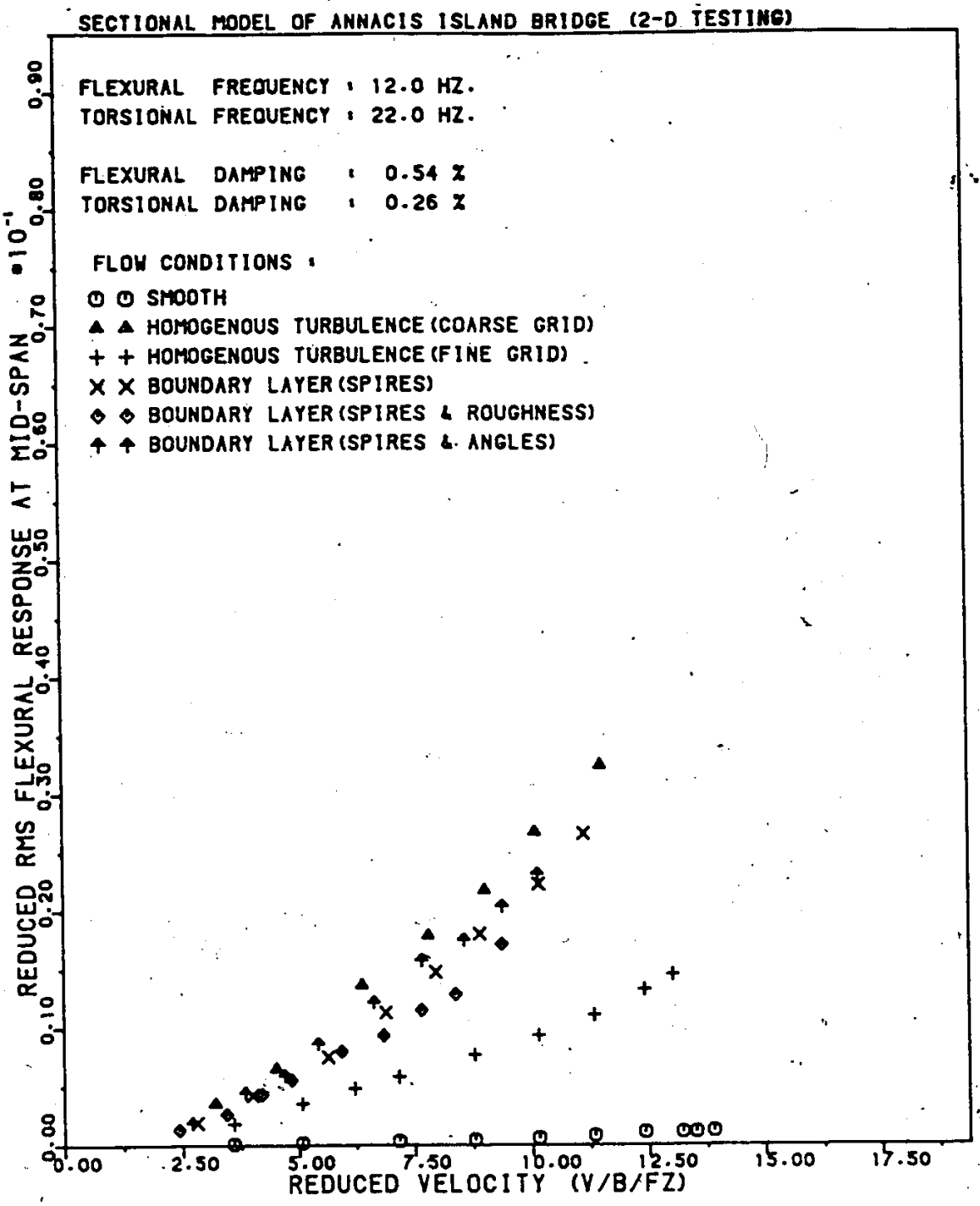

Figure 3.4.8: Buffeting Response against Reduced Velocity (2-D) : FA = 22.0 Hz , Fz = 12.0 Hz

(a) Flexural response

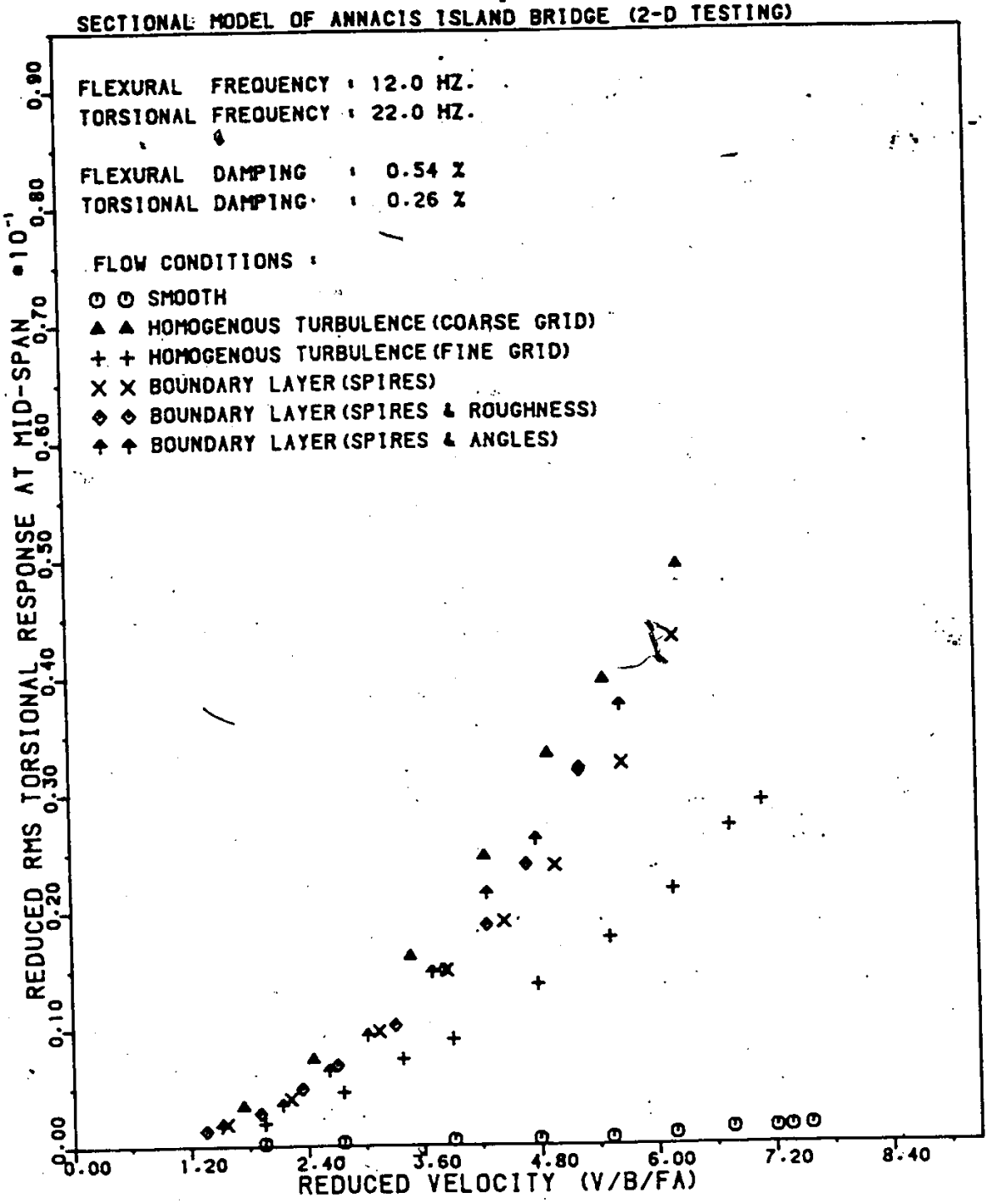

Figure 3.4.8: Buffeting Response against Reduced Velocity (2-D) : FA = 22.0 Hz , Fz = 12.0 Hz

(b) Torsional response

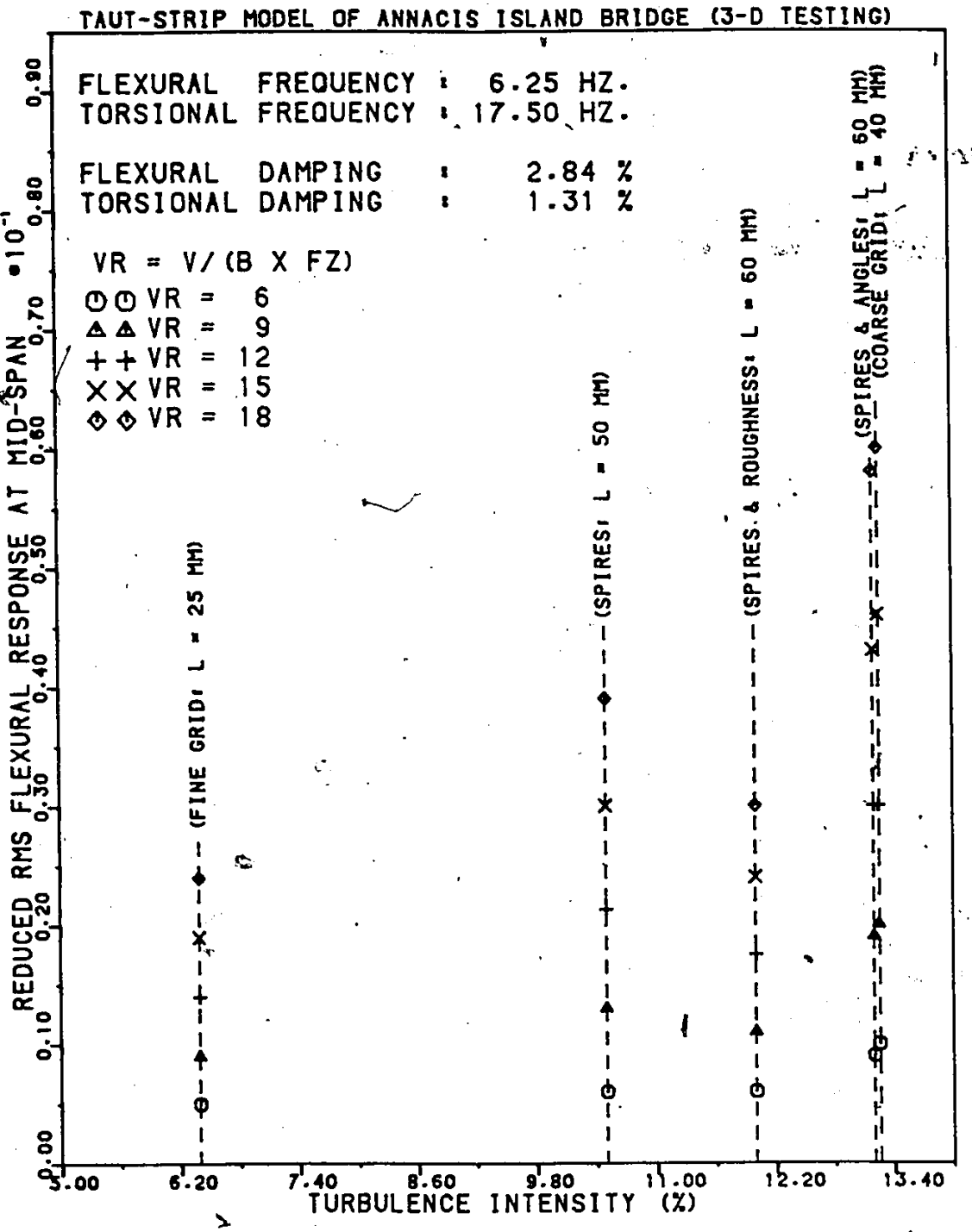

Figure 4.2.1.1: Buffeting response against Turbulence Intensity (3-D) : FA = 17.5 Hz , FZ = 6.25 Hz

(a) Flexural response

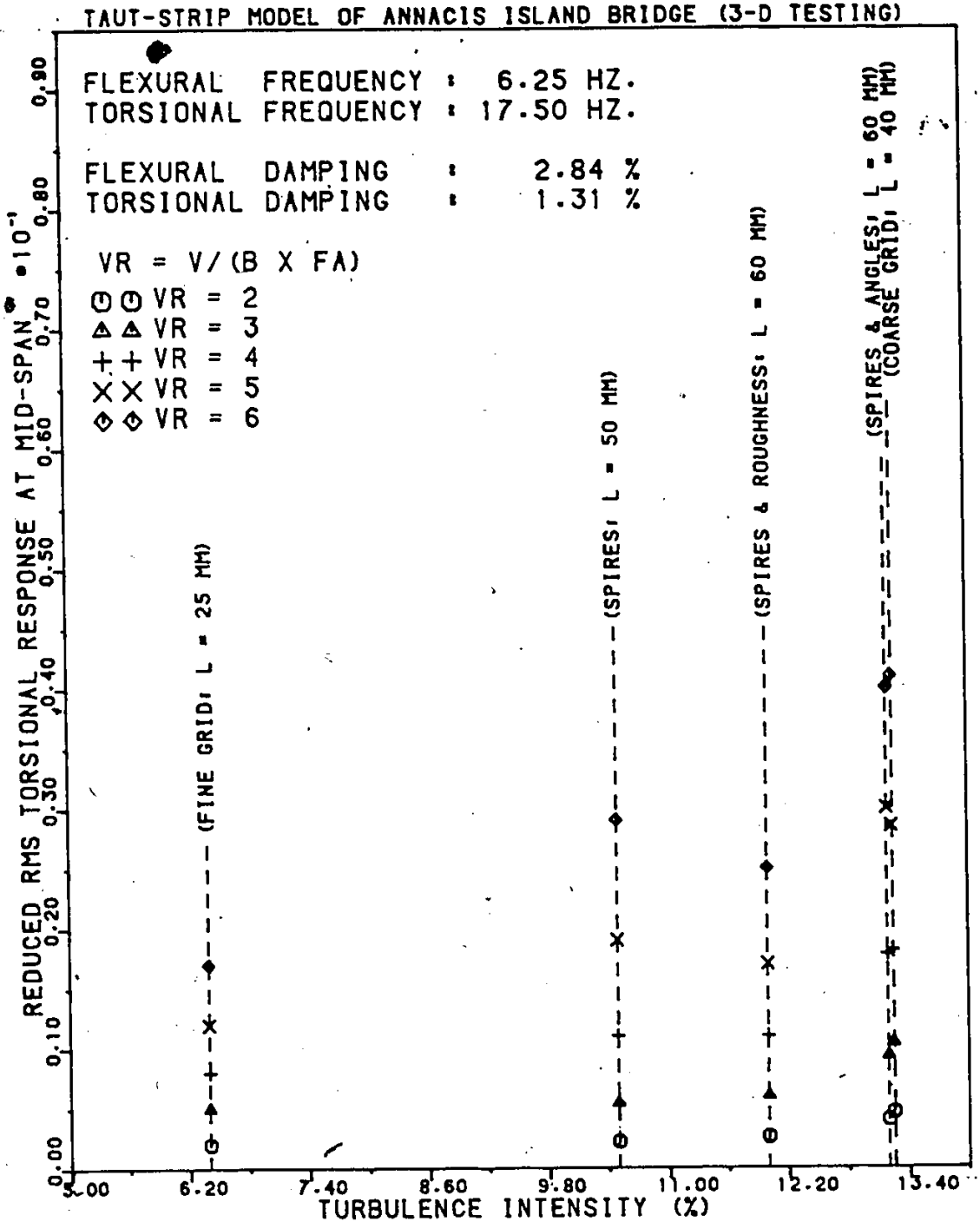

(b) Torsional response

Figure 4.2.1.1: Buffeting response against Turbulence Intensity (3-D) : FA = 17.5 Hz , FZ = 6.25 Hz

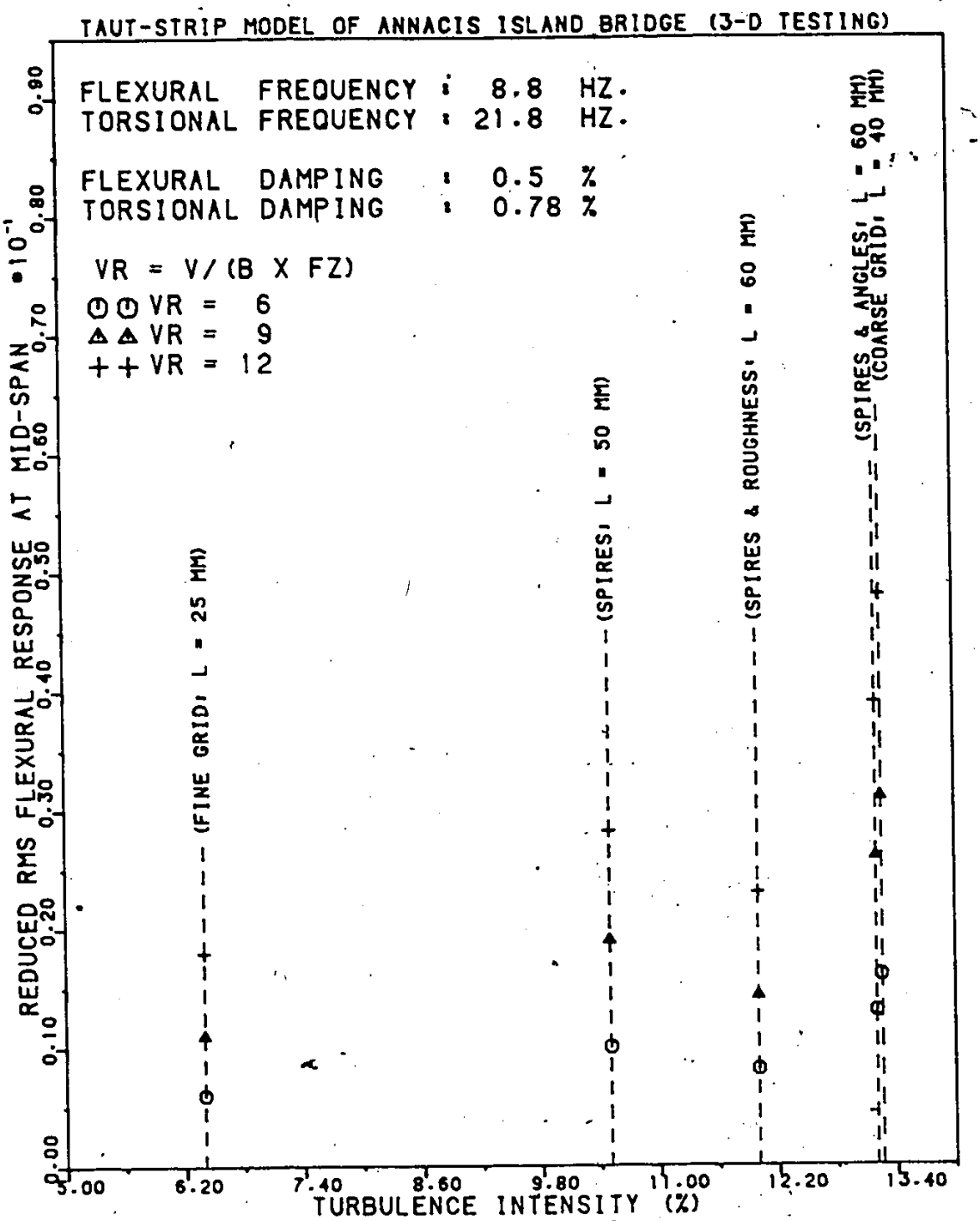

Figure 4.2.1.2: Buffeting response against Turbulence Intensity (3-D) : FA = 21.8 Hz , FZ = 8.8 Hz

(a) Flexural response

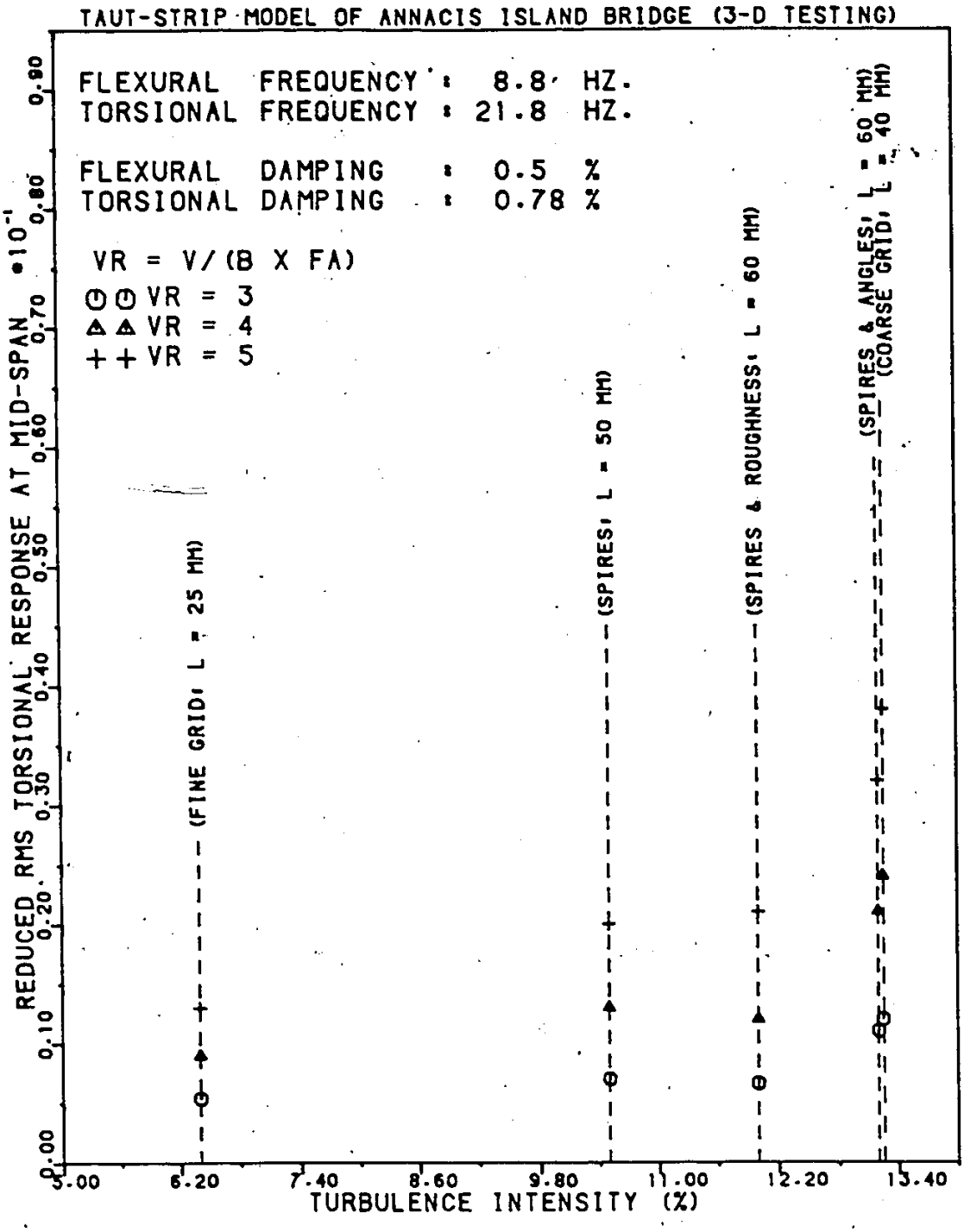

(b) Torsional response

Figure 4.2.1.2: Buffeting response against Turbulence Intensity (3-D) : FA = 21.8 Hz , FZ = 8.8 Hz

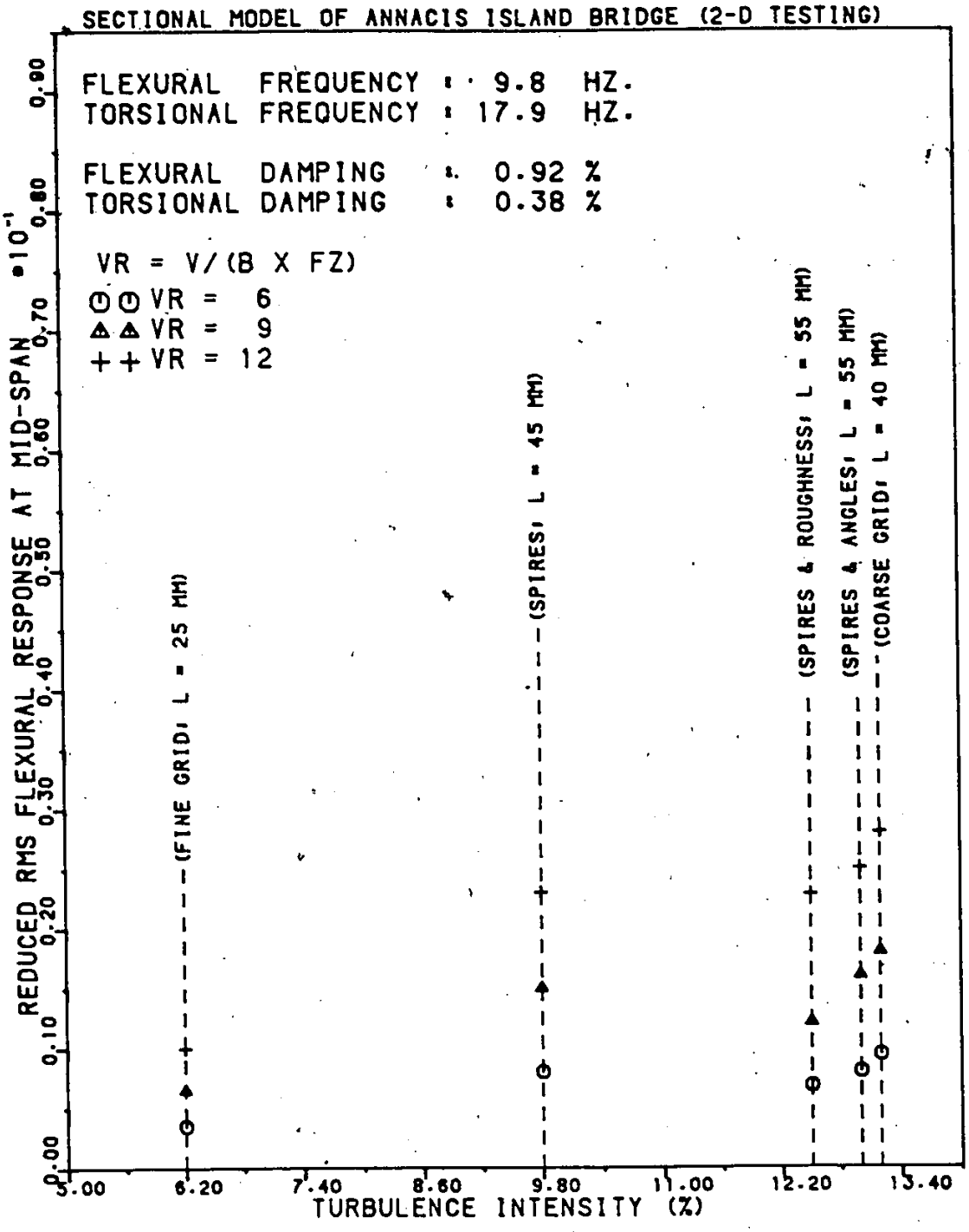

Figure 4.2.2.1: Buffeting response against Turbulence Intensity (2-D) : FA = 17.9 Hz , FZ = 9.8 Hz

(a) Flexural response

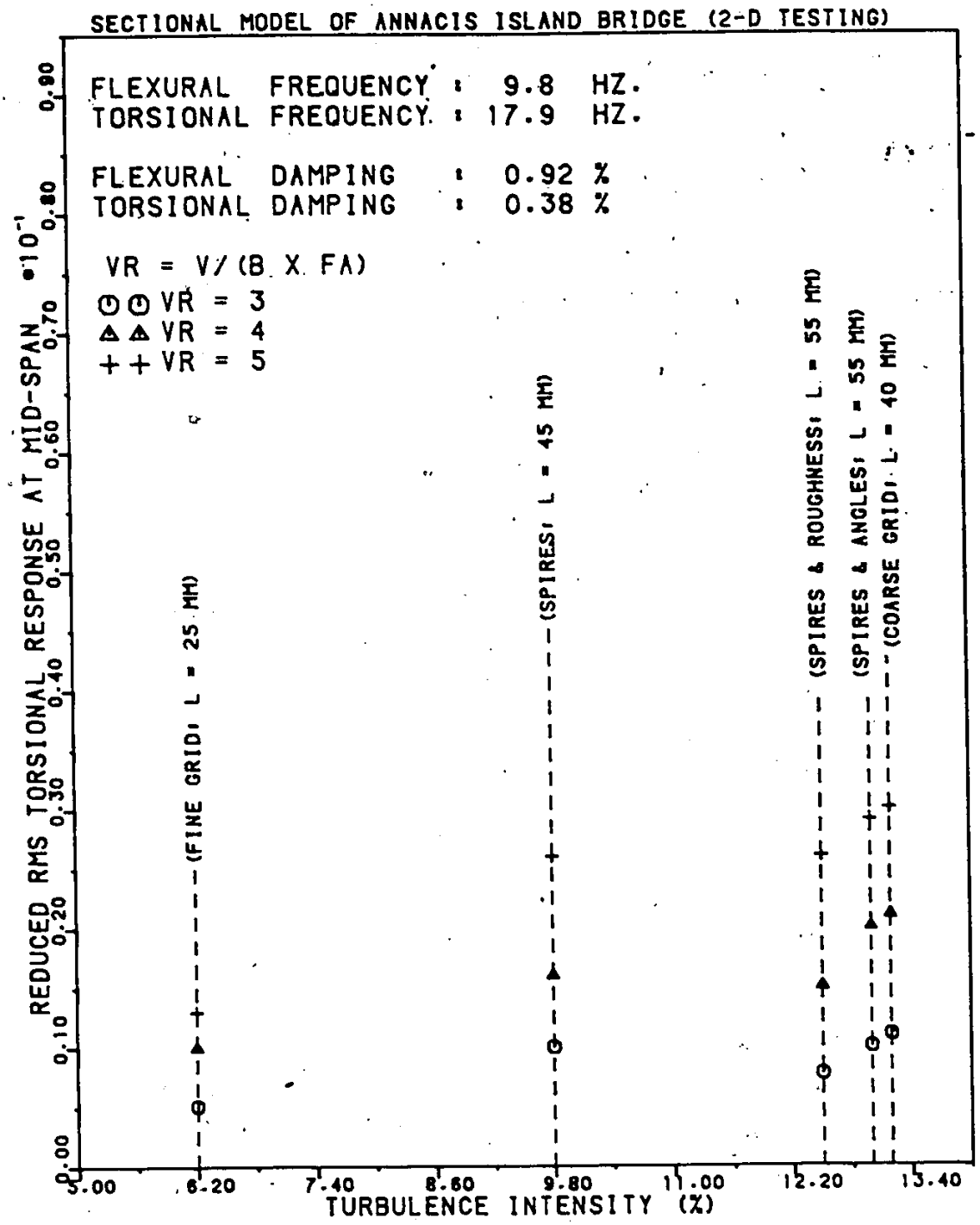

(b) Torsional response

Figure 4.2.2.1: Buffeting response against Turbulence Intensity (2-D) : FA = 17.9 Hz , FZ = 9.8 Hz

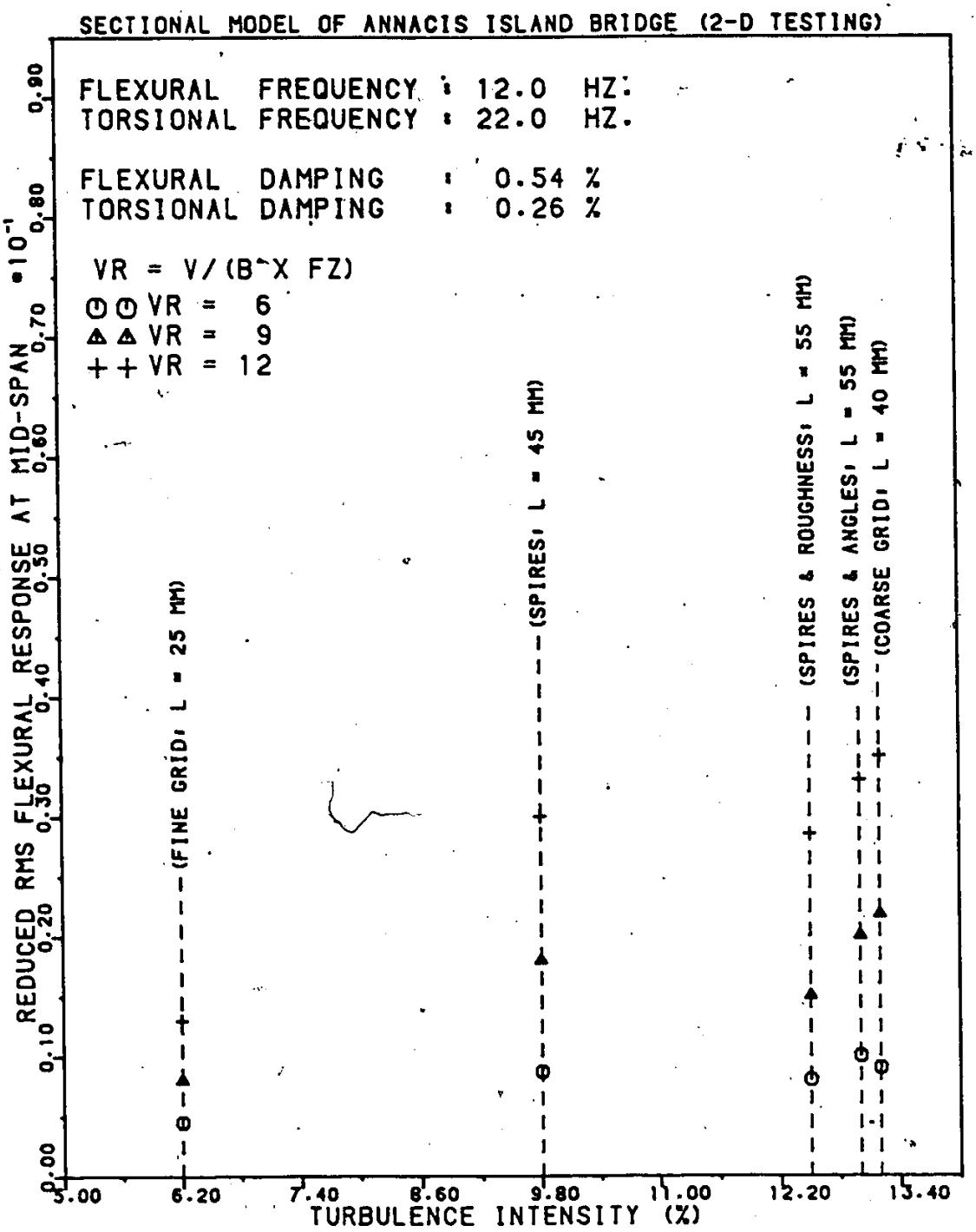

Figure 4.2.2.2: Buffeting response against Turbulence Intensity (2-D) : FA = 22.0 Hz , Fz = 12.0 Hz
(a) Flexural response

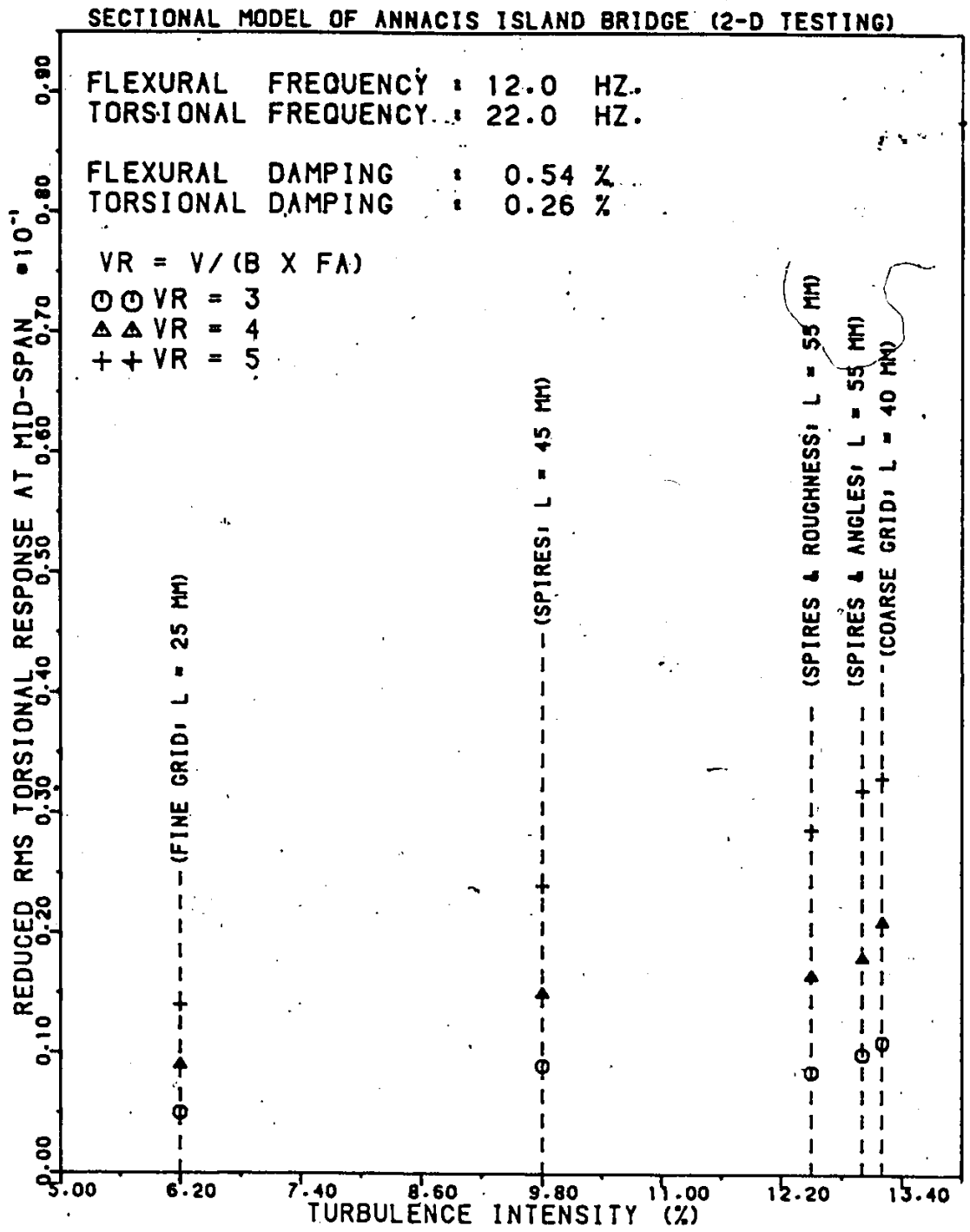

(b) Torsional response

Figure 4.2.2.2: Buffeting response against Turbulence Intensity (2-D) : FA = 22.0 Hz , Fz = 12.0 Hz

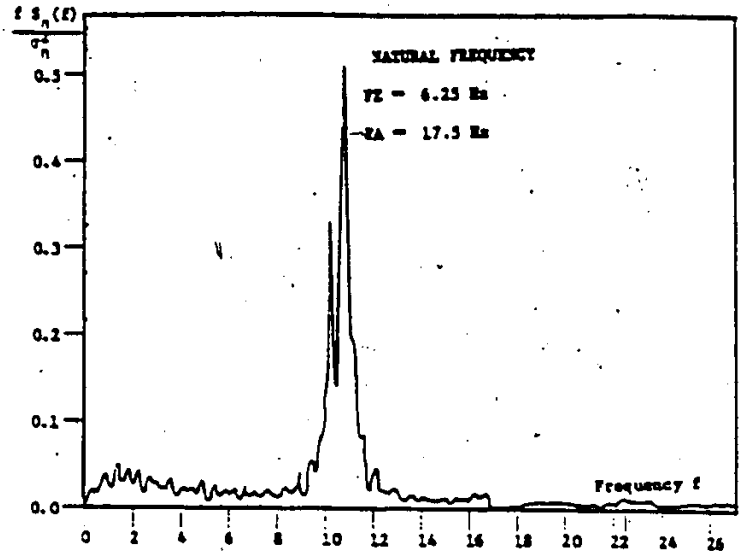

(a) normalized spectrum of vertical bending

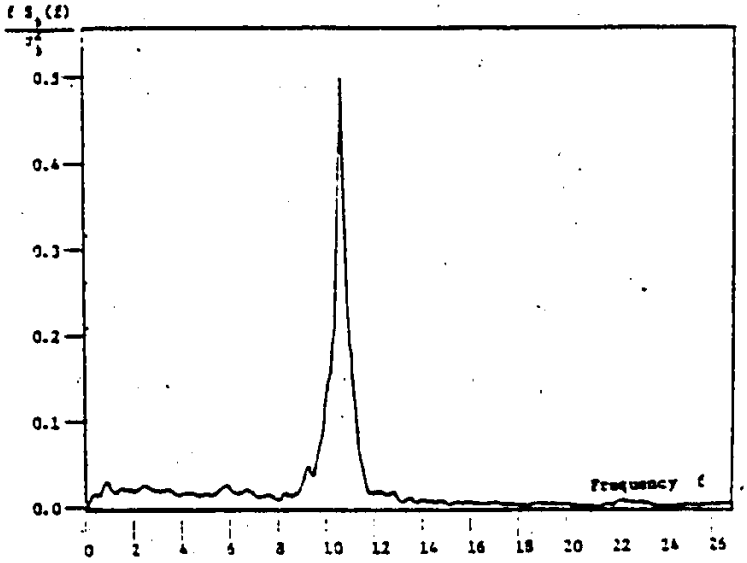

(b) normalized spectrum of torsion

Figure 4.1.1.1: Response spectra of taut strip model at aerodynamic instability

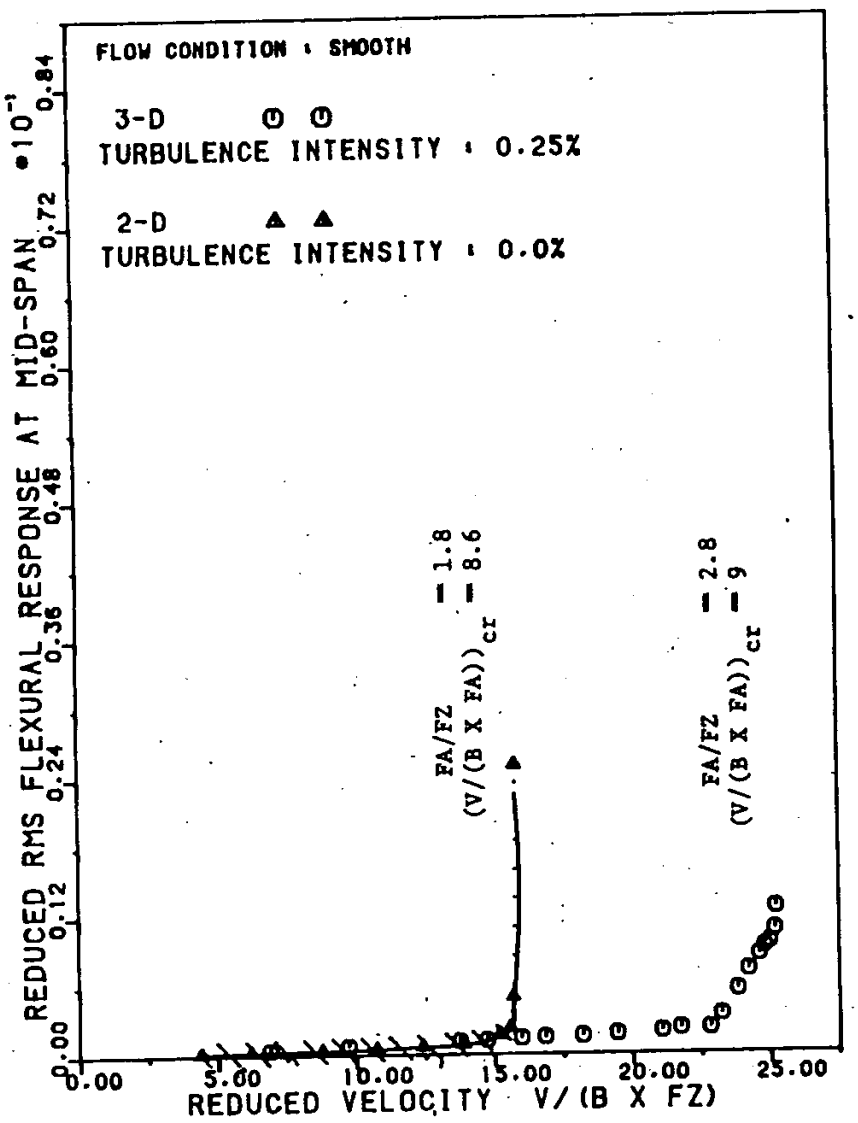

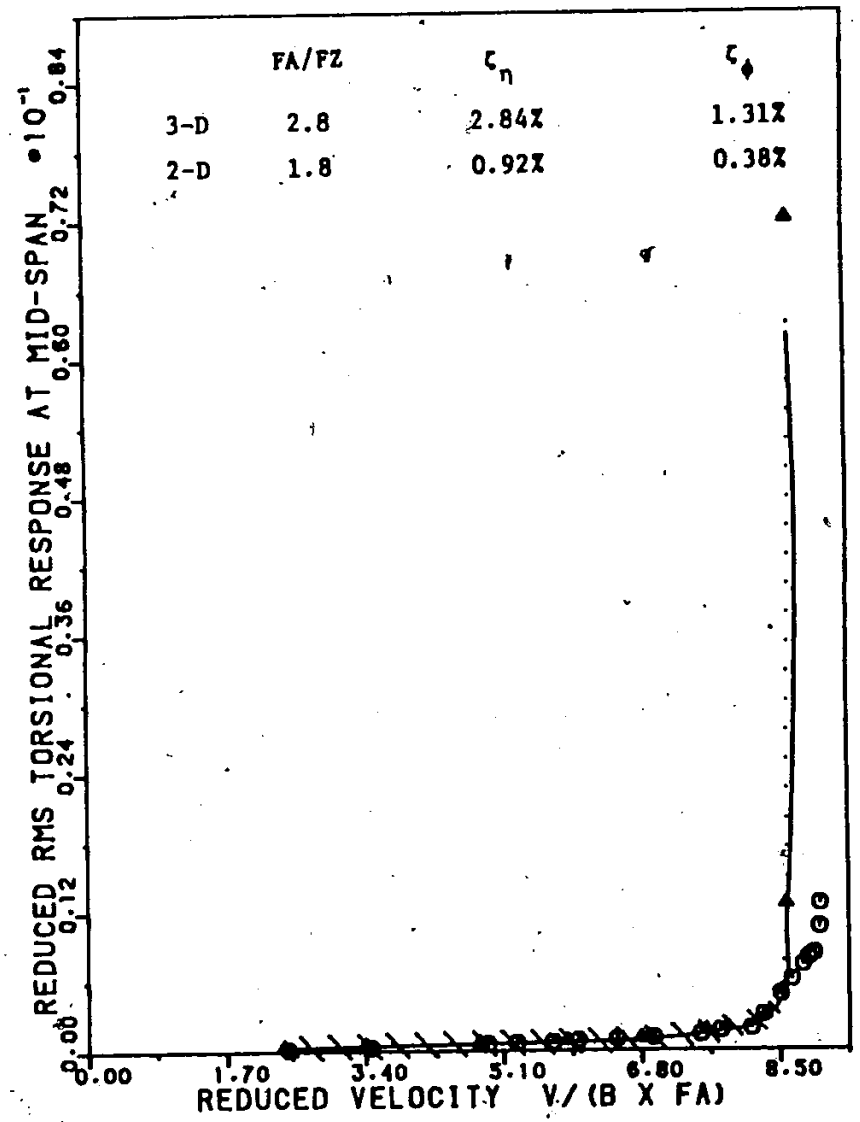

Figure 4.3.1: Comparison of 3-D and 2-D buffeting response : Smooth

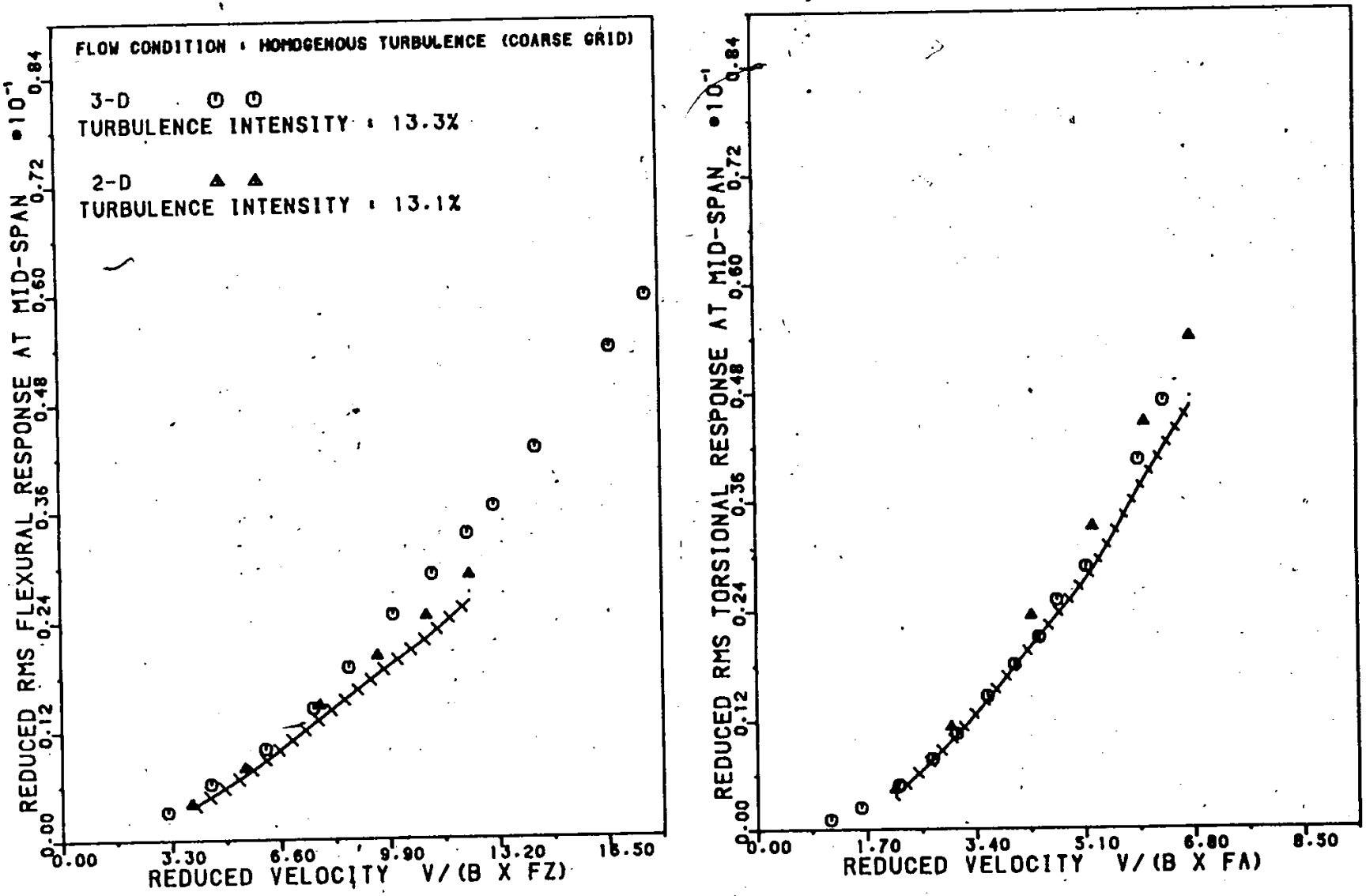

Figure 4.3.1: Comparison of 3-D and 2-D buffeting response : Coarse Grid

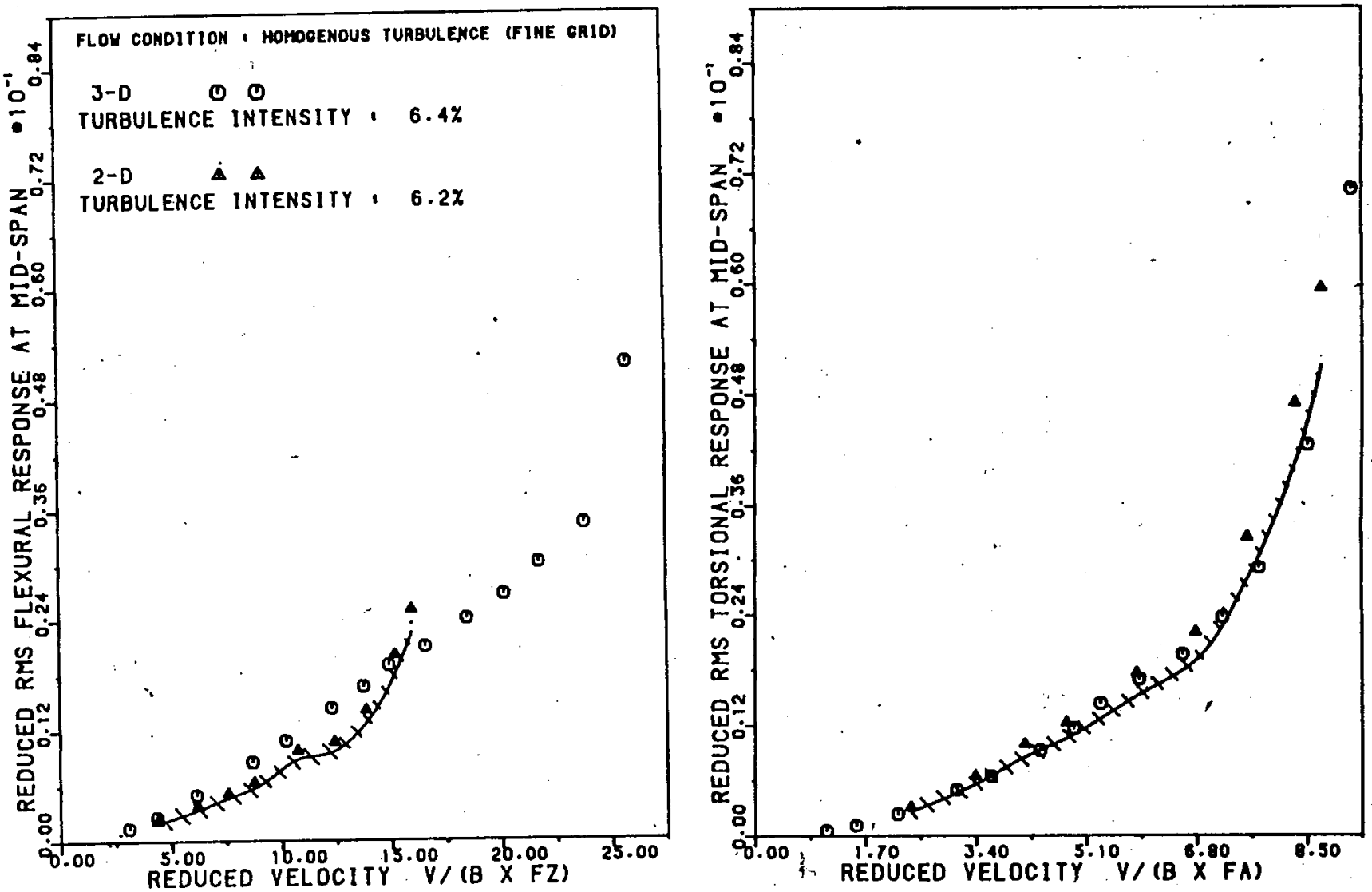

Figure 4.3.1: Comparison of 3-D and 2-D buffeting response : Fine Grid

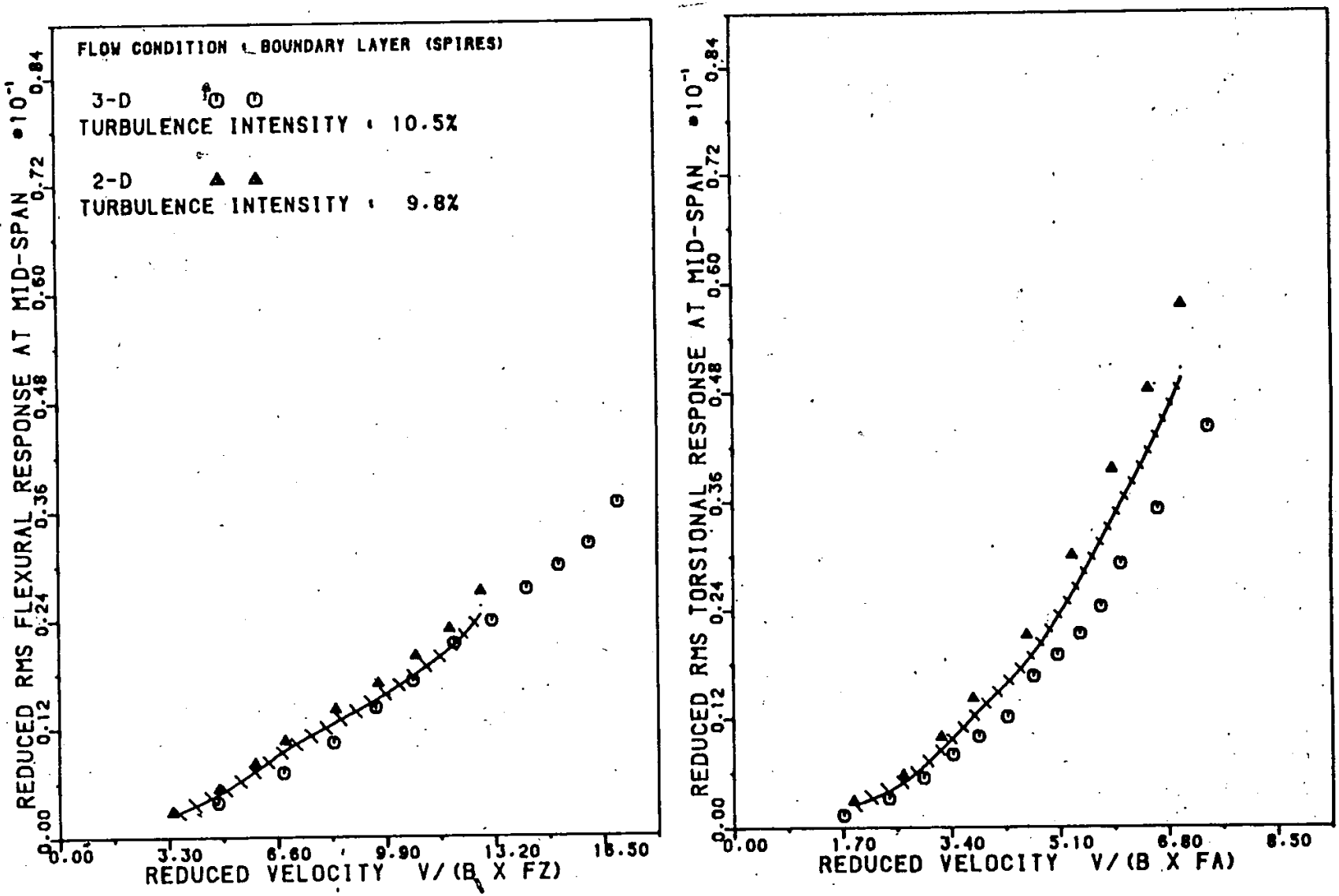

Figure 4.3.1: Comparison of 3-D and 2-D buffeting response : Spires

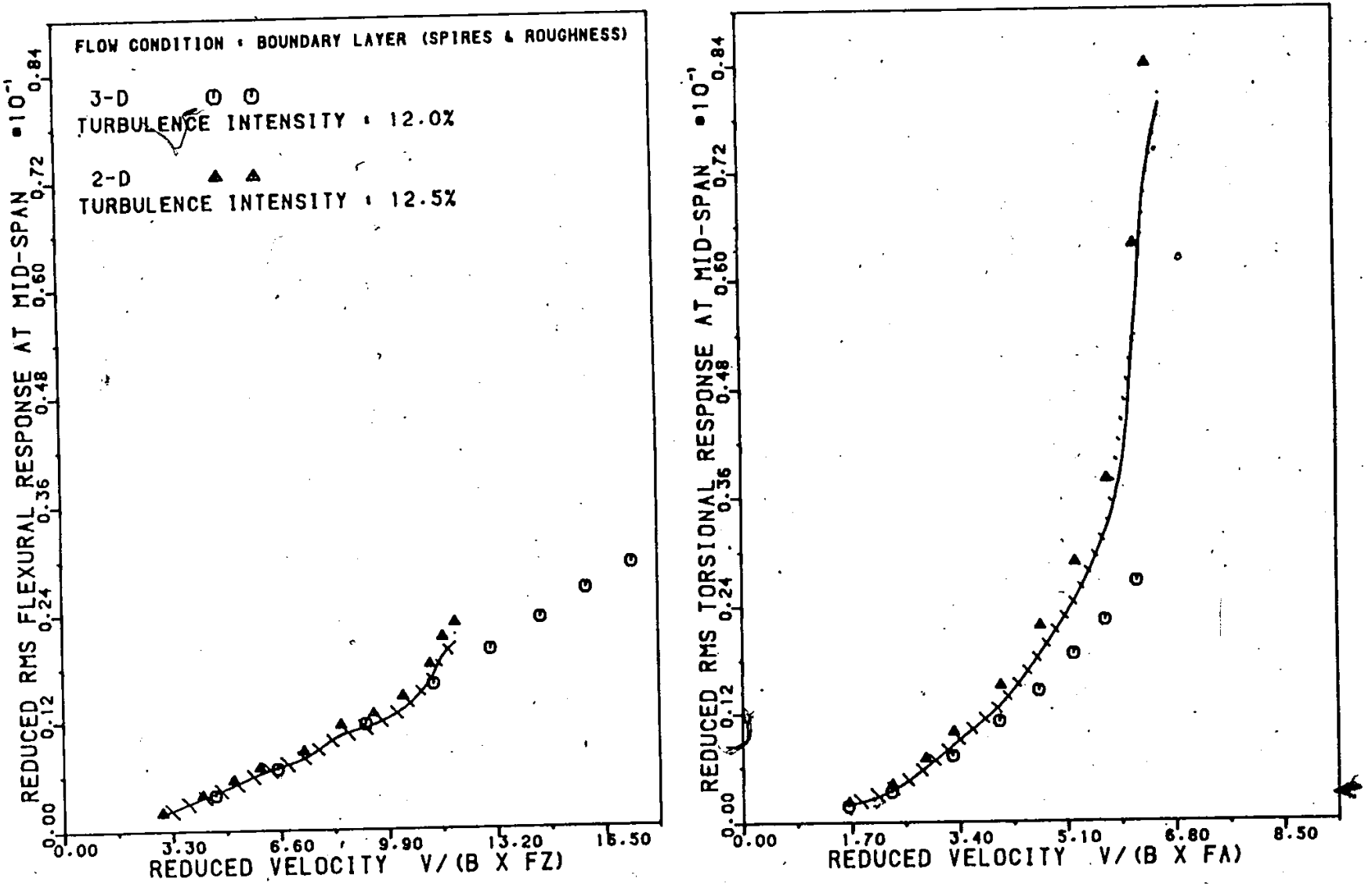

Figure 4.3.1: Comparison of 3-D and 2-D buffeting response : Spires and Roughness

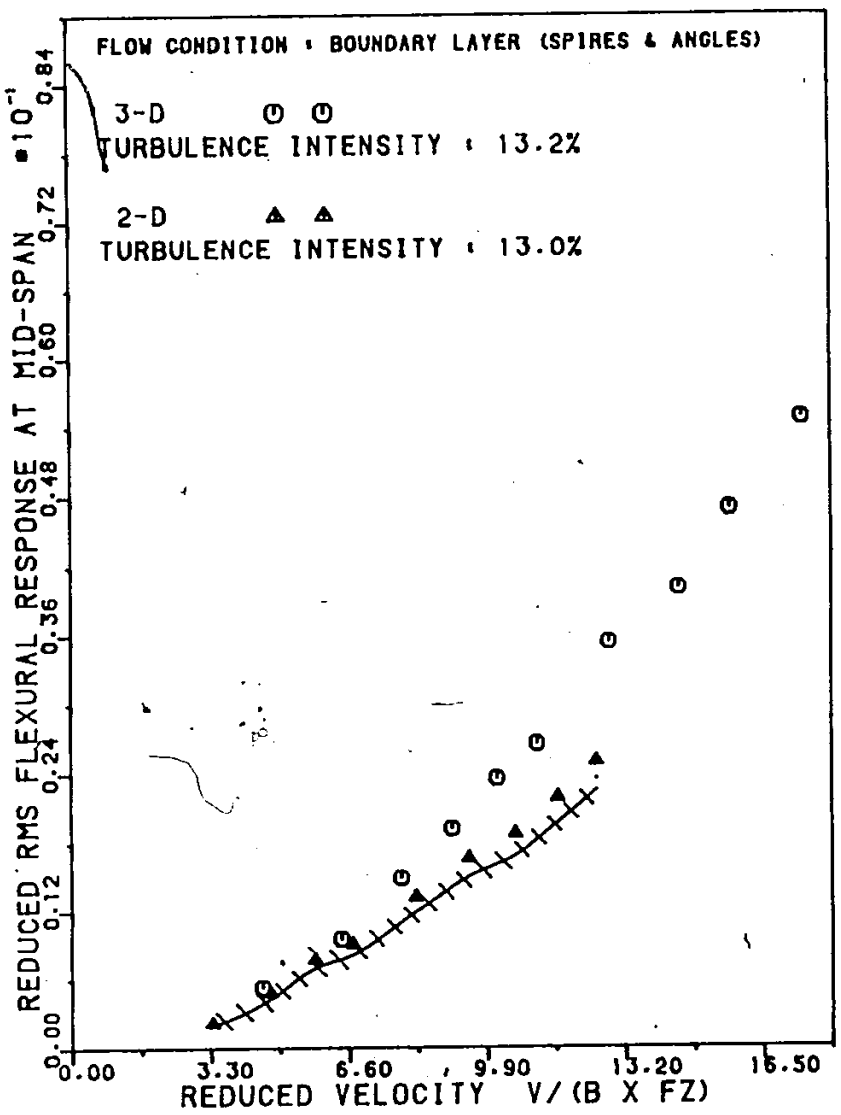

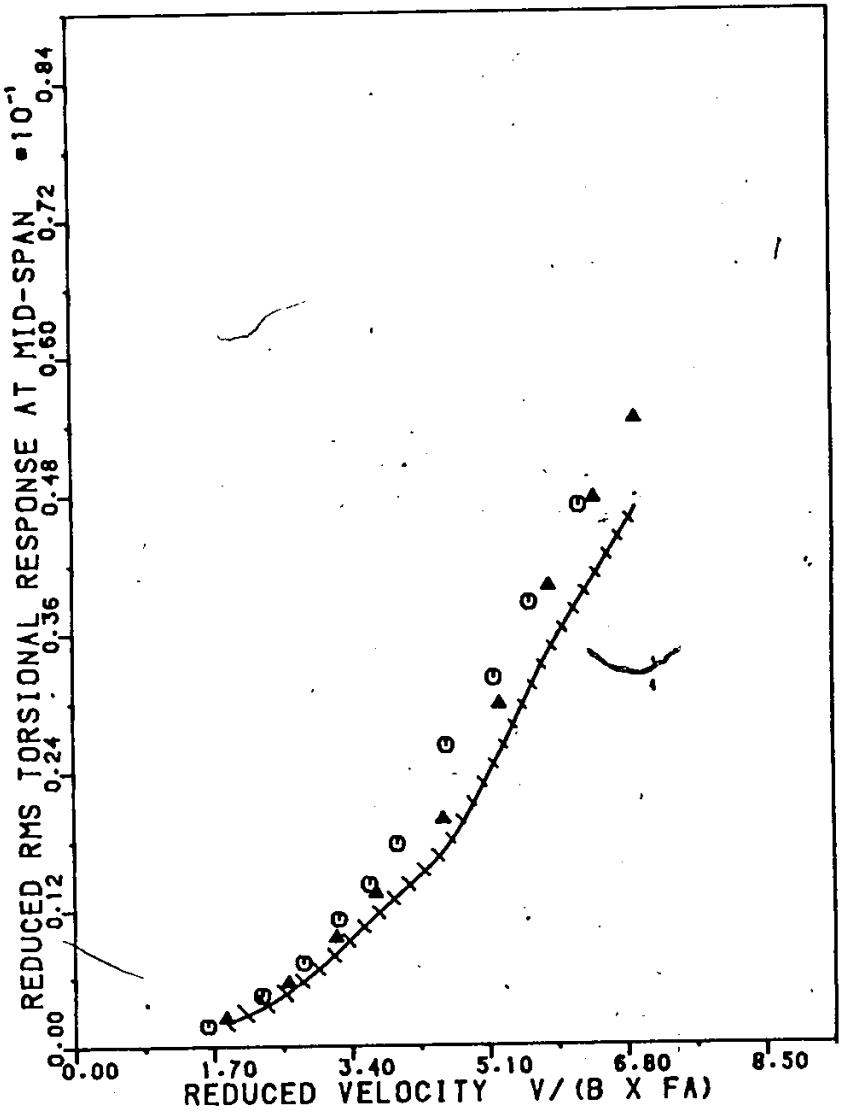

Figure 4.3.1: Comparison of 3-D and 2-D buffeting response : Spires and Angles

Appendix A

CALIBRATION

A.1 FREE VIBRATION

The model was manually excited in either vertical or torsional mode. The corresponding signal trace was recorded by the chart recorder. From this trace, the natural frequency and structural damping can be calculated.

Example :

Torsional (i.e. signal(A-B)/2)

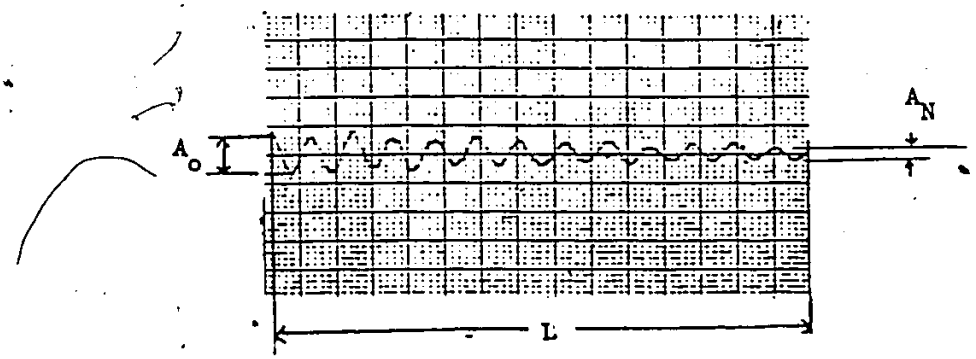

Velocity of chart moving = 100.0 mm/sec.

This is a particular tracing of 3-D model in torsional mode.

$L = 16 \times 5$ mm

N = number of cycles = 14

$$FA = \frac{14 \times 100}{80} = 17.5 \text{ Hz}$$

$A_o = 0.6$ cm.

$A_N = 0.19$ cm.

$$\delta = \frac{1}{14} \log_e \frac{0.6}{0.19} = 0.082$$

$$\zeta_\phi = 100 \times \frac{\delta}{2 \times \pi} = 1.31\%$$

The results of the other schemes are shown in Table A1

A.2 CALIBRATION FOR MODEL RESPONSES

The model deflection was detected usind Kaman displacement transducers at the end of the bridge model immediately outside the wind tunnel. The deflections of both taut wires were measured, and hence, the sum and difference of these two signals would give the vertical and torsional responses, respectively.

A.2.1 Vertical response

Calibration to convert these data to the model deflection was done as follows :

A micrometer head was placed at the centre of the mid-span point of the bridge model. A known magnitude of displacement was given and the corresponding voltage displayed on the voltmeter was recorded. The same process was repeated for a several steps. From the plotting of displacement against outpput voltage, the calibration factor was decided. The results are listed in Table A2 and a general sketch to illustrate the above discription is shown :

A.2.2 Torsional response

In order to assure the pure torsional displacement, on the edge of the girder was pushed by the micrometer head and the middle point of the bridge deck was supported by a pin point to fix the centre of rotion. The results are listed in Table A2 and a general sketch to illustrate the above discription is shown as follow :

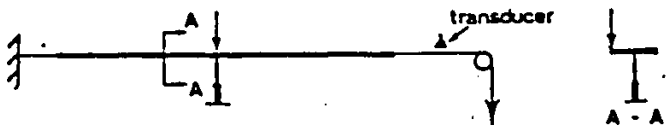

TABLE A1

MODEL	FA/FZ	CALIBRATION VALUES	
		BENDING mm/mv	TORSION degree/mv
3-D	2.8	0.1	0.0018
	2.5	0.1	0.0018
2-D	1.8	0.08	0.0036
	1.79	0.1	0.0036

TABLE A_2

MODEL		FZ(Hz)	FA(Hz)	ζ_n(%)	ζ_ϕ(%)
3-D	1	6.25	17.5	2.8	1.31
	2	8.8	21.8	0.78	0.5
2-D	1	9.8	17.9	0.92	0.38
	2	12.0	22.0	0.54	0.26

Appendix B

PARAMETRIC ANALYSIS

Although the mathematical formulation to calculate the aerodynamic response of bridge deck is complicated, simplified attempts have been made. The following mathematical formulation largely depends on Ref.[12].

B.1 INTRODUCTION TO AERODYNAMIC RESPONSES OF PLATE-LIKE STRUCTURES

The random oscillation of a flat-plate in the wind is a superposition of both the torsional and bending vibrations in their own modes, which can be analysed in each mode separately. However, the aerodynamic instability is a coupled motion in these two modes. Basically, the buffeting response is decided by the aerodynamic forces, aerodynamic admittance function, frequency response function of the system, joint acceptance function and power spectral density of gust. The aerodynamic instability, on the other hand, will be decided from the frequency response function and the aerodynamic forces.

In simplified the analytical approach, employs the combination of equations in vertical bending and torsion together with quasi-steady or unsteady aerodynamic forces can be employed to calculate the response of long span bridges. In doing so, usually, the nonlinear aerodynamic terms are ignored. The experimental results from a paper[10] have indicated that the approach using quasi-steady aerodynamic forces gives rather conservative estimate

of amplitude for bending and even more conservative for torsion. The same paper [8] also suggests that if the difference between bending and torsional frequencies is significant, the neligence of coupling terms can be justified. In the other extreme, when the low frequency ratio(FA/FZ) is given, the aerodynamic coupling force is considered to be the most important factors. Considering both the vertical and torsional vibration of an aerofoil, Theodorsen proposed a theory [7] to describe the unsteady self-excitation forces in steady air flow. His philosophy was to assume a streamline body, with high aspect ratio(i.e. the ratio of the span length to the chord length is infinity), submerged in a steady air flow and vibrated with small amplitude. The application of this theory to calculate the aerodynamic responses can be briefly illustrated in the following sections[12].

B.2 FORMULATION OF THE EQUATIONS OF COUPLED MOTION

Consider the section of a streamlined bridge deck with two degrees of freedom Z & Φ as shown in figure below. The elastic axis and gravity centre were assumed at the centre-chord of the bridge deck. The lateral sway was ignored in the formulation since the lateral motion can be assumed to be negiligibly small.

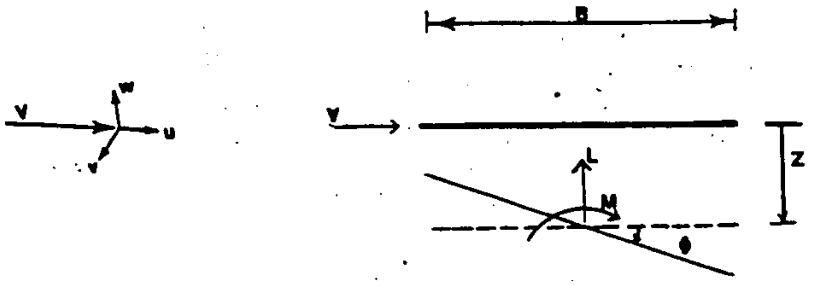

Assuming that the modes of vibration in bending and torsion have an orthogonal relationship between each other , and that each oscillation can be expressed by a linear equation, the equations of motion in can be written in a simplified form as follows :

$$m (\ddot{Z} + 2\zeta_z \omega_z \dot{Z} + \omega_z^2 Z) = -L$$

$$\theta (\ddot{\Phi} + 2\zeta_\phi \omega_\phi \dot{\phi} + \omega_\phi^2 \phi) = M \qquad \text{(B.2.1)}$$

Note : all symbols can be referred to nomenclatures.

B.3 AERODYNAMIC FORCES ACTING ON PLATE

The aerodynamic forces acting on a vibrating model in two modes consist of unsteady self-excitation terms and the random buffeting force. In order to study the aerodynamic problems of the structures in strong wind, it is usually required either to perform aeroelastic tests to measure the induced response, or to conduct aerodynamic tests to investigate the aerodynamic forces. However, for a model with a plate-like shape, the aerodynamic characteristics have already been pointed out in many past investigators. Their results can be used to describe the aerodynamic forces acting on a particular plate-like structure such as the proposed Annacis Island Bridge - concrete version.

The approximate expressions for the unsteady aerodynamic lift and pitching moment, acting on a plate which vibrates in coupled modes of circular frequency ω in a wind stream are :

$$L = -\pi\rho b^3\omega^2 \{ L_z \frac{Z}{b} + L_\phi \phi \} + L_f(t)$$

$$M = \rho b^4\omega^2 \{ M_z \frac{Z}{b} + M_\phi \phi \} + M_f(t) \qquad (B.3.1)$$

where L_z, L_ϕ, M_z, M_ϕ, are the aerodynamic coefficients, which are in terms of Theodorsen's function, C(k), to describe the self-excited forces.

L_f, M_f are the random lift force and pitching moment which are time dependent.

$|\chi_w^m|$ and $|\chi_w^\iota|$ are the aerodynamic admittance function which reflect the aerodynamic effectiveness of the bridge structure in translating velocity fluctuations into vertical and pitching forces.

They are expressed as follows :

$$L_f(t) = \frac{\rho\bar{V}^2}{2} B \frac{\partial C_l}{\partial\phi} \frac{w(t)}{\bar{V}} |\chi_w^\iota| \qquad (B.3.2)$$

$$M_f(t) = \frac{\rho\bar{V}^2}{2} B^2 \frac{\partial C_m}{\partial\phi} \frac{w(t)}{\bar{V}} |\chi_w^m|$$

$$L_z = -\frac{2\pi}{k} C(k) \qquad L_\phi = -\frac{2}{k^2} C(k) - \frac{1}{k}[\, 1 + C(k) \,]$$

$$M_z = \frac{1}{k} C(k) \qquad M_\phi = \frac{1}{k^2} C(k) - \frac{1}{2k}[\, 1 - C(k) \,] \qquad (B.3.3)$$

in which $k = \frac{\omega b}{V}$ = reduced frequency ; $i = \sqrt{-1}$;

$C(k) = F(k) + iG(k)$ [6];

ρ = air density; V = mean wind speed at deck height ; B = width of the model deck;

$b = B/2$; $\frac{\partial C_m}{\partial \phi} = \pi/2$; $\frac{\partial C_l}{\partial \phi} = 2\pi$;

v(t) = vertical instantaneous velocity.

By using the following dimensionless terms

$$\eta = z/b \qquad \beta = FA/FZ$$

$$\mu = \frac{m}{\pi \rho b^2} \qquad \xi = F/FZ$$

$$\nu = \frac{\theta}{\pi \rho b^4}$$

Eq. (B.2.1) can be rewritten as follows :

$$\ddot{\eta} + 2\zeta_z \omega_z \dot{\eta} + \omega_z^2 \eta = -\frac{L}{mb} \qquad (B.3.4)$$

$$\ddot{\phi} + 2\zeta_\phi \omega_\phi \dot{\phi} + \omega_\phi^2 \phi = \frac{M}{\theta}$$

B.4 SOLUTION OF THE EQUATIONS OF COUPLED MOTION

Assuming that the vertical deflection, Z , and the angular rotation, ϕ , are harmonic oscillations with the common frequency, and they can be expressed in the following complex form :

$$Z = \bar{Z}\, e^{i\omega t} \quad \text{and} \quad \phi = \bar{\phi}\, e^{i\omega t} \qquad (B.4.1)$$

From previous eq. (B.3.4) , the solution is given as follows :

$$\begin{vmatrix} \mu(1-\xi^2+i2\zeta_z\xi)-\xi^2L_z & -\xi^2L_\phi \\ -\xi^2M_z & \nu(\beta^2-\xi^2+i2\zeta_\phi\beta\xi)-\xi^2M_\phi \end{vmatrix} \begin{vmatrix} \eta \\ \phi \end{vmatrix} = \begin{vmatrix} -L_f(t) \\ M_f(t) \end{vmatrix} \qquad (B.4.2)$$

Eq. (B.4.2) is written in a simplier form :

$$\begin{bmatrix} A_1 & A_2 \\ A_3 & A_4 \end{bmatrix} \begin{bmatrix} \eta \\ \phi \end{bmatrix} = \begin{bmatrix} L \\ M \end{bmatrix} . \qquad (B.4.3)$$

or

$$\eta = \frac{1}{\Delta}(A_4L - A_2M) = X_{zz}L - X_{z\phi}M$$
$$\phi = \frac{1}{\Delta}(A_1M - A_3L) = X_{\phi\phi}M - X_{\phi z}L \qquad (B.4.4)$$

where

$$\begin{vmatrix} A_1 & A_2 \\ A_3 & A_4 \end{vmatrix} = \Delta \qquad (B.4.5)$$

and X_{zz} , $X_{z\phi}$, $X_{\phi z}$ and $X_{\phi\phi}$ are the aerodynamic frequency response function.

Assuming the cross-spectrum do not have significant effect in the response spectra,

$$S_\eta = (S_L|X_{zz}|^2 + S_M|X_{z\phi}|^2)|J_f|^2$$

$$S_\phi = (S_L|X_{\phi z}|^2 + S_M|X_{\phi\phi}|^2)|J_f|^2 \qquad (B.4.6)$$

in which,

$$S_L = S_w(f)|\chi_w^L|^2|J_f|^2$$

$$S_M = S_w(f)|\chi_w^m|^2|J_f|^2 \qquad (B.4.7)$$

$$|J_f|^2 = \frac{\lambda^2}{\lambda^2+\pi^2} + \frac{2\pi^2(1+e^{-\lambda})}{(\lambda^2+\pi^2)^2} \qquad (B.4.8)$$

$$\lambda = \frac{cf\ell}{V} \qquad (B.4.9)$$

Panofsky's empirical expression for vertical velocity spectrum is used :

$$\frac{fS_w(f)}{\sigma_w^2} = \frac{4\kappa}{(1+4\kappa)^2} \qquad \kappa = \frac{f}{V} h_g \qquad (B.4.10)$$

By integrating the spectra of η and ϕ, RMS of the respective displacement can be found :

$$\sigma_\eta^2 = \int_0^\infty S_\eta(f)df$$

$$\sigma_\phi^2 = \int_0^\infty S_\phi(f)df \qquad (B.4.11)$$

B.5 THE SUMMARY OF PARAMETRIC STUDY

The main parameters which affect on the buffeting responses are the bridge deck height, the space correlation factor of aerodynamic forces, the turbulence intensity, the structural damping, the frequency ratio and the mass parameters. The range of parameters' variation chosen in this study is based on the characteristics of the prototype structure. The corresponding plottings can be referred to the figures at the end of this section. The main results from our present parametric study can be summarized as follows :

1. Effect of deck height

   The deck height affects on the results through velocity spectrum. From Fig. B.5.1, for each reduced velocity, V/(B X FZ), the responses both in bending and torsion are increased gradually with increase of deck height. The effect becomes more pronounced when the wind speed approaches the instability wind speed of the model.

2. Effect of turbulence intensity

   For each particular reduced velocity, V/(B X FZ), the buffeting response is simply proportional to the turbulence intensity (Fig. B.5.2).

3. Effect of correlation factor

The dimensionaless factor, c , of Eq.(B.4.9) is used as a parameter. It affects through the joint acceptance function on the response. The higher the correlation factor, c , is , which means the poorer the space correlation of velocity fluctuation along the bridge deck is, the lower the response would become (Fig. B.5.3).

4. Effect of structural damping

The higher the structural damping is, the lower the response is, in general. Also, the increase of the structural damping would delay the aerodynamic instability. The results are summarized in Fig. B.5.4 and B.5.5.

5. Effect of frequency ratio

When the ratio of torsional frequency to bending frequency increases , the critical wind speed for instability phenomena becomes higher. The change in frequency ratio does not have much effect on buffeting response in bending, but some effects were observed in torsional response (Fig. B.5.6).

6. Effect of mass parameter

The change of the mass parameter has the similar effect of changing the structural damping. The heavy bridge deck results less amplitude in buffeting and higher critical speed for instability. The ratio of

mass moment of inertia to the mass is kept constant throughout this analysis considering the fact that the bridge deck has very similar structural and aerodynamic characteristics of a flat plate (Fig. B.5.7).

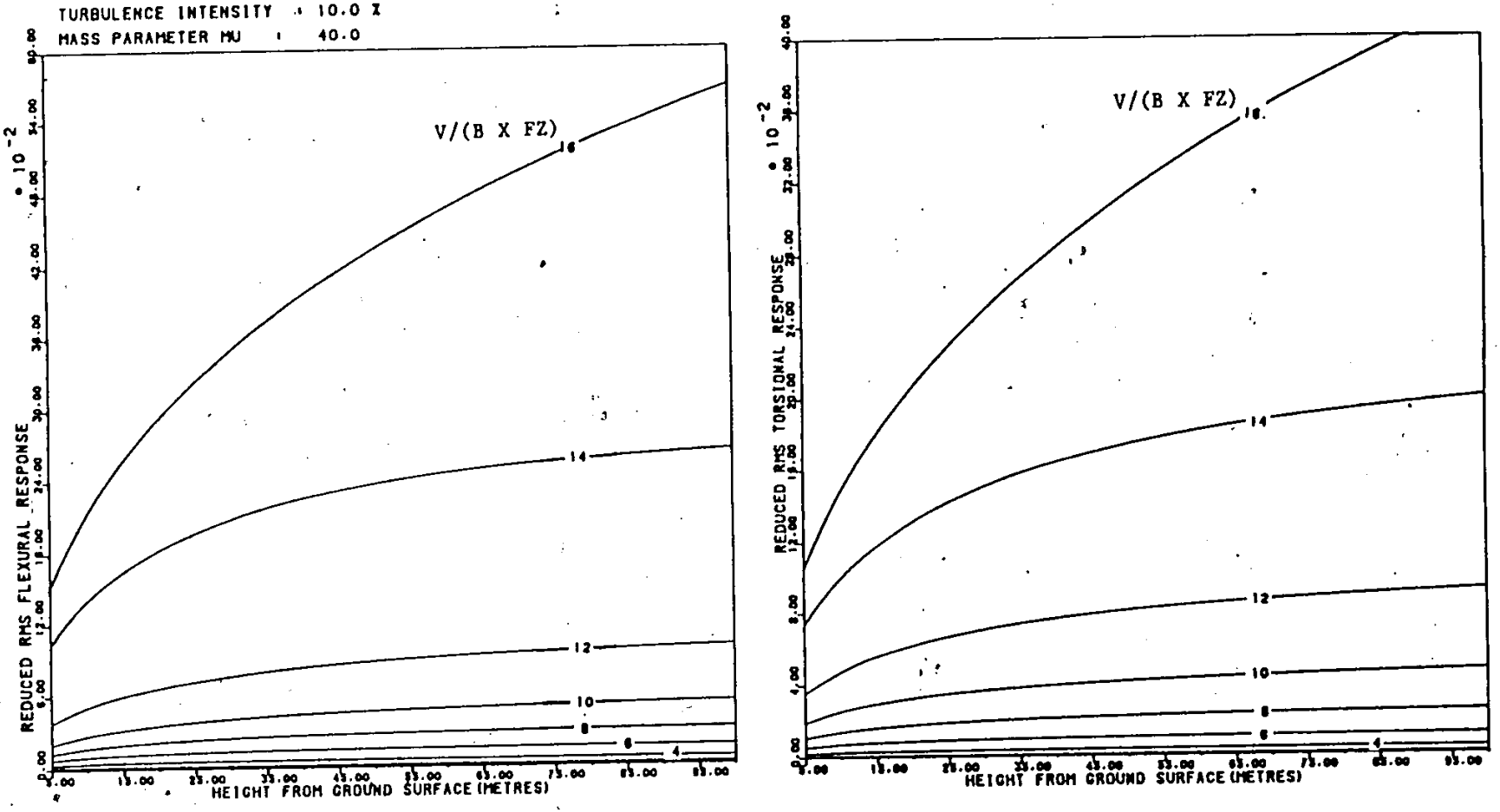

Figure B.5.1: Effect of the deck height

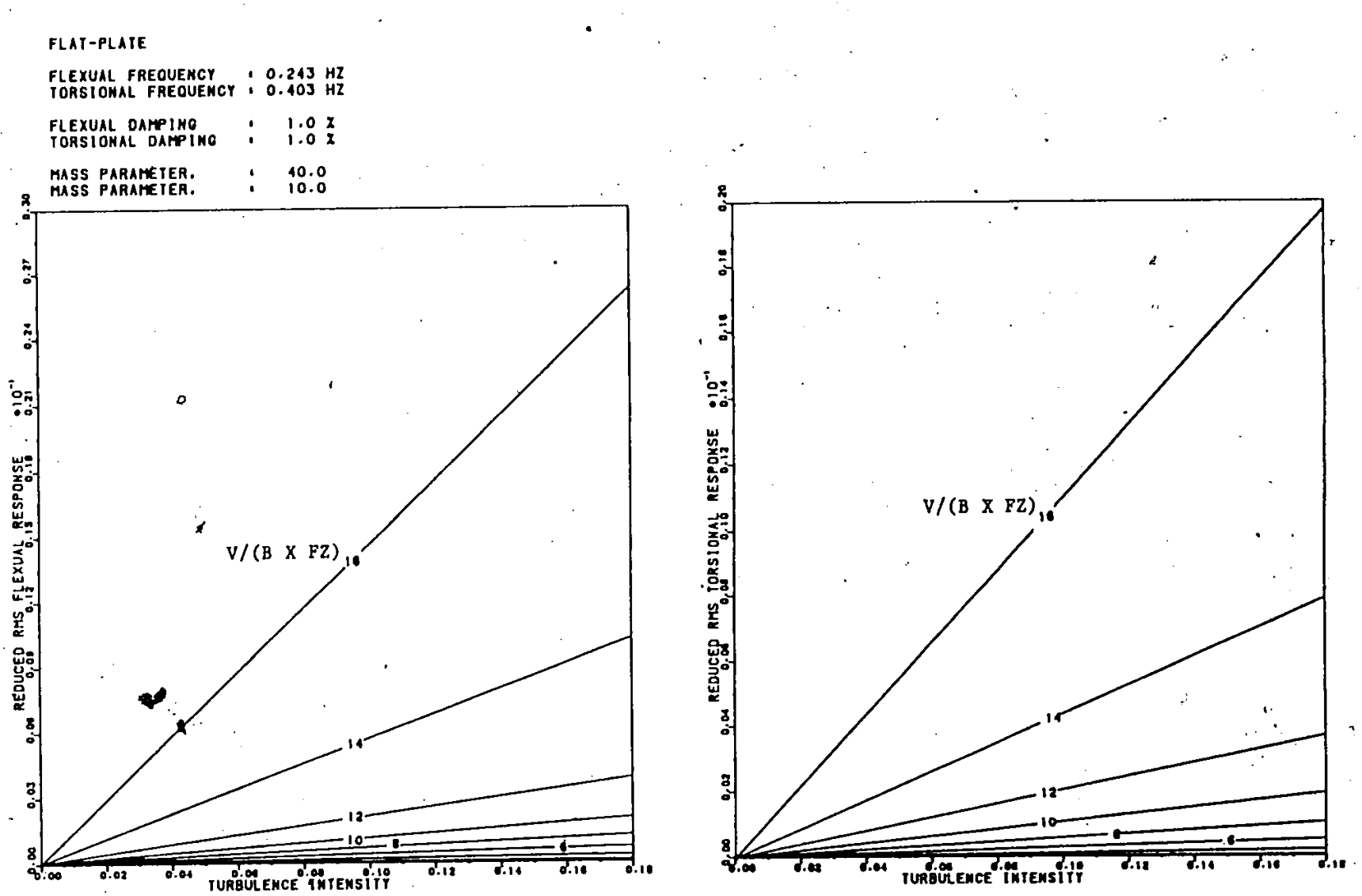

Figure B.5.2: Effect of turbulence intensity

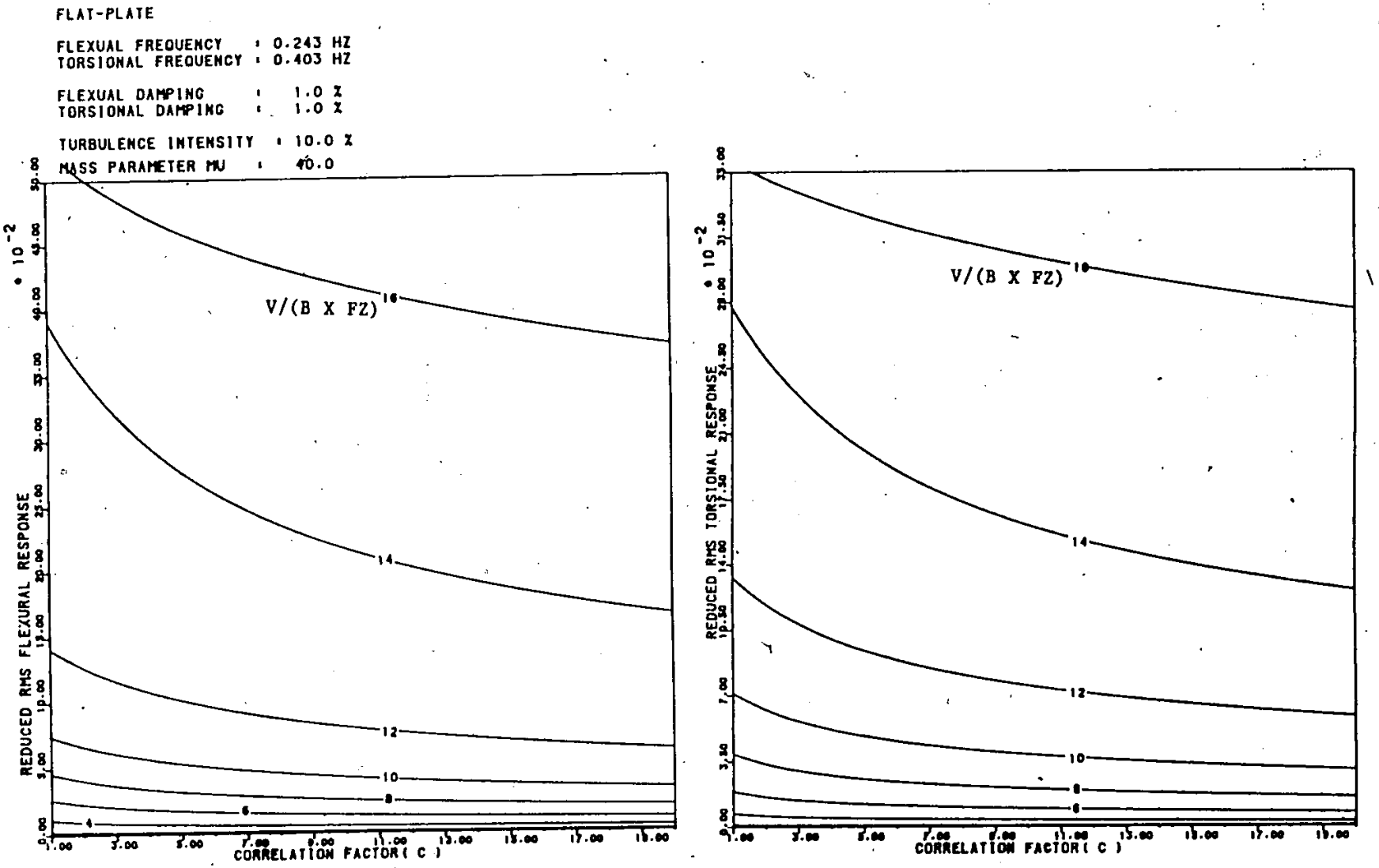

Figure B.5.3: Effect of correlation factor

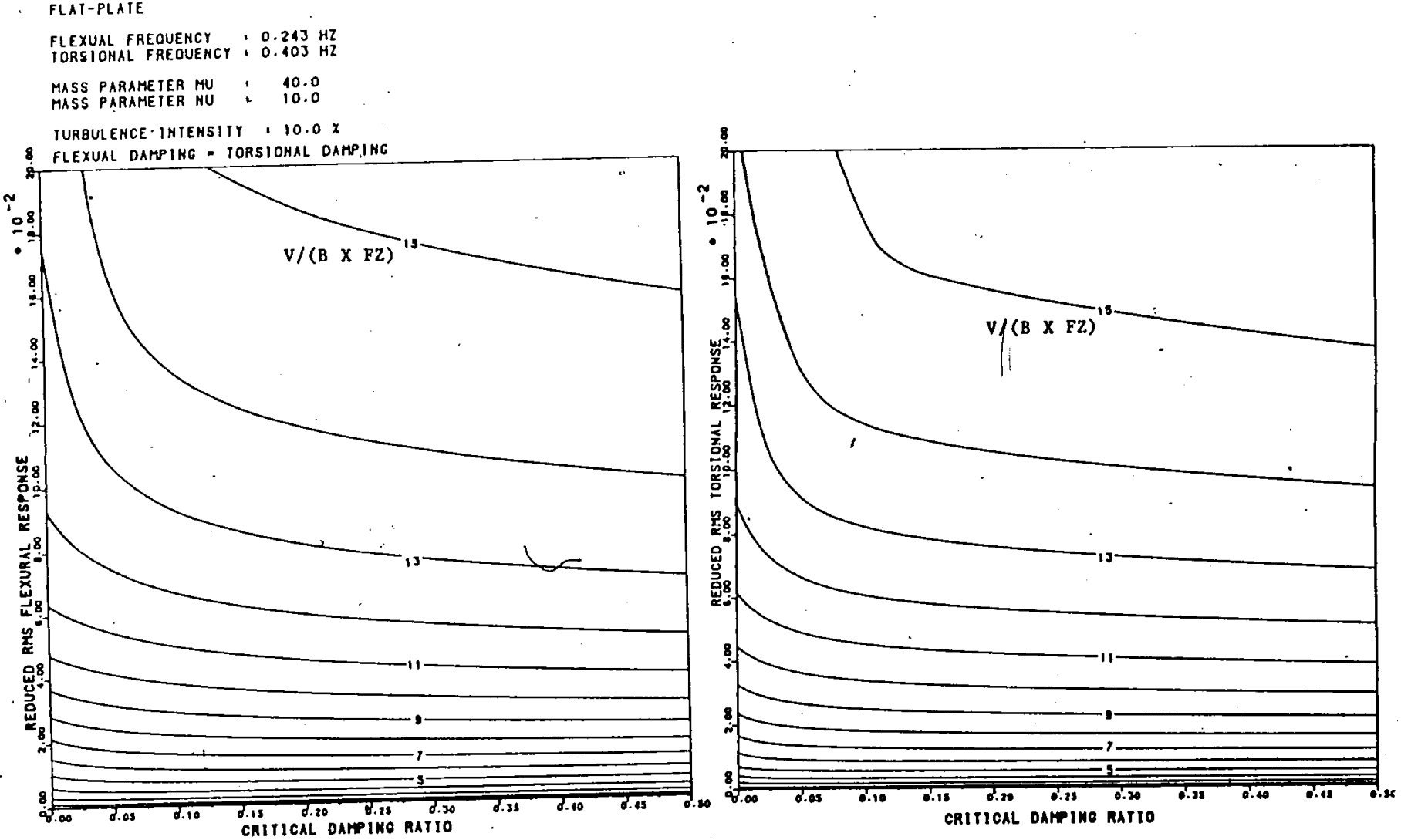

Figure B.5.4: Effect of structural damping

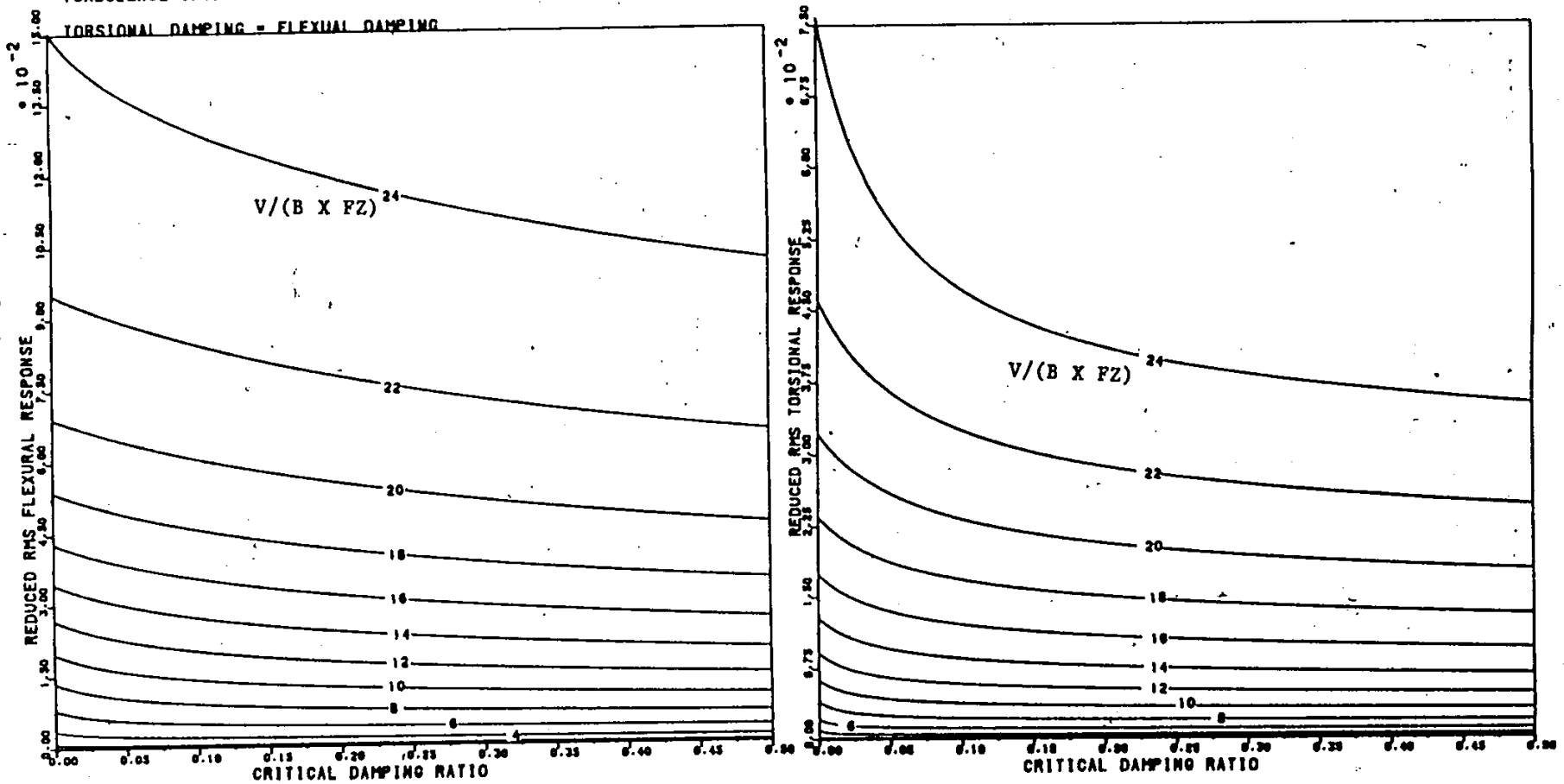

Figure B.5.5: Effect of structural damping

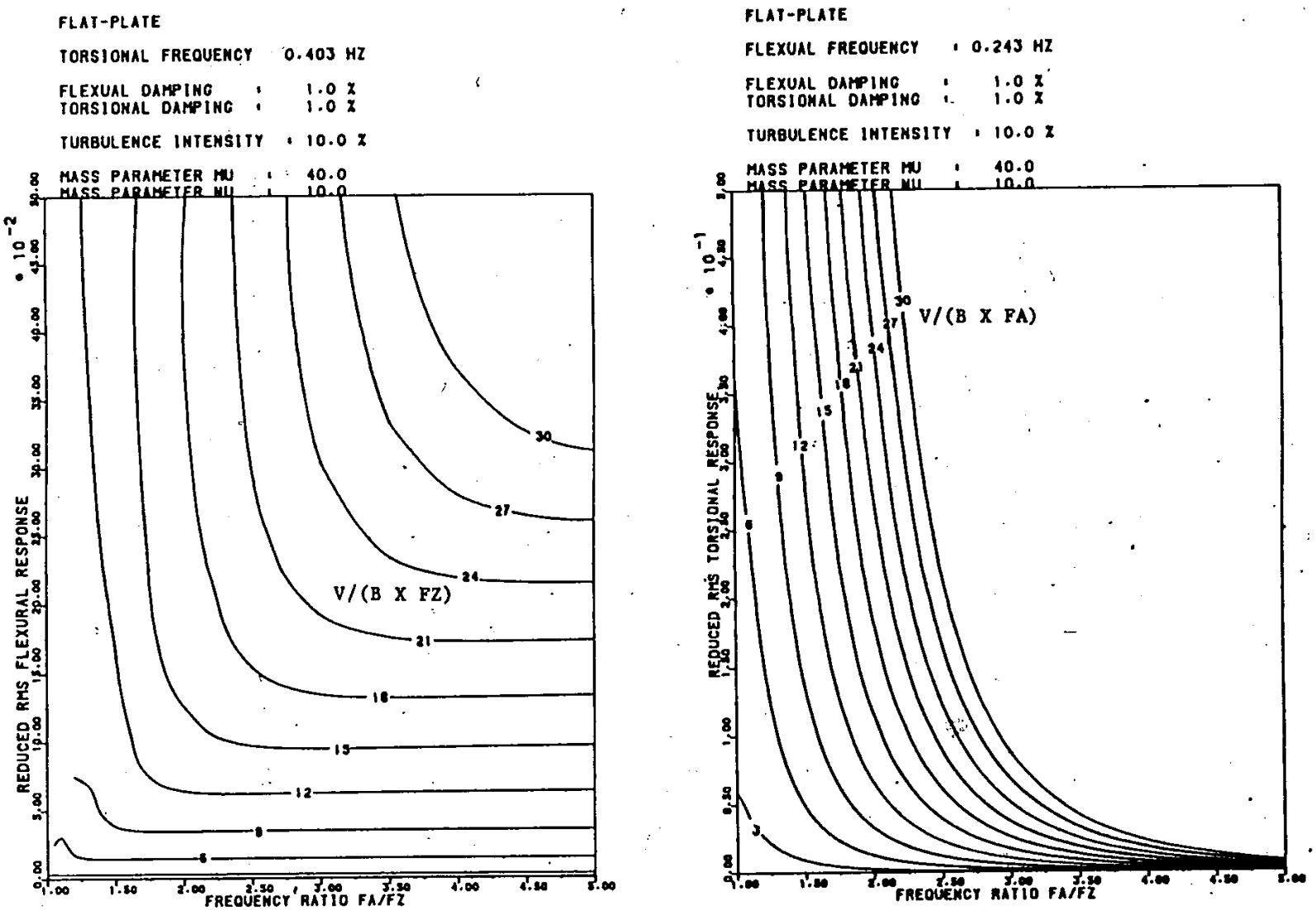

Figure B.5.6: Effect of frequency ratio

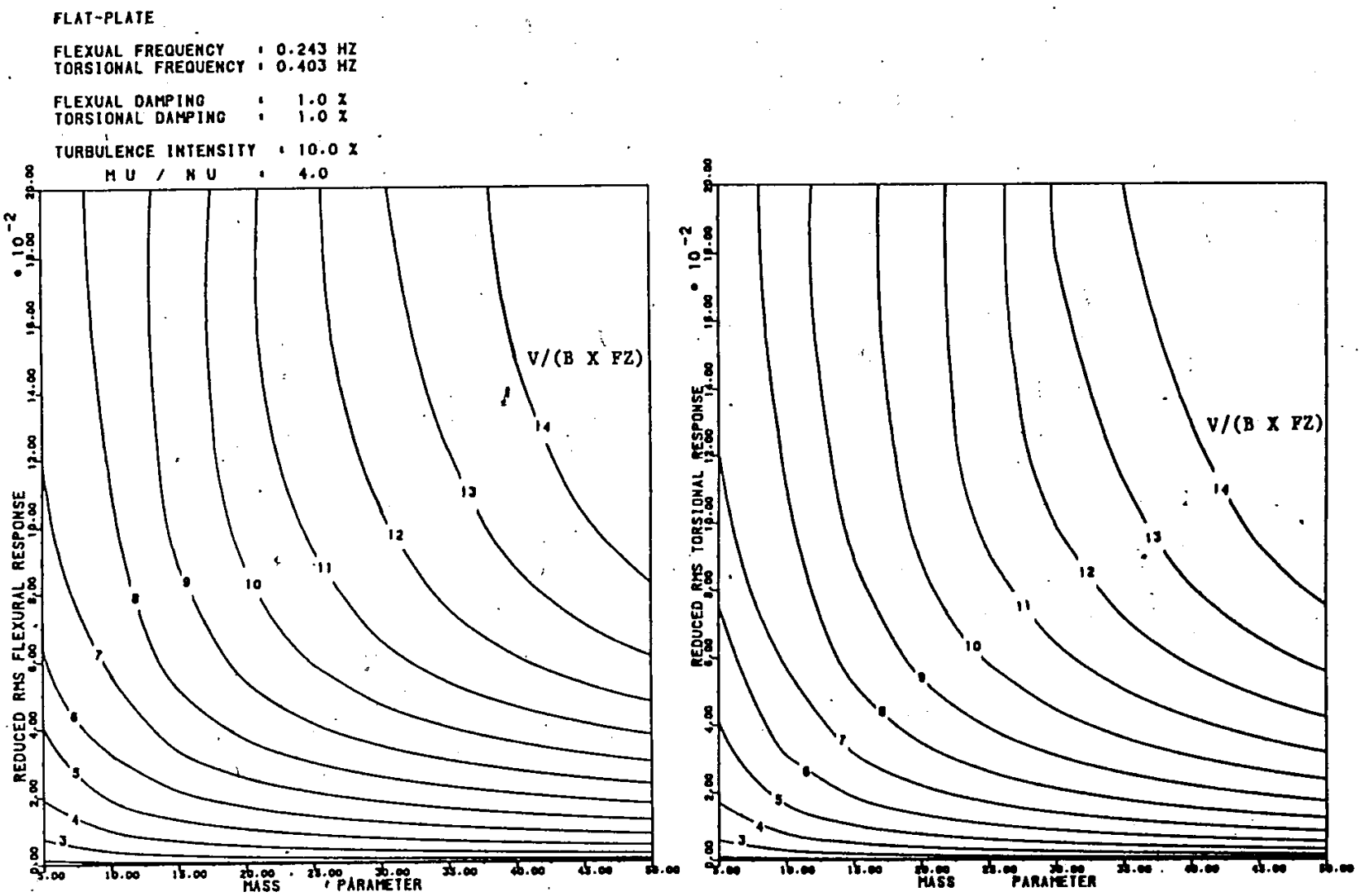

Figure B.5.7: Effect of mass parameter

Appendix C

INTEGRAL LENGTH SCALE OF TURBULENCE, L

Definition :

The integral length scale of turbulence, L, may be considered as the average size of the eddies present in the turbulence. A method of describing the length scale is based on the variation of the correlation coefficient Rx between the values of the component u at two points, separated by the distance X in the direction of the X coordinate as X is varied. The curve of Rx against X represents the statistical distribution of u along the X-axis at any instant. If Rx falls to zero and remains zero, a length L may be defined by the relation :

$$L = \int_0^\infty \bar{R}u(x)\, dx$$

where $\bar{R}u(x)$ is the correlation coefficient

$$\bar{R}u(x) = Ru(x) \,/\, \sigma_u^2$$

$$Ru(x) = \overline{u(0,t) * u(x,t)}$$

$$\sigma_u^2 = Ru(0) = \overline{u(0,t) * u(0,t)}$$

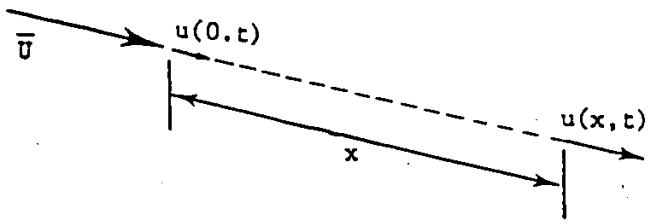

von Kàrmàn defined a normalized spectrum in the u-direction as below :

$$\frac{f\,S_u(f)}{\sigma_u^2} = \frac{4\left(\frac{f\,L_u}{V}\right)}{\left[1 + 70.7\left(\frac{f\,L_u}{V}\right)^2\right]^{5/6}}$$

where L_u = integral length scale of turbulence

$\frac{f\,L_u}{V}$ = reduced frequency

$S_u(f)$ = power spectral density of the wind at frequency f

σ_u^2 = mean-square of the velocity fluctuation

The peak of this spectrum is found at the reduced frequency :

$$\left(\frac{f\,L_u}{V}\right)_{peak} = 0.146$$

Hence the integral length scale of turbulence can be expressed as :

$$L_u = 0.146\left(\frac{V}{f}\right)_{peak}$$

Asumming the von Kàrmàn expression is also applicable to the normalized velocity spectrum in the w-direction, the results obtain from the measured spectra are presented in Table C-1.

The agreement between the measured velocity spectrum and the von Kàrmàn spectrum, in u and w directions, is quite satisfactory. Some typical examples are shown from Figures C-1 to C-5.

TABLE C-1

Integral length scale of turbulence of the measured velocity spectrum

	FLOW CONDITION	u - direction			w - direction		
		$\overline{V}$, m/s	$(f)_p$, Hz	Lu, mm	$\overline{V}$, m/s	$(f)_p$, Hz	Lw, mm
3-D	Coarse Grid	7.766	28	40	7.766	28	40
	Fine Grid	7.766	45	25	7.766	45	25
	Spires	7.766	23	50	7.766	25	45
	Spires and - roughness	7.766	19	60	7.766	21	55
	Spires and - angles	7.766	19	60	7.766	21	55
2-D	Coarse Grid	5.491	20	40	5.491	20	40
	Fine Grid	5.491	32	25	5.491	32	25
	Spires	5.491	16	50	5.491	18	45
	Spires and - roughness	5.491	13.5	60	5.491	14.5	55
	Spires and - angles	5.491	13.5	60	5.491	14.5	55

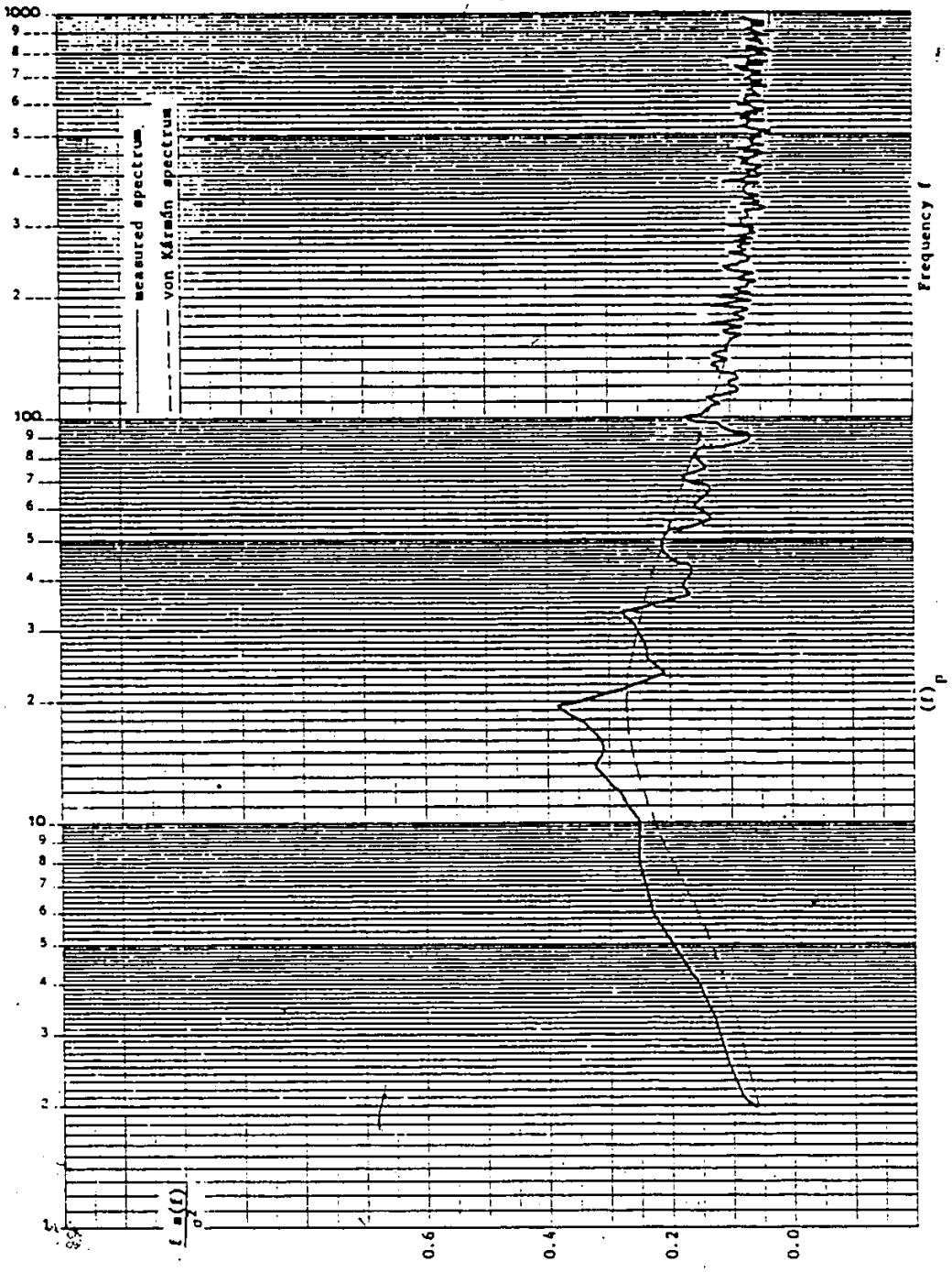

Figure C.1: Velocity spectrum : Homogenous Turbulence (Coares grid) (u-direction) (2-D)

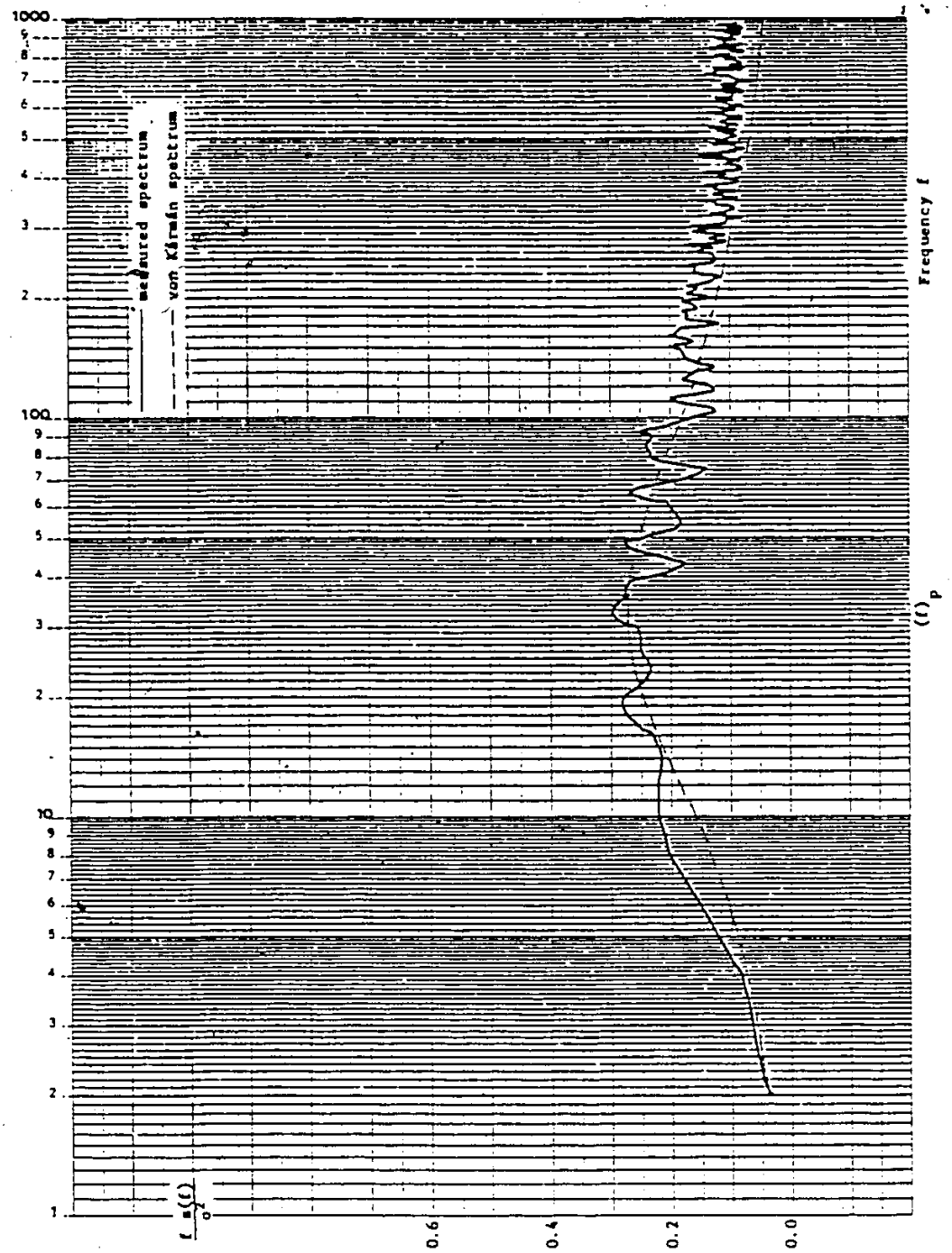

Figure C-2: Velocity spectrum : Homogenous Turbulence (Fine grid) (u-direction) (2-D)

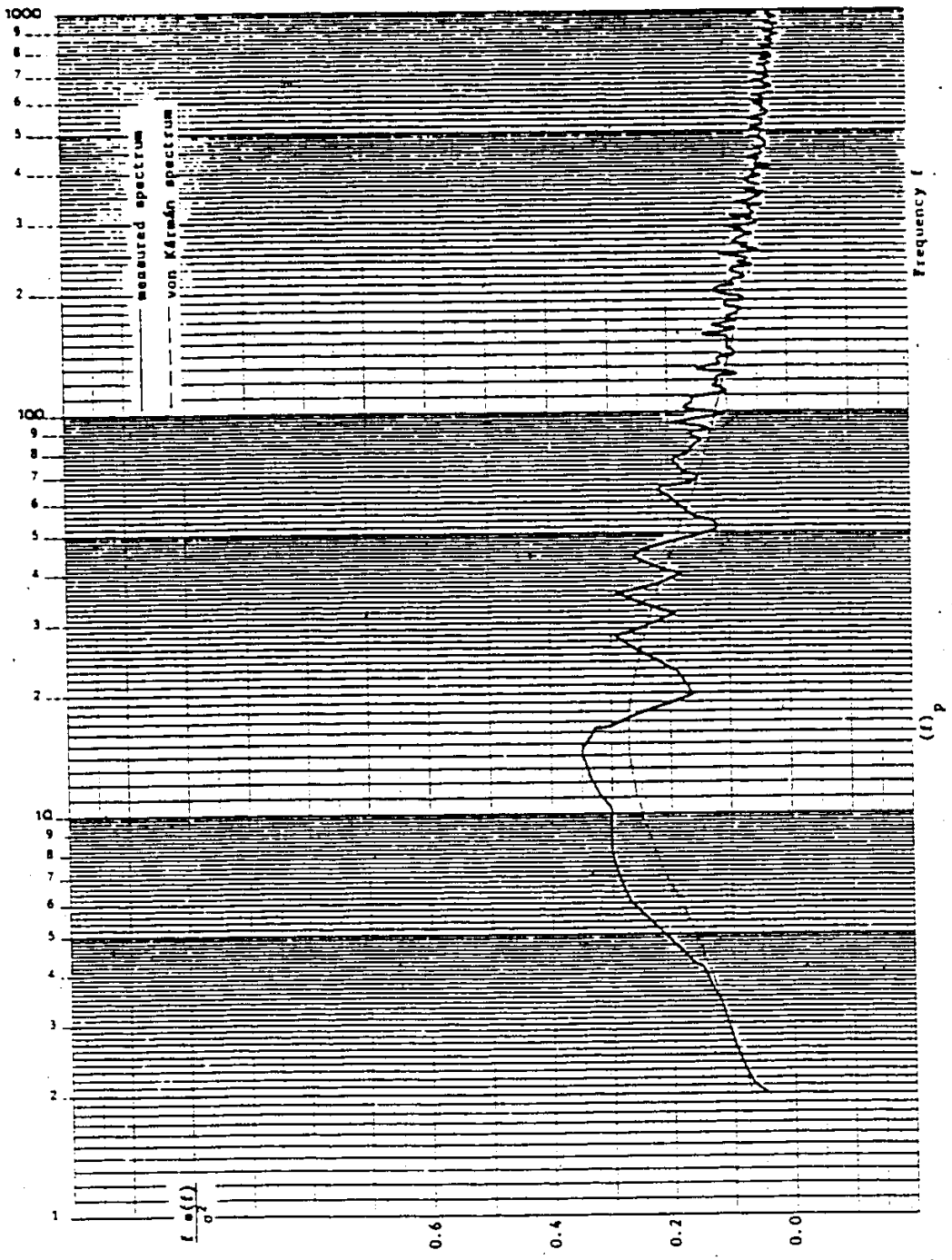

Figure C.3: Velocity spectrum :Boundary layer flow (Spires) (u-direction)(2-D)

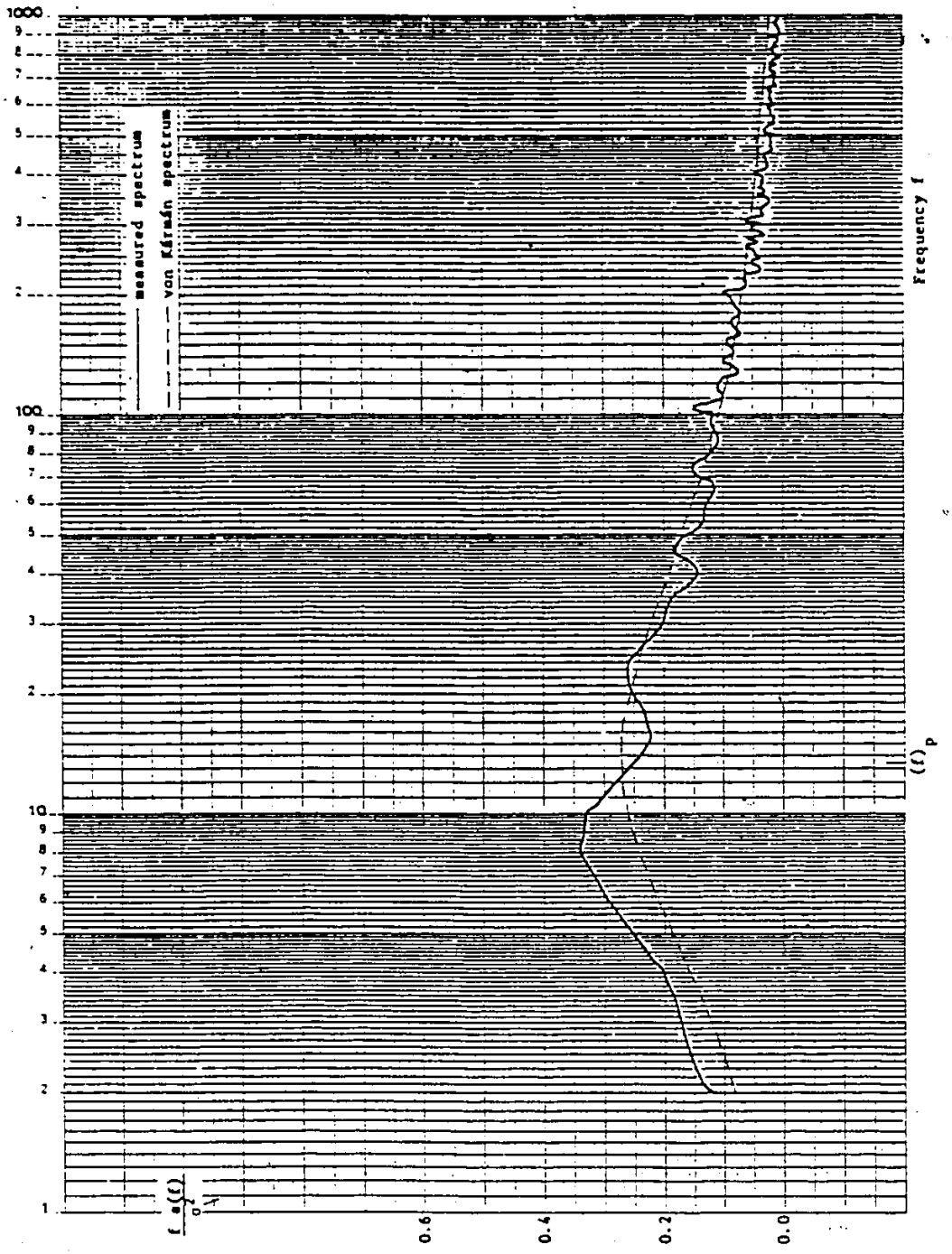

Figure C.4: Velocity spectrum : Boundary layer flow (Spires and Roughness) (u-direction) (2-D)

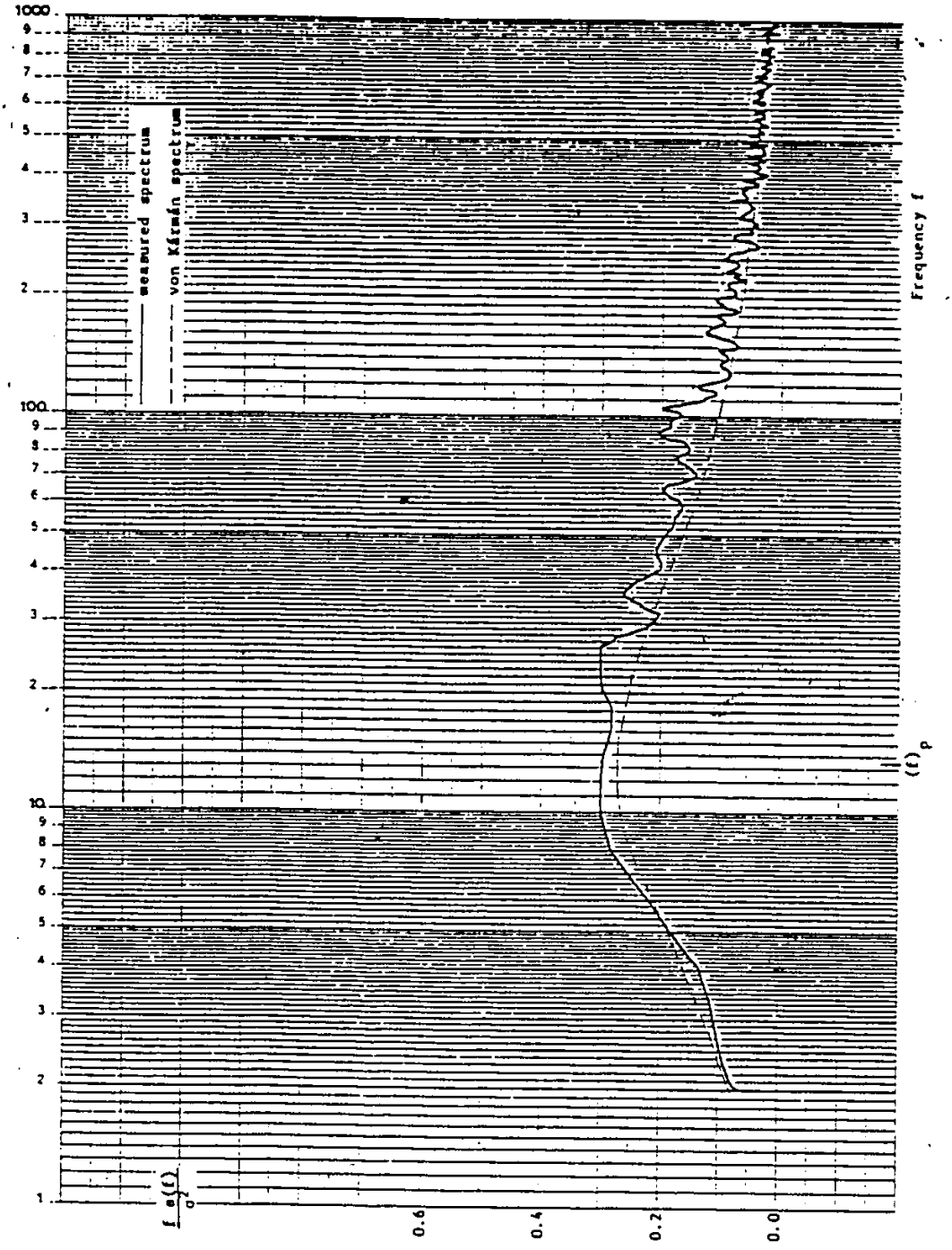

Figure C.5: Velocity spectrum : Boundary layer flow (Spires and Angles) (u-direction) (2-D)

Appendix D

RESPONSE OF 1/500-SCALE TAUT STRIP MODEL AND SECTIONAL MODEL

Z = HEIGHT FROM TUNNEL FLOOR

VZ = VELOCITY AT ELEVATION, Z

VG = GRADIENT VELOCITY

X = DISTANCE FROM TUNNEL WALL

VX = VELOCITY AT A DISTANCE, X, FROM WALL.

TABLE D-1

RESPONSE AT FLOW CONDITION : SMOOTH (BARE TUNNEL)

1/500-SCALE TAUT STRIP MODEL TEST
FLEXURAL FREQUENCY = 6.25 TORSIONAL FREQUENCY =17.50
FLEXURAL DAMPING = 2.84 TORSIONAL DAMPING =1.31
TURBULENCE INTENSITY , IW : 0.25%

V/(B X FZ)	REDUCED FLEXURAL RESPONSE	V/(B X FA)	REDUCED TORSIONAL RESPONSE
6.9	0.0005	2.5	0.0002
9.7	0.0008	3.5	0.0003
13.7	0.0012	4.9	0.0006
14.7	0.0013	5.3	0.0007
16.0	0.0014	5.7	0.0007
16.8	0.0015	6.0	0.0009
18.2	0.0016	6.5	0.0010
19.4	0.0017	6.9	0.0011
21.1	0.0019	7.5	0.0014
21.7	0.0022	7.8	0.0017
22.8	0.0022	8.1	0.0018
23.2	0.0034	8.3	0.0031
23.8	0.0055	8.5	0.0048
24.2	0.0071	8.6	0.0060
24.6	0.0085	8.8	0.0073
24.8	0.0092	8.9	0.0079
25.0	0.0095	8.9	0.0083
25.2	0.0106	9.0	0.0106
25.2	0.0125	9.0	0.0126

TABLE D-2

RESPONSE AT FLOW CONDITION : HOMOGENOUS TURBULENCE (COARSE GRID)

1/500-SCALE TAUT STRIP MODEL TEST

FLEXURAL FREQUENCY = 6.25 TORSIONAL FREQUENCY =17.50

FLEXURAL DAMPING = 2.84 TORSIONAL DAMPING =1.31

TURBULENCE INTENSITY , IW : 13.3%

V/(B X FZ)	REDUCED FLEXURAL RESPONSE	V/(B X FA)	REDUCED TORSIONAL RESPONSE
3.2	0.0032	1.1	0.0011
4.5	0.0062	1.6	0.0024
6.1	0.0100	2.2	0.0049
7.6	0.0145	2.7	0.0078
8.7	0.0189	3.1	0.0106
10.0	0.0246	3.6	0.0147
11.2	0.0291	4.0	0.0181
12.3	0.0335	4.4	0.0211
13.1	0.0365	4.7	0.0251
14.4	0.0429	5.1	0.0287
16.6	0.0538	5.9	0.0405
17.7	0.0595	6.3	0.0470

TABLE D-3

RESPONSE AT FLOW CONDITION : HOMOGENOUS TURBULENCE (FINE GRID)

1/500-SCALE TAUT STRIP MODEL TEST

FLEXURAL FREQUENCY = 6.25 TORSIONAL FREQUENCY =17.50

FLEXURAL DAMPING = 2.84 TORSIONAL DAMPING =1.31

TURBULENCE INTENSITY , IW : 6.4%

V/(B X FZ)	REDUCED FLEXURAL RESPONSE	V/(B X FA)	REDUCED TORSIONAL RESPONSE
3.1	0.0015	1.1	0.0006
4.3	0.0026	1.6	0.0012
6.1	0.0050	2.2	0.0023
8.7	0.0086	3.1	0.0050
10.2	0.0109	3.6	0.0065
12.3	0.0144	4.4	0.0093
13.7	0.0168	4.9	0.0117
14.9	0.0190	5.3	0.0144
16.6	0.0210	5.9	0.0170
18.4	0.0241	6.6	0.0197
20.2	0.0267	7.2	0.0237
21.7	0.0302	7.8	0.0291
23.8	0.0344	8.5	0.0425
25.7	0.0518	9.2	0.0702

TABLE D-4

RESPONSE AT FLOW CONDITION : BOUNDARY LAYER FLOW (SPIRES)

1/500-SCALE TAUT STRIP MODEL TEST

FLEXURAL FREQUENCY = 6.25 TORSIONAL FREQUENCY =17.50

FLEXURAL DAMPING = 2.84 TORSIONAL DAMPING =1.31

TURBULENCE INTENSITY, IW : 10.5%

V/(B X FZ)	REDUCED FLEXURAL RESPONSE	V/(B X FA)	REDUCED TORSIONAL RESPONSE
4.8	0.0039	1.7	0.0014
6.8	0.0071	2.4	0.0032
8.3	0.0104	3.0	0.0054
9.6	0.0143	3.4	0.0080
10.7	0.0172	3.8	0.0100
12.0	0.0213	4.3	0.0121
13.1	0.0238	4.7	0.0166
14.2	0.0274	5.1	0.0189
15.2	0.0299	5.4	0.0213
16.1	0.0324	5.7	0.0243
17.0	0.0368	6.1	0.0291
18.6	0.0401	6.6	0.0351
20.8	0.0484	7.4	0.0441

TABLE D-5

RESPONSE AT FLOW CONDITION : BOUNDARY LAYER FLOW (SPIRES & ROUGHNESSES)

1/500-SCALE TAUT STRIP MODEL TEST

FLEXURAL FREQUENCY = 6.25 TORSIONAL FREQUENCY =17.50

FLEXURAL DAMPING = 2.84 TORSIONAL DAMPING =1.31

TURBULENCE INTENSITY , IW : 12.0%

V/(B X FZ)	REDUCED FLEXURAL RESPONSE	V/(B X FA)	REDUCED TORSIONAL RESPONSE
4.6	0.0038	1.6	0.0017
6.5	0.0066	2.3	0.0033
9.2	0.0115	3.3	0.0072
11.3	0.0160	4.0	0.0111
13.0	0.0198	4.7	0.0145
14.6	0.0233	5.2	0.0186
16.0	0.0265	5.7	0.0224
17.4	0.0292	6.2	0.0266

TABLE D-6

RESPONSE AT FLOW CONDITION : BOUNDARY LAYER FLOW (SPIRES & ANGLES)

1/500-SCALE TAUT STRIP MODEL TEST

FLEXURAL FREQUENCY = 6.25 TORSIONAL FREQUENCY =17.50

FLEXURAL DAMPING = 2.84 TORSIONAL DAMPING =1.31

TURBULENCE INTENSITY , IW : 13.2%

V/(B X FZ)	REDUCED FLEXURAL RESPONSE	V/(B X FA)	REDUCED TORSIONAL RESPONSE
4.5	0.0053	1.6	0.0019
6.4	0.0096	2.3	0.0045
7.9	0.0149	2.8	0.0074
9.1	0.0192	3.2	0.0112
10.1	0.0236	3.6	0.0142
11.1	0.0266	4.0	0.0178
12.8	0.0354	4.6	0.0263
14.5	0.0401	5.2	0.0320
15.7	0.0469	5.6	0.0385
17.5	0.0548	6.2	0.0469

TABLE D-7

RESPONSE AT FLOW CONDITION : SMOOTH (BARE TUNNEL)

1/500-SCALE TAUT STRIP MODEL TEST

FLEXURAL FREQUENCY = 8.80 TORSIONAL FREQUENCY =21.80

FLEXURAL DAMPING = 0.50 TORSIONAL DAMPING =0.78

TURBULENCE INTENSITY , IW : 0.25%

V/(B X FZ)	REDUCED FLEXURAL RESPONSE	V/(B X FA)	REDUCED TORSIONAL RESPONSE
4.9	0.0003	2.0	0.0002
6.9	0.0005	2.8	0.0002
9.8	0.0007	3.9	0.0004
12.0	0.0010	4.8	0.0006
13.8	0.0011	5.6	0.0007
15.4	0.0014	6.2	0.0010
17.6	0.0018	7.1	0.0012
19.5	0.0023	7.9	0.0020

TABLE D-8

RESPONSE AT FLOW CONDITION : HOMOGENOUS TURBULENCE (COARSE GRID).

1/500-SCALE TAUT STRIP MODEL TEST

FLEXURAL FREQUENCY = 8.80 TORSIONAL FREQUENCY =21.80

FLEXURAL DAMPING = 0.50 TORSIONAL DAMPING =0.78

TURBULENCE INTENSITY , IW : 13.3%

V/(B X FZ)	REDUCED FLEXURAL RESPONSE	V/(B X FA)	REDUCED TORSIONAL RESPONSE
3.6	0.0071	1.4	0.0024
5.0	0.0118	2.0	0.0054
7.1	0.0214	2.9	0.0118
8.7	0.0293	3.5	0.0175
10.1	0.0382	4.1	0.0243
11.3	0.0437	4.5	0.0306
12.3	0.0493	5.0	0.0381
13.3	0.0560	5.4	0.0454

TABLE D-9

RESPONSE AT FLOW CONDITION : HOMOGENOUS TURBULENCE (FINE GRID)

1/500-SCALE TAUT STRIP MODEL TEST

FLEXURAL FREQUENCY = 8.80 TORSIONAL FREQUENCY =21.80

FLEXURAL DAMPING = 0.50 TORSIONAL DAMPING =0.78

TURBULENCE INTENSITY , IW : 6.4%

V/(B X FZ)	REDUCED FLEXURAL RESPONSE	V/(B X FA)	REDUCED TORSIONAL RESPONSE
4.9	0.0045	2.0	0.0023
6.9	0.0077	2.8	0.0044
8.5	0.0102	3.4	0.0069
9.8	0.0131	3.9	0.0085
12.0	0.0177	4.8	0.0124
13.8	0.0200	5.6	0.0156
15.4	0.0225	6.2	0.0196
17.0	0.0254	6.9	0.0225
18.0	0.0307	7.3	0.0293

TABLE D-10

RESPONSE AT FLOW CONDITION : BOUNDARY LAYER FLOW (SPIRES)

1/500-SCALE TAUT STRIP MODEL TEST

FLEXURAL FREQUENCY = 8.80 TORSIONAL FREQUENCY =21.80

FLEXURAL DAMPING = 0.50 TORSIONAL DAMPING =0.78

TURBULENCE INTENSITY , IW : 10.5%

V/(B X FZ)	REDUCED FLEXURAL RESPONSE	V/(B X FA)	REDUCED TORSIONAL RESPONSE
3.8	0.0035	1.5	0.0011
5.4	0.0080	2.2	0.0029
6.6	0.0112	2.7	0.0052
7.6	0.0142	3.1	0.0072
9.3	0.0196	3.8	0.0109
10.8	0.0242	4.3	0.0161
12.0	0.0282	4.9	0.0197
13.2	0.0317	5.3	0.0247
14.4	0.0379	5.8	0.0290

TABLE D-11

RESPONSE AT FLOW CONDITION : BOUNDARY LAYER FLOW (SPIRES & ROUGHNESSES)

1/500-SCALE TAUT STRIP MODEL TEST

FLEXURAL FREQUENCY = 8.80 TORSIONAL FREQUENCY =21.80

FLEXURAL DAMPING = 0.50 TORSIONAL DAMPING =0.78

TURBULENCE INTENSITY , IW : 12.0%

V/(B X FZ)	REDUCED FLEXURAL RESPONSE	V/(B X FA)	REDUCED TORSIONAL RESPONSE
3.3	0.0030	1.3	0.0009
4.6	0.0052	1.9	0.0021
6.5	0.0091	2.6	0.0050
7.3	0.0111	3.0	0.0066
8.0	0.0125	3.2	0.0079
9.3	0.0149	3.7	0.0106
10.3	0.0184	4.2	0.0127
11.3	0.0212	4.6	0.0164
12.3	0.0232	5.0	0.0206

TABLE D-12

RESPONSE AT FLOW CONDITION : BOUNDARY LAYER FLOW (SPIRES & ANGLES)

1/500-SCALE TAUT STRIP MODEL TEST

FLEXURAL FREQUENCY = 8.80 TORSIONAL FREQUENCY =21.80

FLEXURAL DAMPING = 0.50 TORSIONAL DAMPING =0.78

TURBULENCE INTENSITY , IW : 13.2%

V/(B X FZ)	REDUCED FLEXURAL RESPONSE	V/(B X FA)	REDUCED TORSIONAL RESPONSE
3.2	0.0040	1.3	0.0011
4.6	0.0077	1.8	0.0027
6.4	0.0147	2.6	0.0072
7.9	0.0196	3.2	0.0112
9.1	0.0257	3.7	0.0163
10.2	0.0296	4.1	0.0207
11.2	0.0345	4.5	0.0272
12.1	0.0391	4.9	0.0315

TABLE D-13

RESPONSE AT FLOW CONDITION : SMOOTH (BARE TUNNEL)

1/500-SCALE SECTIONAL MODEL TEST

FLEXURAL FREQUENCY = 9.80 TORSIONAL FREQUENCY =17.90

FLEXURAL DAMPING = 0.92 TORSIONAL DAMPING =0.38

TURBULENCE INTENSITY , IW : 0.0%

V/(B X FZ)	REDUCED FLEXURAL RESPONSE	V/(B X FA)	REDUCED TORSIONAL RESPONSE
4.4	0.0002	2.4	0.0004
6.2	0.0003	3.4	0.0005
8.8	0.0004	4.8	0.0007
10.7	0.0005	5.9	0.0009
12.4	0.0007	6.8	0.0011
13.9	0.0009	7.6	0.0017
15.2	0.0017	8.3	0.0030
15.6	0.0023	8.5	0.0050
15.7	0.0050	8.6	0.0126
15.8	0.0250	8.7	0.0720

TABLE D-14

RESPONSE AT FLOW CONDITION : HOMOGENOUE TURBULENCE (COARSE GRID)

1/500-SCALE SECTIONAL MODEL TEST

FLEXURAL FREQUENCY = 9.80 TORSIONAL FREQUENCY =17.90

FLEXURAL DAMPING = 0.92 TORSIONAL DAMPING =0.38

TURBULENCE INTENSITY , IW : 13.1%

V/(B X FZ)	REDUCED FLEXURAL RESPONSE	V/(B X FA)	REDUCED TORSIONAL RESPONSE
3.9	0.0040	2.1	0.0045
5.5	0.0079	3.0	0.0113
7.8	0.0148	4.3	0.0234
9.6	0.0202	5.2	0.0331
11.0	0.0244	6.0	0.0446
12.3	0.0289	6.8	0.0540

TABLE D-15

RESPONSE AT FLOW CONDITION : HOMOGENOUS TURBULENCE (FINE GRID)

1/500-SCALE SECTIONAL MODEL TEST

FLEXURAL FREQUENCY = 9.80 TORSIONAL FREQUENCY =17.90

FLEXURAL DAMPING = 0.92 TORSIONAL DAMPING =0.38

TURBULENCE INTENSITY , IW : 6.2%

V/(B X FZ)	REDUCED FLEXURAL RESPONSE	V/(B X FA)	REDUCED TORSIONAL RESPONSE
4.4	0.0022	2.4	0.0030
6.2	0.0037	3.4	0.0065
7.6	0.0052	4.2	0.0099
8.8	0.0063	4.8	0.0123
10.7	0.0098	5.9	0.0176
12.4	0.0107	6.8	0.0220
13.9	0.0142	7.6	0.0324
15.2	0.0201	8.3	0.0470
15.9	0.0251	8.7	0.0594

TABLE D-16

RESPONSE AT FLOW CONDITION : BOUNDARY LAYER FLOW (SPIRES)

1/500-SCALE SECTIONAL MODEL TEST

FLEXURAL FREQUENCY = 9.80 TORSIONAL FREQUENCY =17.90

FLEXURAL DAMPING = 0.92 TORSIONAL DAMPING =0.38

TURBULENCE INTENSITY , IW : 9.8%

V/(B X FZ)	REDUCED FLEXURAL RESPONSE	V/(B X FA)	REDUCED TORSIONAL RESPONSE
3.4	0.0028	1.9	0.0029
4.8	0.0053	2.6	0.0057
5.9	0.0080	3.2	0.0099
6.8	0.0106	3.7	0.0141
8.4	0.0140	4.6	0.0211
9.7	0.0169	5.3	0.0300
10.8	0.0199	5.9	0.0395
11.8	0.0229	6.5	0.0482
12.8	0.0271	7.0	0.0575

TABLE D-17

RESPONSE AT FLOW CONDITION : BOUNDARY LAYER FLOW (SPIRES & ROUGHNESSES)

1/500-SCALE SECTIONAL MODEL TEST

FLEXURAL FREQUENCY = 9.80 TORSIONAL FREQUENCY =17.90

FLEXURAL DAMPING = 0.92 TORSIONAL DAMPING =0.38

TURBULENCE INTENSITY , I_H : 12.5%

V/(B X FZ)	REDUCED FLEXURAL RESPONSE	V/(B X FA)	REDUCED TORSIONAL RESPONSE
3.0	0.0019	1.7	0.0022
4.2	0.0039	2.3	0.0041
5.2	0.0054	2.9	0.0069
6.0	0.0068	3.3	0.0099
7.3	0.0086	4.1	0.0151
8.5	0.0115	4.7	0.0217
9.5	0.0127	5.2	0.0288
10.4	0.0146	5.7	0.0376
11.2	0.0182	6.2	0.0638
11.6	0.0212	6.4	0.0840
12.0	0.0228	6.6	0.0925

TABLE D-18

RESPONSE AT FLOW CONDITION : BOUNDARY LAYER FLOW (SPIRES AND ANGLES)

1/500-SCALE SECTIONAL MODEL TEST

FLEXURAL FREQUENCY = 9.80 TORSIONAL FREQUENCY =17.90

FLEXURAL DAMPING = 0.92 TORSIONAL DAMPING =0.38

TURBULENCE INTENSITY , IW : 13.0%

V/(B X FZ)	REDUCED FLEXURAL RESPONSE	V/(B X FA)	REDUCED TORSIONAL RESPONSE
3.3	0.0022	1.9	0.0025
4.7	0.0048	2.6	0.0055
5.8	0.0078	3.2	0.0095
6.7	0.0091	3.7	0.0135
8.2	0.0133	4.5	0.0199
9.5	0.0167	5.2	0.0298
10.6	0.0188	5.9	0.0400
11.6	0.0219	6.4	0.0475
12.5	0.0250	6.9	0.0544

TABLE D-19

RESPONSE AT FLOW CONDITION : SMOOTH FLOW (BARE TUNNEL)

1/500-SCALE SECTIONAL MODEL TEST

FLEXURAL FREQUENCY =12.00 TORSIONAL FREQUENCY =22.00

FLEXURAL DAMPING = 0.54 TORSIONAL DAMPING =0.26

TURBULENCE INTENSITY , IW : 0.0%

V/(B X FZ)	REDUCED FLEXURAL RESPONSE	V/(B X FA)	REDUCED TORSIONAL RESPONSE
3.6	0.0001	2.0	0.0002
5.1	0.0002	2.8	0.0003
7.2	0.0003	3.9	0.0004
8.8	0.0004	4.8	0.0005
10.1	0.0006	5.5	0.0006
11.3	0.0008	6.2	0.0009
12.4	0.0011	6.8	0.0014
13.2	0.0011	7.2	0.0014
13.5	0.0011	7.4	0.0015
13.9	0.0012	7.6	0.0016

TABLE D-20

RESPONSE AT FLOW CONDITION : HOMOGENOUS TURBULENCE (COARSE GRID)

1/500-SCALE SECTIONAL MODEL TEST

FLEXURAL FREQUENCY =12.00 TORSIONAL FREQUENCY =22.00

FLEXURAL DAMPING = 0.54 TORSIONAL DAMPING =0.26

TURBULENCE INTENSITY , IW : 13.1%

V/(B X FZ)	REDUCED FLEXURAL RESPONSE	V/(B X FA)	REDUCED TORSIONAL RESPONSE
3.2	0.0036	1.7	0.0034
4.5	0.0066	2.5	0.0074
6.4	0.0137	3.5	0.0161
7.8	0.0179	4.3	0.0246
9.0	0.0218	4.9	0.0333
10.1	0.0268	5.5	0.0396
11.5	0.0324	6.3	0.0493

TABLE D-21

RESPONSE AT FLOW CONDITION : HOMOGENOUS TURBULENCE (FINE GRID)

1/500-SCALE SECTIONAL MODEL TEST

FLEXURAL FREQUENCY =12.00 TORSIONAL FREQUENCY =22.00

FLEXURAL DAMPING = 0.54 TORSIONAL DAMPING =0.26

TURBULENCE INTENSITY , IW : 6.2%

V/(B X FZ)	REDUCED FLEXURAL RESPONSE	V/(B X FA)	REDUCED TORSIONAL RESPONSE
3.6	0.0019	2.0	0.0019
5.1	0.0036	2.8	0.0046
6.2	0.0048	3.4	0.0074
7.2	0.0058	3.9	0.0090
8.8	0.0077	4.8	0.0137
10.1	0.0094	5.5	0.0176
11.3	0.0111	6.2	0.0217
12.4	0.0133	6.8	0.0271
13.0	0.0145	7.1	0.0292

TABLE D-22

RESPONSE AT FLOW CONDITION : BOUNDARY LAYER FLOW (SPIRES)

1/500-SCALE SECTIONAL MODEL TEST

FLEXURAL FREQUENCY =12.0 TORSIONAL FREQUENCY =22.00

FLEXURAL DAMPING = 0.54 TORSIONAL DAMPING =0.28

TURBULENCE INTENSITY , IW : 9.8%

V/(B X FZ)	REDUCED FLEXURAL RESPONSE	V/(B X FA)	REDUCED TORSIONAL RESPONSE
2.8	0.0019	1.6	0.0019
4.0	0.0043	2.2	0.0040
5.6	0.0075	3.1	0.0097
6.9	0.0113	3.9	0.0149
8.0	0.0148	4.5	0.0191
8.9	0.0180	5.0	0.0238
10.2	0.0223	5.7	0.0325
11.1	0.0266	6.2	0.0432

TABLE D-23

RESPONSE AT FLOW CONDITION : BOUNDARY LAYER FLOW (SPIRES & ROUGHNESSES)

1/500-SCALE SECTIONAL MODEL TEST

FLEXURAL FREQUENCY =12.0 TORSIONAL FREQUENCY =22.0

FLEXURAL DAMPING = 0.54 TORSIONAL DAMPING =0.26

TURBULENCE INTENSITY , IW : 12.5%

V/(B X FZ)	REDUCED FLEXURAL RESPONSE	V/(B X FA)	REDUCED TORSIONAL RESPONSE
2.4	0.0013	1.4	0.0013
3.4	0.0027	1.9	0.0028
4.2	0.0043	2.3	0.0049
4.8	0.0056	2.7	0.0068
5.9	0.0080	3.3	0.0102
6.8	0.0093	3.8	0.0149
7.7	0.0115	4.3	0.0188
8.4	0.0129	4.7	0.0239
9.4	0.0172	5.2	0.0319

TABLE D-24

RESPONSE AT FLOW CONDITION : BOUNDARY LAYER FLOW (SPIRES AND ANGLES)

1/500-SCALE SECTIONAL MODEL TEST

FLEXURAL FREQUENCY =12.0 TORSIONAL FREQUENCY =22.0

FLEXURAL DAMPING = 0.54 TORSIONAL DAMPING =0.26

TURBULENCE INTENSITY , IW : 13.5%

V/(B X FZ)	REDUCED FLEXURAL RESPONSE	V/(B X FA)	REDUCED TORSIONAL RESPONSE
2.7	0.0019	1.5	0.0017
3.8	0.0045	2.1	0.0035
4.7	0.0059	2.6	0.0064
5.4	0.0087	3.0	0.0094
6.6	0.0122	3.7	0.0147
7.7	0.0158	4.3	0.0215
8.6	0.0175	4.8	0.0261
9.4	0.0204	5.2	0.0321
10.1	0.0232	5.7	0.0374

Appendix E

RESULTS OF FLOW MEASUREMENT

TABLE E-1

FLOW MEASUREMENTS AT FLOW CONDITION : SMOOTH (2-D)

HEIGHT FROM TUNNEL FLOOR Z (CM.)	VELOCITY RATIO (VZ/VG)	TURBULENCE INTENSITY(U) (%)	TURBULENCE INTENSITY(W) (%)
2.5	0.953	5.404	3.310
3.8	0.989	2.734	1.790
5.1	0.997	1.162	1.033
5.6	1.000	0.741	0.869

TABLE E-2

FLOW MEASUREMENTS AT FLOW CONDITION : HOMOGENOUS TURBULENCE(COARSE GRID) (2-D)

HEIGHT FROM TUNNEL FLOOR Z (CM.)	VELOCITY RATIO (VZ/VG)	TURBULENCE INTENSITY(U) (%)	TURBULENCE INTENSITY(W) (%)
7.6	0.851	15.507	13.502
10.2	0.877	15.345	13.179
11.1	0.890	14.756	12.839
12.7	0.921	14.331	12.338
15.2	0.958	13.206	11.257

TABLE E-3

FLOW MEASUREMENTS AT FLOW CONDITION : HOMOGENOUS TURBULENCE(FINE GRID) (2-D)

HEIGHT FROM TUNNEL FLOOR Z (CM.)	VELOCITY RATIO (VZ/VG)	TURBULENCE INTENSITY(U) (%)	TURBULENCE INTENSITY(W) (%)
11.1	0.987	6.817	6.099
12.7	0.993	7.066	6.126

TABLE E-4

FLOW MEASUREMENTS AT FLOW CONDITION : BOUNDARY LAYER(SPIRES)
(2-D)

HEIGHT FROM TUNNEL FLOOR Z (CM.)	VELOCITY RATIO (VZ/VG)	TURBULENCE INTENSITY(U) (%)	TURBULENCE INTENSITY(W) (%)
2.5	0.682	12.506	10.665
5.1	0.707	11.891	10.205
7.6	0.736	11.860	10.066
10.2	0.763	11.646	10.000
12.7	0.802	10.803	9.598
15.2	0.837	10.000	9.231
17.8	0.870	9.138	8.324
20.3	0.899	8.127	7.698
22.9	0.925	6.929	6.685
25.4	0.944	5.898	5.864
30.5	0.973	3.970	4.069
35.6	0.989	2.345	2.572
40.6	0.999	1.193	1.289
45.7	1.000	0.741	0.676

TABLE E-5

FLOW CONDITIN : BOUNDARY LAYER(SPIRES & ROUGHNESS) (2-D)

HEIGHT FROM TUNNEL FLOOR Z (CM.)	VELOCITY RATIO (VZ/VG)	TURBULENCE INTENSITY(U) (%)	TURBULENCE INTENSITY(W) (%)
7.6	0.570	20.395	15.367
10.2	0.634	16.853	13.350
12.7	0.681	14.468	11.915
15.2	0.744	12.381	10.130
17.8	0.805	10.840	9.720
20.3	0.850	9.470	8.636
22.9	0.901	8.036	7.500
25.4	0.924	6.690	6.551
30.5	0.966	4.433	4.600
35.6	0.988	2.606	2.997
40.6	0.998	1.613	1.806
45.7	1.001	0.836	0.836

TABLE E-6

FLOW MEASUREMENTS AT FLOW CONDITION : BOUNDARY LAYER(SPIRES & ANGLES) (2-D)

HEIGHT FROM TUNNEL FLOOR Z (CM.)	VELOCITY RATIO (VZ/VG)	TURBULENCE INTENSITY(U) (%)	TURBULENCE INTENSITY(W) (%)
2.5	0.539	19.104	17.493
5.1	0.573	19.270	16.348
7.6	0.620	18.182	15.584
10.2	0.658	16.732	14.384
12.7	0.682	14.953	13.585
15.2	0.728	13.510	12.246
17.8	0.773	12.073	10.991
20.3	0.811	10.754	10.000
22.9	0.842	9.564	8.875
25.4	0.875	8.131	7.837
30.5	0.918	5.367	5.647
35.6	0.941	3.488	3.659
40.6	0.959	1.812	1.980
45.7	0.969	1.130	0.930

TABLE E-7

FLOW MEASUREMENTS AT FLOW CONDITION : SMOOTH (3-D)

HEIGHT FROM TUNNEL FLOOR Z (CM.)	VELOCITY RATIO (VZ/VG)	TURBULENCE INTENSITY(U) (%)	TURBULENCE INTENSITY(W) (%)
0.5	0.648	13.978	9.808
1.5	0.931	7.658	4.786
2.5	0.969	5.208	2.819
3.5	0.984	2.820	1.691
4.5	0.998	1.685	1.018
26.0	0.998	0.476	0.028

TABLE E-8

FLOW MEASUREMENTS AT FLOW CONDITION : HOMOGENOUS TURBULENCE(COARSE GRID) (3-D)

HEIGHT FROM TUNNEL FLOOR Z (CM.)	VELOCITY RATIO (VZ/VG)	TURBULENCE INTENSITY(U) (%)	TURBULENCE INTENSITY(W) (%)
9.5	0.721	18.699	13.959
11.0	0.731	18.366	13.585
13.5	0.758	15.658	12.982

TABLE E-9

FLOW MEASUREMENTS AT FLOW CONDITION : HOMOGENOUS TURBULENCE(FINE GRID) (3-D)

HEIGHT FROM TUNNEL FLOOR Z (CM.)	VELOCITY RATIO (VZ/VG)	TURBULENCE INTENSITY(U) (%)	TURBULENCE INTENSITY(W) (%)
9.5	0.986	7.356	6.620
11.0	0.995	7.185	6.492
13.0	0.997	7.060	6.550

TABLE E-10

FLOW MEASUREMENTS AT FLOW CONDITION : BOUNDARY LAYER(SPIRES)
(3-D)

HEIGHT FROM TUNNEL FLOOR Z (CM.)	VELOCITY RATIO (VZ/VG)	TURBULENCE INTENSITY(U) (%)	TURBULENCE INTENSITY(W) (%)
6.0	0.691	14.545	11.727
8.0	0.729	14.483	11.078
10.0	0.760	13.678	10.744
13.4	0.799	12.510	10.071
16.8	0.842	10.966	9.399
20.5	0.889	9.261	8.059
25.5	0.932	6.237	6.136
30.1	0.945	4.520	4.420
36.5	0.968	2.414	2.596
41.0	0.977	1.221	1.511
44.7	0.982	0.800	0.928

TABLE E-11

FLOW MEASUREMENTS AT FLOW CONDITIN : BOUNDARY LAYER
(SPIRES & ROUGHNESS) (3-D)

HEIGHT FROM TUNNEL FLOOR Z (CM.)	VELOCITY RATIO (VZ/VG)	TURBULENCE INTENSITY(U) (%)	TURBULENCE INTENSITY(W) (%)
9.5	0.651	17.957	11.847
11.5	0.668	15.364	11.136
16.0	0.717	12.489	9.441
20.0	0.832	10.284	8.279
24.0	0.888	7.858	6.833
28.0	0.938	5.469	5.375.
32.0	0.947	3.719	4.040
36.0	0.964	2.457	2.709
40.0	0.981	1.548	1.625

TABLE E-12

FLOW MEASUREMENTS AT FLOW CONDITION : BOUNDARY LAYER(SPIRES & ANGLES) (3-D)

HEIGHT FROM TUNNEL FLOOR Z (CM.)	VELOCITY RATIO (VZ/VG)	TURBULENCE INTENSITY(U) (%)	TURBULENCE INTENSITY(W) (%)
9.5	0.625	20.031	14.127
11.5	0.655	16.216	13.194
13.0	0.692	14.535	12.219
16.0	0.734	13.408	11.070
22.0	0.813	10.693	9.018
28.0	0.875	7.049	6.564
35.0	0.924	3.868	3.937
40.0	0.953	2.331	2.537
44.0	0.966	1.550	1.783

TABLE E-13

FLOW MEASUREMENTS AT FLOW CONDITION : 90 INCHES FROM THE SPIRES

DISTANCE FROM TUNNEL WALL X (IN.)	VELOCITY RATIO (VX/VG)	TURBULENCE INTENSITY(U) (%)	TURBULENCE INTENSITY(W) (%)
1.9	0.781	11.294	8.533
3.7	0.823	11.220	9.812
5.3	0.833	11.399	10.124
6.8	0.822	11.991	10.384
8.5	0.810	11.919	10.250
10.0	0.805	11.795	10.356
11.8	0.782	11.687	10.700
13.3	0.777	11.636	10.600
15.0	0.779	12.066	10.537
16.4	0.779	12.479	10.496
19.6	0.779	12.392	10.533
21.2	0.777	12.298	10.642
22.8	0.783	11.929	10.695
24.4	0.781	11.753	10.680
25.9	0.803	11.231	10.429
27.7	0.802	11.847	10.402
29.1	0.814	11.976	10.198
30.7	0.837	11.111	9.919
32.3	0.825	10.929	9.680
34.1	0.782	11.317	8.642

TABLE E-14

FLOW MEASUREMENTS AT FLOW CONDITION : 45 INCHES FROM THE SPIRES

DISTANCE FROM TUNNEL WALL X (IN.)	VELOCITY RATIO (VX/VG)	TURBULENCE INTENSITY(U) (%)	TURBULENCE INTENSITY(W) (%)
2.1	0.767	17.556	14.322
3.9	0.784	16.954	14.819
5.3	0.805	18.265	15.188
6.9	0.793	18.806	15.597
8.6	0.771	20.492	15.609
10.2	0.764	19.477	16.357
11.9	0.753	17.949	16.239
13.5	0.752	18.870	16.260
15.2	0.769	18.787	15.565
16.7	0.788	18.750	15.359
19.9	0.776	19.212	15.104

Appendix F

COMPUTER PROGRAM

```
**********************************************
*                                            *
*         RESPONSE CALCULATION               *
*                                            *
**********************************************
      COMPLEX*16 CMPLX,HO,H1,DEN,CC,ZL,AL,ZM,AM,BZ,BA,
     *AA1,AA2,AA3,AA4
      COMPLEX*16 DEL,CC1,CC2,CC3,CC4,CC5,CC6
&&&&&&&&&&&&&&&&&&&&&&&&&&&&&&&&&&&&&&&&&&&&&&&&&&&&
C                                                   &
C  PI  = 3.142857.....                              &
C  SL  : SLOPE OF LIFT FORCE COEFFICIENT            &
C  SM  : SLOPE OF MOMENT COEFFICIENT                &
C  BET : FREQUENCY RATIO FA/FZ                      &
C   SP : SPAN LENGTH OF THE BRIDGE                  &
C  AMU : MASS RATIO                                 &
C  ANU : MASS MOMENT OF INERTIA RATIO               &
C   HG : DECK HEIGHT                                &
C   BB : LINEAR DIMENSION OF THE BRIDGE DECK        &
C   CC : CORRELATION FACTOR                         &
C   TI : TURBULENCE INTENSITY                       &
C   ZZ : FLEXURAL DAMPING                           &
C   ZA : TORSIONAL DAMPING                          &
C   FZ : FLEXURAL FREQUENCY                         &
C   FA : TORSIONAL FREQUENCY                        &
C                                                   &
C&&&&&&&&&&&&&&&&&&&&&&&&&&&&&&&&&&&&&&&&&&&&&&&&&&&&
```

```
      PI=4.*ATAN(1.)
      SL=2.*PI
      SM=PI/2
       FZ=AFZ(1)
       SP=440.
       FA=AFZ(1)*1.66
       BET=FA/FZ
       ANU=10.0
       AMU=40.0
       ZZ1=ZZ(1)*100.0
       ZZZ=ZZ(1)
       ZAA=ZZZ
       TI=TUI(1)*100.0
C*****************************************************
C                                                     *
C  IX   :  FREQUENCY FROM 0.05 FZ TO 5 FZ             *
C  XI   :  F/FZ                                      *
C  VR(III) : REDUCED VELOCITY                         *
C*****************************************************
       DO 1 III=1,JJJ
       V(III)=FLOAT(III)*K
       DO 6 I=1,KOUNT
C*****************************************************
C                                                     *
C  SSZ = SQUARE OF RMS OF VERTICAL RESPONSE           *
C  SSA = SQUARE OF RMS OF TORSIONAL RESPONSE          *
C                                                     *
```

```
C*****************************************************
      SSZ=0.0
      SSA=0.0
      DO 10 IX=1,100
      XI=FLOAT(IX)*0.05
C*****************************************************************
C                                                                *
C  APPROXIMATION OF THEODERSON'S FUNCTION :  F(K) + IG(K)        *
C                                                                *
C*****************************************************************
      AK=PI*XI/VR(III)
      HO=CMPLX(1.0,-0.0455/AK)
      H1=CMPLX(1.0,-0.30/AK)
      CC=1.0-0.165/HO-0.335/H1
      CC1=-2.0*CC/AK
C*****************************************************************
C                                                                *
C  USING THEODERSON'S FUNCTION,                                  *
C THE NONLINEAR FORCES CAN BE APPROXIMATE : ZL, AL, ZM, AM*
C                                                                *
C*****************************************************************
      ZL=CMPLX(-1.0-AIMAG(CC1),REAL(CC1))
      CC2=CC1/AK
      CC3=(-CC-1.0)/AK
      AL=CMPLX(REAL(CC2)-AIMAG(CC3),AIMAG(CC2)+REAL(CC3))
      CC4=CC/AK
      ZM=CMPLX(-AIMAG(CC4),REAL(CC4))
```

```
      CC5=CC4/AK
      CC6=(CC-1.0)/2.0/AK
      AM=CMPLX(-0.125+REAL(CC5)-AIMAG(CC6),AIMAG(CC5)+REAL(CC6))
C*************************************************************
C                                                             *
C  FORM THE FREQUENCY RESPONSE FUNCTION : A1, A2, A3, A4      *
C DEL : THE DETERMINANT OF THE FREQUENCY RESPONSE FUNCTION    *
C                                                             *
*************************************************************
      BZ=CMPLX(1.-XI*XI,2.*XI*ZZZ)
      BA=CMPLX(BET**2-XI**2,2.*BET*XI*ZAA)
      AA1=AMU*BZ-ZL*XI**2
      AA2=-AL*XI**2
      AA3=-(ZM*XI**2)
      AA4=ANU*BA-AM*XI**2
      DEL=AA1*AA4-AA2*AA3
      R1=CDABS(AA4/DEL)
      R2=CDABS(AA2/DEL)
      R3=CDABS(AA3/DEL)
      R4=CDABS(AA1/DEL)
C*****************************************
C                                        *
C   FORM THE RESPONSE SPECTRUM           *
C                                        *
C*****************************************
      A=(SL*VR(III)**2/(PI**3))**2
      B=PI**2*2*XI/VR(III)+1
```

```
C*****************************************
C                                         *
C   FORM THE VELOCITY SPECTRUM            *
C                                         *
C*****************************************
      C=6.0*HG(I)*(TI**2)/BB/VR(III)
      D=(4.*HG(I)*XI/BB/VR(III)+1.)**2
      G=(2.*SM/SL)**2
C*****************************************
C                                         *
C  THE JOINT ACCEPTANCE FUNCTION          *
C  CC : CORRELATION FACTOR                *
C*****************************************
      HX=CC*SP*XI/BB/VR(III)
      HQ=HX**2+PI**2
      IF (HX.GT.15) PP=0.0
      IF (HX.LE.15) PP=EXP(-HX)
      H=(4*HX/HQ)+8.*PI**2*(PP+1.)/HQ**2
C*************************************************
C                                                 *
C  CALCULATE THE CORRESPONDING RMS RESPONSE       *
C        TO EACH FREQUENCY                        *
C*************************************************
      SZ=(R1**2+G*R2**2)*H*A*C/B/D
      SA=(R3**2+G*R4**2)*H*A*C/B/D
C*************************************************
C                                                 *
```

```
C  SUM UP THE SQUARE OF RMS RESPONSE          *
C       FOR EACH FREQUENCY                     *
C***************************************************
        SSZ=SSZ+SZ*0.05
        SSA=SSA+SA*0.05
   10   CONTINUE
    6   CONTINUE
    1   CONTINUE
```